On the Development of a Real-Time Embedded Digital Controller for Heavy Truck Semiactive Suspensions

By

Neil McLellan

Thesis Submitted to the Faculty of Virginia Tech in partial fulfillment of the requirements for the degree of

Master of Science

In

Electrical Engineering

Approved:

William T. Baumann, Co-Chairman	Mehdi Ahmadian, Co-Chairman

John S. Bay

June, 1998

Blacksburg, VA

Keywords: Suspension, Magneto-Rheological, Semiactive, Skyhook, Embedded, Controller, Heavy, Truck

Abstract

A digital controller was designed for a semiactive primary suspension for a class 8 highway truck. The controller used a skyhook policy (where the semiactive damper simulates a damper between the sprung mass and an inertial reference) to control magneto-rheological dampers placed on the truck ‘s primary suspension in response to measurements made by accelerometers placed on the axle and the truck frame. The completed system was then tested for both random noise (on highway driving) and impulse (speed bump) response. The test results showed that for the damping tuning and controller arrangements used in this study, semiactive dampers do not offer any significant benefits in reducing overall vibration levels at the truck frame or axles. The semiactive dampers, however, provided better control of the dynamic transients, such as roll and pitch induced by hitting speed bumps, as compared to passive dampers. Further assessment of the magneto-rheological damper’s tuning and the skyhook control policy is needed to establish any definitive conclusions on the potential benefits of semiactive magneto-rheological suspensions for heavy trucks.

Acknowledgements

I would like to thank Dr. Mehdi Ahmadian for his guidance on this project. I would also like to thank Dr. Bill Baumann and Dr. John Bay for serving on my graduate committee, and Dave Simon for his participation in this project.

Additionally, the financial support provided by the Federal Highway Administration (FWHP) through the Center for Transportation Research (CTR) at Virginia Tech is greatly acknowledged. The support of Lord Corporation, Cary, NC, in providing the magneto-rheological dampers and fluid, and Volvo Heavy Trucks, Florence, KY, in providing the class 8 truck that was used in this study is also greatly appreciated.

I also wish to thank my parents, Doug and Libby, for providing the funding for the large majority of my education, and my brother and sister, Kevin and Molly, for cutting into these funds and forcing me to attempt to graduate. Finally, I would like to thank Cliff Lee for helping me pass Freshman Statics.

Contents

List of Figures

List of Tables

Chapter 1
Introduction

The purpose of this chapter is to provide an overview of the application of semiactive primary suspensions in ground vehicles, in particular class 8 heavy on-highway trucks. It further outlines the objectives of this research, the approach for accomplishing the objectives, and the outline of this thesis.

1.1 Overview

In this study, a controller was designed for use in a semiactive suspension for a heavy on-highway truck. The controller was to take acceleration data and apply an on/off skyhook policy (where the semiactive damper simulates a damper between the sprung mass and an inertial reference) to four semiactive primary suspensions. The semiactive suspension consisted of the passive dampers retrofitted with magneto-rheological technology. The system was used to evaluate the potential benefits of semiactive magneto-rheological primary suspensions in controlling the steady state and transient dynamics of a class 8 heavy truck.

1.2 Objectives

The primary objectives of this research were:

1) To design and prototype a real-time digital embedded controller that can be used for semiactive suspensions on a heavy truck, and

2) To use the controller to evaluate the performance of a semiactive primary suspension in improving the stability and handling of a heavy truck.

1.3 Approach

To achieve the research objectives, a controller was designed. This controller was then constructed and programmed to implement a semiactive on/off skyhook policy. The controller took as inputs two accelerometer readings for each wheel, one for the axle near the wheel and one for the frame above it. The controller integrates these to provide the velocity of the axle and frame, calculates the relative velocity, and then switches a magneto-rheological damper on or off based on the sign of the product of relative velocity and velocity of the frame, in accordance with the on/off skyhook policy.

The controller was tested and debugged in the laboratory, and then installed on the truck for road testing. Semiactive dampers were placed on four of the wheels and connected to the controller. Data was recorded from eleven accelerometers placed on the truck. Eight were the axle and frame accelerometers used by the controller for each wheel, while three were placed tri-

axially in the cab. The data were collected during a series of road tests to record the performance of semiactive and passive dampers in response to both random noise (on highway driving), and impulse (speed bump) disturbances. The highway driving provided frequency data for typical driving, while the speed bump data allowed for analysis of the transient response to what was approximately an impulse disturbance.

The data were later analyzed, using Matlab, to assess the potential benefits of the semiactive primary dampers, as compared to passive dampers. The highway data were analyzed in the frequency domain as an auto power spectrum. The speed bump data were analyzed in the time domain by taking measures of the magnitudes of peaks, the decay rate of transients, and the RMS around the time of the hit. The speed bump acceleration data were also integrated to provide displacement data , which were evaluated in the same way as the acceleration data (magnitudes, decay rate, RMS).

1.4 Outline

The following chapters describe the work that was performed in designing and testing of the real-time embedded controller for the semiactive system, and the results obtained in the experiment. Chapter 2 presents background material relevant to this study. Chapter 3 describes the pre-existing damper hardware

that was incorporated into our semiactive primary suspension. Chapter 4 describes the design of the controller hardware and software, along with the debugging and bench testing of the controller. In Chapter 5, the method for collecting data on the overall system on the vehicle is explained and the data are presented and analyzed. Chapter 6 includes conclusions that are drawn from the analysis in Chapter 5 , along with recommendations for further study.

Chapter 2

Background

This section provides a background on topics relevant to the design of this controller and its associated damper hardware. First, issues relevant to vehicle suspensions are discussed, including the choice of a passive, active, or semiactive suspension; technologies with which to implement semiactive controllers; and the frequencies that are important for a suspension to control. The section concludes with a summary of past studies on semiactive damping and magneto-rheological devices.

2.1 Suspensions

A vehicle suspension traditionally consists of a spring and damper in parallel. The spring supports the static weight of the mass, while the damper dissipates the energy from disturbances. The damping constant of the damper determines both the stability of the vehicle and the comfort of the travelers, as shown in Figure 2.1. A stiff damper (a damper with a large damping constant) provides good stability, keeping the tires in contact with the road and preventing jackknifing and other problems, but will transfer much of the road input to the passenger, causing

an uncomfortable ride. Conversely,a soft damper (a damper with a low damping constant) will disturb the travelers less, but it lowers the stability of the vehicle.

This discomfort and corresponding fatigue on the driver is an especially important consideration for on-highway trucks, in which the driver is subjected to the rigors of driving for long periods. In addition, a vehicle with stiff damping is also more likely to cause cargo damage due to larger vibrations transferred from the road to the cargo bed. The design of a suspension must make a compromise between stability and comfort.

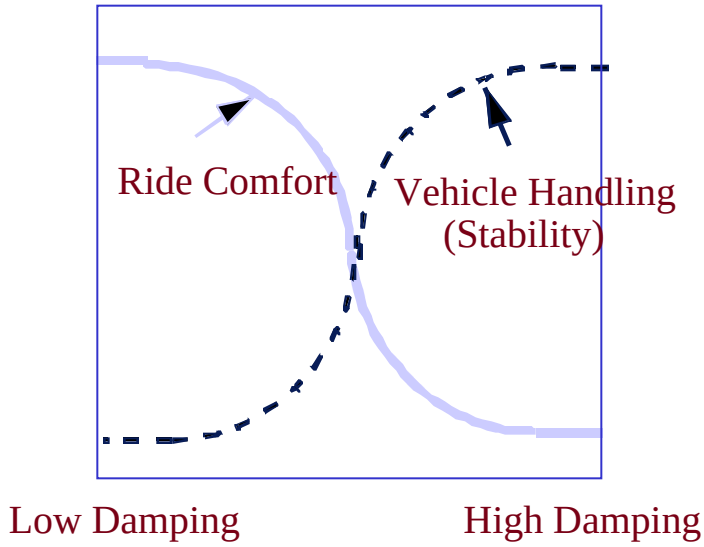

Figure 2.1. Damping Compromise.

2.2 Types of Suspension

The traditional suspensions on vehicles use a passive damper. Passive dampers commonly have a bilinear damping value, such as is shown in Figure 2.2. To improve performance, it has been suggested that an active suspension

mechanism may be used, where an actuator applies a force to directly oppose vibrations, as shown in Figure 2.3. Such a system, however, requires large amounts of power and is thus somewhat impractical for most applications. In addition, if such a system should fail, a vehicle would be left with no damping, which can yield an unstable condition.

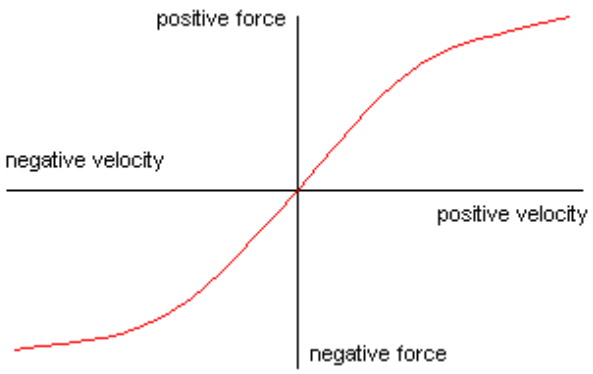

Figure 2.2. Force vs. Velocity Curve for a Passive Damper.

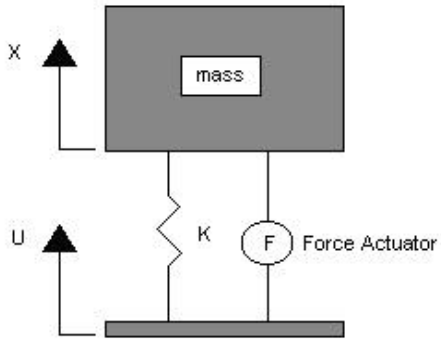

Figure 2.3. Fully Active Suspension Schematic.

Because of the difficulties encountered in using a fully active suspension, it is often more practical to use a semiactive suspension. A semiactive suspension uses a damping element, but unlike a passive damper, the semiactive damper can vary its damping, as shown in Figure 2.4. The semiactive suspension can provide performance comparable to the optimal fully active suspension, while using significantly less power. In addition, the semiactive suspension can provide some level of damping even if power is lost, making it safer than a fully active suspension.

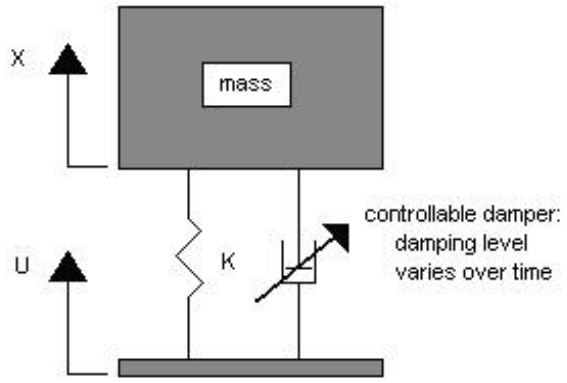

Figure 2.4. Semiactive Suspension Schematic.

2.3 Skyhook Policy

In controlling the vibration of a suspended body, such as the body of a vehicle, it has been shown that the so-called "skyhook" dampers provide the optimal control [1, 2], minimizing the vibration of the suspended body. As shown in Figure 2.5, skyhook damping suggests placing a damper between the suspended body and

some inertial frame of reference. Of course, for vehicle applications, this is not practical, as the damper is placed between two moving bodies (i.e. the body and the axle.) Thus, semiactive dampers are controlled to emulate the skyhook damper to the extent possible. As illustrated in Figure 2.6, this is accomplished by turning on the damper when it can apply a force in the direction of a true skyhook damper, and turning it off when it cannot. In an "on/off" skyhook policy, the on-state damping coefficient will be fixed, whereas a continuous skyhook policy would make the damping coefficient proportional to the sprung body velocity.

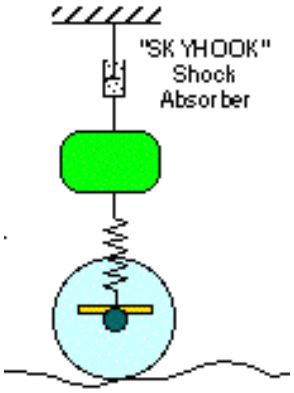

Figure 2.5. Skyhook Damper Arrangement [3].

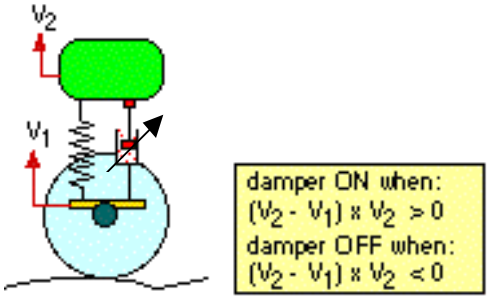

Figure 2.6. Semiactive Skyhook Damper Arrangement [3].

2.4 Implementing Semiactive Dampers

There are two methods for creating a damper with variable damping: changing the size of the orifice through which the hydraulic fluid passes, and changing the properties of the fluid itself. The orifice size can be changed by using a motor or some other actuator to open and close it. To implement a damper where the properties of the fluid change, there are two types of materials available; electro-rheological (ER) and magneto-rheological (MR) fluids.

As the names suggest, electro-rheological fluids are a class of fluids in which the rheological properties of the fluid are changed by subjecting the fluid to an electric field. Similarly, magneto-rheological fluids are fluids that change when subjected to a magnetic field. As shown in Table 2.1, the primary advantages of magneto-rheological fluids, in comparison to electro-rheological fluids, are that they:

- Require much smaller electrical voltages
- Can provide much higher shear strain rates

Table 2.1. Comparison of Properties of Typical ER and MR Fluids [4].

Property	ER Fluid	MR Fluid
Yield Strength (Field)	2-5 kPa (3-5 kV/mm) Field Limited by Breakdown	50-100 kPa (150-250 kA/m) Field Limited by Saturation
Viscosity (No Field)	0.2-0.3 Pa-s @25°C	0.2-0.3 Pa-s @25°C
Operating Temperature	+10 to +90 °C (ionic, DC) -25 to +125 °C (non-ionic, AC)	-40 to +150 °C (Limited by Carrier Fluid)
Current Density	2-15 mA/cm^2 (4kV/mm, 25°C) (x10 – x100 @ 90°C)	Can Energize with Permanent Magnets
Specific Gravity	1-2.5	3-4
Ancillary Materials	Any (Conductive Surfaces)	Iron/Steel
Color	Any, Opaque or Transparent	Brown, Black, Gray/Opaque

Therefore, magneto-rheological fluids have been evaluated to be practical for many applications, such as vehicle dampers, in which electro-rheological fluids have proven to be impractical.

2.4.1 Magneto-Rheological Fluids

Magneto-rheological fluids contain metallic particles suspended in a hydraulic carrier. Since the rheological properties of the fluid are controlled by passing it through a magnetic field, electromagnetic means (such as a coil of wire) are often used to energize the fluid and control its shear strain rate. If the coil is placed

such that the fluid passes through it as the damper compresses and extends, then the damping rate of the damper can be controlled. Such a controllable damper is described in Section 3.1.

2.5 Frequency Response

The frequencies most uncomfortable to humans, and therefore, those that the system described in this paper needs to control, are in the 0.5Hz-10Hz range [5]. The range 0.5-0.75 Hz can be associated with motion sickness or “seasickness” [5]. A 1Hz signal, however, is not uncomfortable; it is near the frequency of a walking person. It is also relatively close to the body heave of most cars; therefore, it seems normal to most drivers and passengers [5].

The frequencies that the human body is most sensitive to in the vertical (heave), fore-aft (pitch), and lateral (roll) directions are shown in Figures 2.7-2.8. Note that a plateau is reached for the lateral and fore-aft directions between 1Hz and 2Hz, and a plateau for the vertical direction is reached between 4Hz and 8Hz, again showing how the frequencies of interest for comfort are at 10Hz and below.

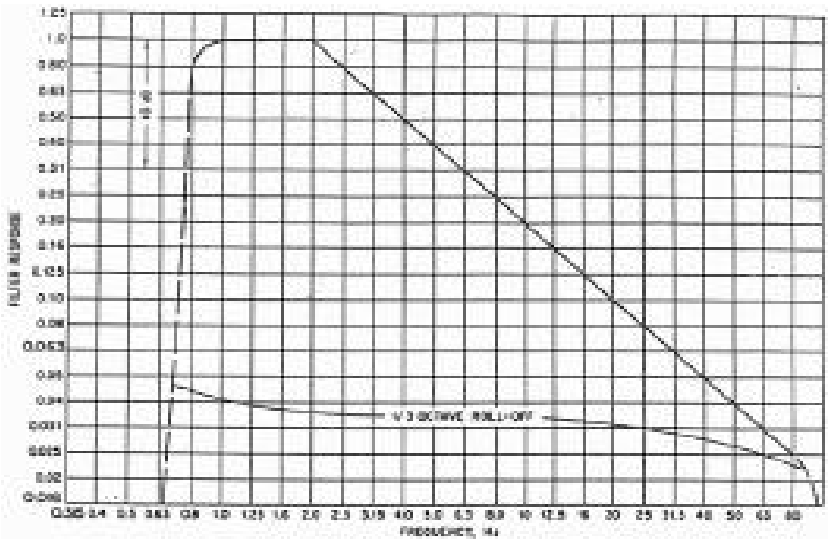

Figure 2.7. Human Body Sensitivity to Vibrations in the Fore-Aft and Lateral Directions [6].

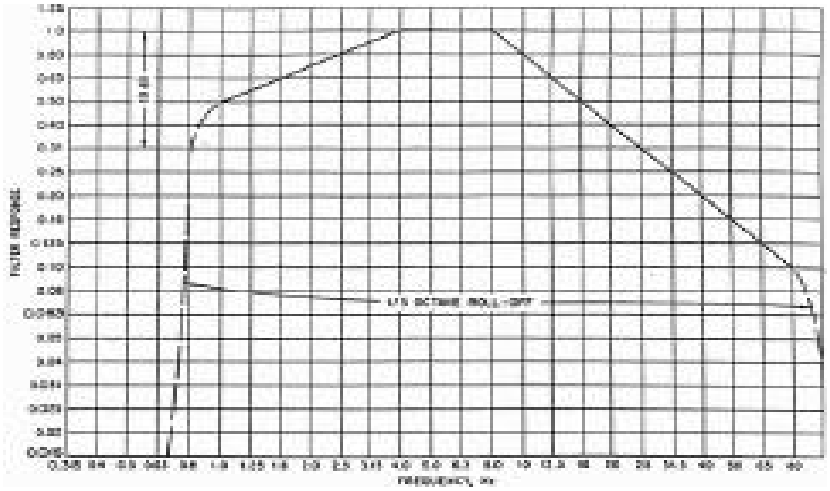

Figure 2.8. Human Body Sensitivity to Vibrations in the Vertical Direction [6].

2.6 Past Studies

Most of the past studies that are related to semiactive suspensions and/or magneto-rheological systems include simulation analysis of the systems. There are a relatively much smaller number of studies that address the experimental

evaluation of the systems. We will next review some of the past studies of semiactive vehicle suspensions and magneto-rheological devices.

2.6.1 Vehicle Suspensions

One of the earlier studies of skyhook damping was conducted by Krasnicki [7]. In this study, a single degree of freedom system with a prototype semiactive damper using the skyhook policy is compared to results obtained from computer simulation. The damper consisted of a hydraulic actuator with an electro-hydraulic servo-valve modulating the controlling orifice area. The system was subjected to both sinusoidal and random vibration input. Transmissibility and signal/waveform data were collected and compared to those obtained in computer simulation. The semiactive damping was found to improve vibration isolation.

Another paper by Krasnicki [8] involves an "on/off" damper. It assumes either zero damping or a constant passive damping value. The on/off damper differs from the continuous skyhook policy in that the force generated by the damper will be proportional to the relative velocity of the sprung and unsprung mass rather than the absolute velocity of the sprung mass. The damper is evaluated in the same manner as in [7]. The on/off damper was found to provide

improvements over a passive system, but it had limitations when compared to an active damper, especially at higher frequencies.

Semiactive suspensions have been tested on a motorcycle in studies by McMichael, Boonchanta, and Krasnicki [9, 10, 11], where they were placed on the rear wheel of a Yamaha YZ-250 dirt bike. An all analog controller was built and tested. Problems with the accelerometer being sensitive to the lean of the motorcycle and with low frequency drift in the analog implementation caused the system to show limited performance.

Semiactive systems have also been tested on a ten-wheeled tank in a study by Miller and Nobles [12]; it is worth noting here that in that case, only four of the ten wheels were given the semiactive dampers. In this study, a microprocessor-based controller was built. The system was tested on a 10-axis road simulator and compared to the same vehicle with passive dampers. Significant reduction in the absorbed power was achieved (13%-40%).

Semiactive dampers have previously been tested on a large truck by Ahmadian [13]. In this study, semiactive dampers were put on all six wheels, with the capability to switch between a variety of control configurations for each axle. The acceleration data were taken at the B-post, a point in the truck cab behind the driver at approximately shoulder height, and were evaluated by measuring the peak intensity in various frequency bands. The truck was driven on highway

and city roads, and the semiactive damping was found to provide improvements in controlling beaming motion, the first bending mode of the truck frame.

Semiactive dampers have also been used for suspensions other than the primary suspension, such as secondary suspensions at vehicle cabs and seats. For instance, a semiactive magneto-rheological seat suspension for heavy truck and farm equipment applications was recently developed and made commercially available by Lord Corporation. In studies conducted jointly between the Advanced Vehicle Dynamics Laboratory at Virginia Tech and Lord Corporation, it was shown that the magneto-rheological semiactive systems can provide significant improvements over active dampers for such applications [14]. It was also found that the discontinuities from switching the damper on and off present in skyhook control policies caused some passenger discomfort, and a policy to remove these discontinuities and improve comfort was developed.

A similar effect related to these discontinuities has been found when a semiactive scheme is applied to the primary suspension. On the primary suspension, these effects cause noise, the noise being the sound of the tire suddenly releasing stored energy as the damper is turned off. Methods for reducing or eliminating this noise are discussed in a paper by Miller and Nobles [15].

Another application of semiactive dampers that has been studied is in Maglev trains, as both secondary and primary suspensions, in a paper by Cai and Chen [16]. A one-dimensional vehicle with two degrees of freedom was simulated under various active and semiactive control policies. The transient and frequency response showed that such policies can improve vehicle response and comfort.

2.6.2 Simulations

A number of simulations have been performed for semiactive systems, some comparing them to active systems, and some presenting alternate methods to skyhook control.

2.6.2.1 Skyhook Simulations

In papers by Margolis [17, 18] procedures are given for comparing passive, active, and semiactive systems using bond graphs. The bond graph method is a pictorial representation of the energy storage, dissipation, and exchange mechanisms of a system. In [17], they are used to determine when a system can benefit by active or semiactive damping, and if semiactive damping can adequately emulate active damping, by using them to obtain frequency transmissibility data. In [18], bond graphs are used to determine frequency response based on the energy dissipation per cycle, using an approximate

“effective” damping ratio, equal to the active system damping ratio multiplied by the percent “on time” for the semiactive components. Once this effective damping ratio is calculated, it is easy to obtain the state equations and then the frequency response.

In a study by Ahmadian, Reichert, and Song [19], a harmonic analysis of semiactive suspensions is done for a suspension subjected to a pure tone input. It is shown that semiactive suspensions decrease the resonance peak without worsening the isolation at higher frequencies. Both on-off and continuous skyhook semiactive suspensions were simulated in this study.

In another study by Ahmadian [20], a multiple-degree-of-freedom system is simulated. The systems include the heave and pitch in a vehicle. Alternative semiactive policies to skyhook control, called groundhook, wherein the wheel is connected by a damper to an inertial frame of reference and hybrid control (a combination of groundhook and skyhook) are offered and compared to a passive suspension. These alternative control policies will be further addressed in the next section. It was shown that each type of suspension system provides a different compromise between controlling the sprung and unsprung body dynamics, with the hybrid control attempting to provide the compromise suitable for most applications.

2.6.2.2 Other Policies

The skyhook control is only optimal in the sense of minimizing vibration transmission to the sprung body (i.e., vehicle body). It has the disadvantage of increasing wheel hop, and it does not consider rattlespace. The wheelhop is increased because the skyhook policy is simulating a situation in which there is no damping for the wheel. Increased wheelhop means less control of the vehicle when it is not in contact with the ground, and increased pavement damage when it comes back in contact with the ground. The rattlespace is defined as the space provided between the axle and vehicle body for the suspension; this rattlespace must not be exceeded by compression of the suspension or else very jarring impacts will occur. Therefore, other variations of the skyhook may be needed to improve other aspects of the suspension.

To minimize the wheelhop, it is possible to connect the wheel to a skyhook (in this case called a groundhook), but this creates the opposite problem of increasing the vibration of the body, as now the body has effectively no damping. A hybrid method combining the best aspects of groundhook and skyhook is discussed in a paper by Ahmadian [21] as a potential alternative to provide a more acceptable compromise for a wider range of applications.

In a paper by Kimbrough [22], a bilinear model is used to develop various control schemes. A bilinear model is a system that adds non-linearities to standard, time invariant, linear equations, while still allowing some of the desirable properties of the linear equations to be used in analysis. The control schemes developed using these methods are simulated and evaluated for a variety of properties including passenger acceleration, velocity between passenger and sprung mass, tire deflection, and suspension excursion. The controller developed was found to lower the passenger acceleration and passenger relative velocity.

Another study using the bilinear model is by Hrovat, Margolis, and Hubbard [23]. In [23], a two-degree-of-freedom model was simulated. A Linear Quadratic Regulator (LQR) solution for a linear system for the controller was used as a starting point, and then numerical methods were used to find an optimal controller for the nonlinear system. The controller was then simulated, although the only improvement resulting from the optimization was that the new control scheme required fewer control switchings than the LQR control.

In a study by Yi and Hedrick [24], the possibility of controlling tire force using semiactive schemes is discussed. A bilinear model is also used here. Semiactive dampers using a stepper motor to control a variable orifice were tested on a half-car test rig andevaluated for frequency and transient response using the control policies developed. The semiactive system was found to be

capable of controlling the dynamic tire force, reducing it over a wide frequency range in comparison to a passive damper.

A semiactive control scheme is simulated using finite element modeling in a paper by Khulief and Sun [25]. In this study, a multibody flexible vehicle is simulated. Structural vibrations are simulated by dividing the chassis into equal elements and modeling their interaction. The condition simulated is the vehicle hitting a small bump. The semiactive suspension is shown to be able to suppress structural vibrations outside the range of passive suspensions.

The robustness of optimal control schemes for active suspensions is discussed in [26]. Both LQ (Linear Quadratic) and LQG (Linear Quadratic Gaussian) control policies are developed for a quarter-car model. The LQG policy takes into account static load uncertainties (uncertainties in the weight and distribution of the load) and tire behavior uncertainties (such as variations in tire pressure). The policies are simulated for impulse response and are compared. The LQG controller was found to not cause significant performance loss in reduction of vibration, while providing stability from static load and tire behavior uncertainties.

In a paper by Redfield [27], the feasibility of low bandwidth semiactive schemes is studied. These low bandwidth semiactive policies require only sensing and actuation at the bandwidth of the sprung mass, whereas a policy such as

skyhook requires sensing of the relative velocity, which requires a higher bandwidth. The lower bandwidth schemes are more economical to implement. The paper discusses some low bandwidth policies and simulates them on a quarter-car model, showing that they can provide benefits approximating those of higher bandwidth schemes.

Other studies have shown improvements over a skyhook scheme by using adaptive learning. In a study by Bellizi and Bouc [28], an adaptive control scheme is developed for a variable orifice semiactive damper. The adaptive control scheme changes its feedback law parameters continuously in an effort to match the non-linear semiactive system to a reference linear system with the desired properties. In the adaptive control scheme used, it is not necessary to know the exact equations for the non-linear terms, as the system only uses measured responses. The system was simulated for response to low passed white noise. The adaptive controller was found to be able to reduce both the frequency and amplitude of the resonant peak when compared to a passive damper.

2.6.3 Magneto-Rheological Fluids

A number of studies have addressed the properties of MR fluids. In a paper by Shulman et al. [29], the physical properties of magneto-rheological fluids are described in terms of a stationary model, that is, a model in which the structure

formed when the magnetic particles align themselves in the presence of a magnetic field is considered as a stationary structure through which the carrier medium must pass. The increase in viscosity is attributed to the extra energy required to push the carrier through these structures. This model is verified by experimental measurements of steady state effective rheological and magnetic characteristics.

In a paper by Ashour, Rogers, and Kordonsky [30], an inverse MR fluid is discussed, that is, a fluid whose viscosity decreases with increased magnetic field. An inverse MR fluid first forms a solid state when magnetic field is applied, but past a critical level of magnetic field it returns to a liquid state. Constant shear rheological measurements are made to confirm this. The inverse magnetic fluid consists of nonmagnetic particles in a magnetizable fluid.

2.6.3.1 Other Applications of MR Fluids

The properties of MR fluids have been used in devices other than dampers. There have been items of exercise equipment, in particular a bench press and a stair climber, that use MR fluids to provide a variable resistance [31]. Other applications of MR fluid have been suggested, such as hydraulic actuators and magnofluid seals [32]. MR fluids have also been suggested for use in viscometers

[33]. These MR viscometers offer improvements over traditional methods of measuring viscosity by allowing for measurement in a wider range of viscosities.

2.7 Motivation of this Study

The following chapters describe the design of a controller for semiactive dampers, and the testing of the controller. The controller was intended to be a prototype of what could be a commercial system. This controller makes use of an on/off skyhook policy. The on/off skyhook policy was chosen because of its ease of implementation. The controller was designed with the possibility of implementing other control schemes in mind, but the on/off skyhook was the policy tested . It was desired to see if this simple and easy-to-implement scheme provided worthwhile performance benefits in reality before progressing to more complex schemes. The controller is described in Chapter 4.

The dampers to be controlled made use of magneto-rheological fluid technology. Four of these dampers were placed on four of the wheels of a class 8 truck cab. These dampers are described in Chapter 3. The class 8 truck has some differences from other vehicles; it has a secondary suspension between the frame and cab, and it is affected by the towing of the trailer.

In the testing of the controller, acceleration data were recorded for two road conditions, hitting a speed bump and highway driving. In addition to

mounting three accelerometers triaxially at the B-post in the cab as in [13] and recording them, an additional eight accelerometers, two at each wheel, are recorded. These wheel accelerometers measure the acceleration at the axle and the frame above it near each wheel. The testing is described further in Chapter 5.

Chapter 3
Semiactive Primary Suspension Hardware

This chapter describes the hardware that was used for road-testing the real-time embedded controller that was developed in this study. We will describe the magneto-rheological dampers that were used with the controller, as well as the system installation of the class 8 heavy truck that was used for our road tests.

3.1 Dampers

The six twin-tube magneto-rheological dampers that were used in this study were provided by Lord Corporation, Cary, NC. A schematic of the damper is shown in Figure 3.1. Each damper is equipped with two electromagnetic coils for creating a magnetic circuit through which the fluid can pass. One coil is used on the compression stroke, and the other is used for the extension stroke. The two separate coils have different numbers of windings, as it is desired to have different damping coefficients for compression and extension. These different damping coefficients are needed because compression occurs twice as fast as extension, and these different damping coefficients cause the damping force to be equal for both compression and extension.

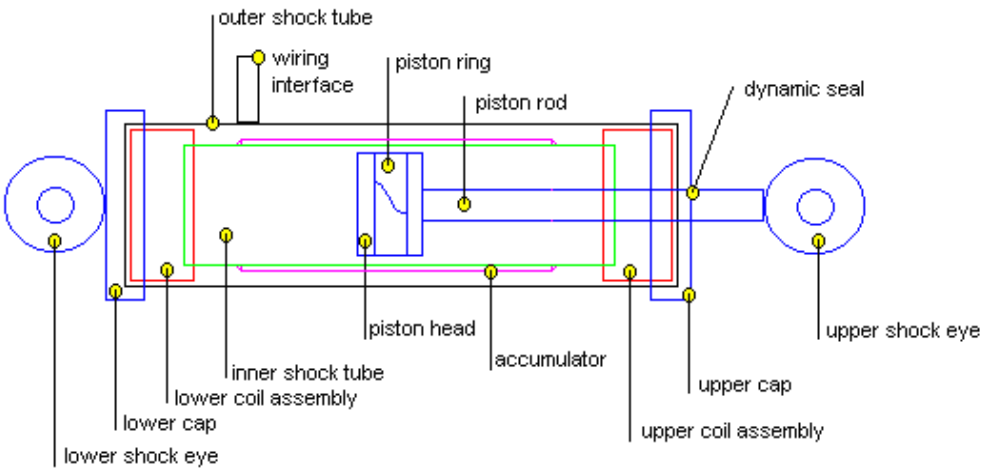

Figure 3.1. A Twin-Tube Magneto-Rheological Damper Schematic.

The piston pushes fluid into the outer tube from the inner tube as it is compressed or extended, passing it through one of the coils. Check valves allow the fluid to enter freely through the opposite side to fill in the volume on the other side of the piston head as it moves away. A tight seal is formed with the inner tube by the piston ring, which keeps fluid from flowing past the piston head. The dynamic seal in the upper cap is composed of two o-rings and a Teflon seal in order to contain the fluid in the damper, but allow for the movement of the piston rod.

The accumulator, made of closed-cell foam, was necessary to allow for changes in the volume of the fluid as it was heated, and also to allow for the added volume of the piston rod as it enters the damper. A traditional twin-tube damper normally uses air in the outer tube to accommodate volume changes of

the fluid, but the MR fluid in this damper must be isolated from the air. A length of high pressure tubing around the wiring interface also acts as a secondary accumulator. The wiring interface provides the external connection to provide current to the damper coils.

The disassembled damper's primary components are shown in Figure 3.2. Topmost is the piston rod, while in the middle is the inner shock tube with the coils to either side of it. Bottommost is the outer shock tube.

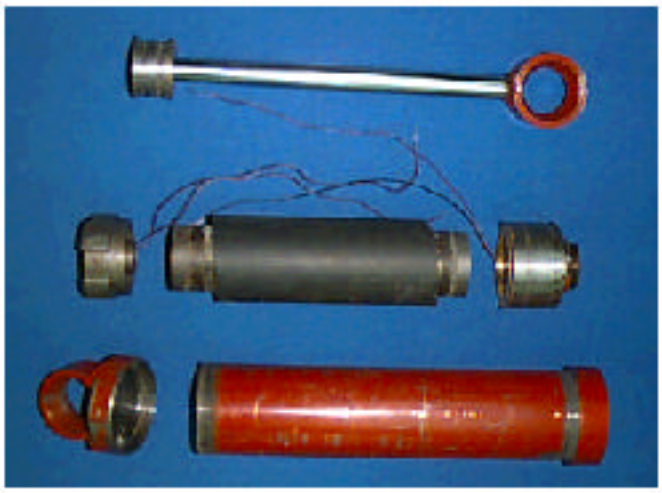

Figure 3.2. A Twin-Tube Magneto-Rheological Damper, Partially Disassembled.

The fully assembled prototype MR damper is shown in Figure 3.3.

Figure 3.3. A Prototype Twin-Tube Magneto-Rheological Damper.

The force velocity curves for the original passive dampers and the semiactive dampers with minimum and maximum electrical current are shown in Figure 3.4.

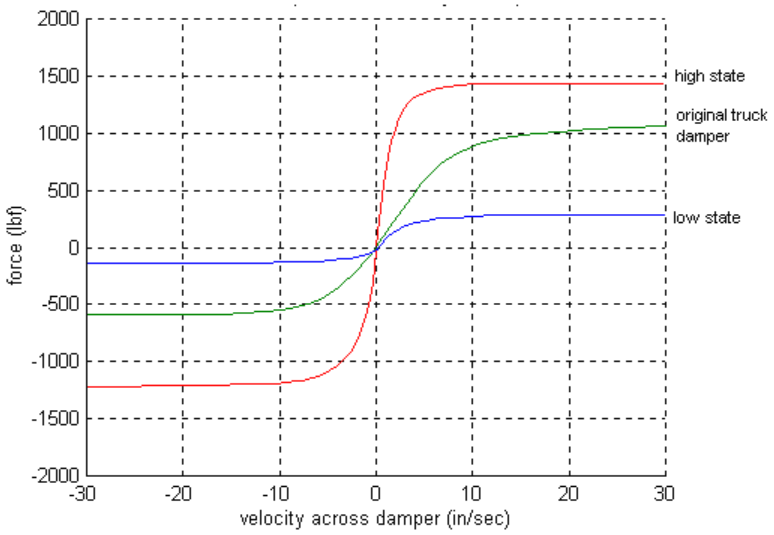

Figure 3.4. Force Velocity Curves.

3.2 Test Vehicle

The completed system was tested on a Volvo VN series class 8 truck, shown in Figure 3.5. Although the cab has three axles, the magneto-rheological semiactive system was installed on only two of the axles, the front axle and the rear tandem axle. Two dampers, one on each side, were placed on each axle. The semiactive dampers on the rearmost wheels must also control the middle pair.

Figure 3.5. Volvo VN Class 8 Truck Used for Road Testing.

3.3 Other Equipment

An AC power inverter was used to power the controller with 110 VAC, as well as other accessories that were used for conducting the tests, such as the Digital Audio Tape (DAT) recorder and the transducer signal conditioner (for the accelerometers). The controller and all associated hardware were to operate off this power supply, rather than directly from the battery. This made it easier to

bench test and debug the controller, as it could operate off a wall outlet. This also meant that when placed in the truck, the controller would be isolated from the noisy battery supply, as the inverter would clean up the power signal significantly.

Chapter 4
Controller Development

The real-time embedded controller that was designed and prototyped for this study takes in the sensor readings from the body and axle accelerometers and then supplies the damper coils with an appropriate current based on this information. The on/off skyhook control policy is used, where the damper coils are provided with 3A of current when the absolute velocity of the frame and the relative velocity between the frame and axle are of the same sign, and 0A are provided when the velocities are of opposite sign. This policy is implemented in software on a Motorola 68HC11 EVBU. An integrator converts the acceleration signals to velocity, and then an A/D (Analog-to-Digital) chip converts them to digital signals which are read by the EVBU. A D/A (Digital-to-Analog) converter and a voltage-to-current converter convert the digital output from the EVBU into a current signal that drives the coils of the magneto-rheological damper.

The following sections will summarize the operation of this controller. The first section will describe the hardware and its various components. This will be followed by a description of the software implemented in the microcontroller

component. This section will conclude with a description of the debugging of the controller.

4.1 Controller Hardware

The controller is shown in Figure 4.1. There are eight input connections for the eight accelerometers, two for each wheel. The controller has six output connections; each of these connections connects to the two coils of a damper, although only four dampers were used in the vehicle testing. Five power connections supply power to the controller, connecting to one 5V power supply for the digital logic, two 12V power supplies for the 1.5Ω coils, and two 24V power supplies for the 3.5Ω coils. The two coils have different resistances as a result of having different numbers of windings in order to provide different damping coefficients for compression and extension. The power supplies are contained in a separate casing, shown in Figure 4.2.

Figure 4.1. The Controller.

Figure 4.2. The Controller Power Supply Cabinet.

The hardware can be divided into different elements, as shown in Figure 4.3. First, the body and axle accelerometers are used for measuring the absolute acceleration of the body and axles. The absolute velocities are obtained using an integrator, described in Section 4.1.2. The microcontroller board, which is described in Section 4.1.4, reads the digital values of the velocities and uses them to calculate a damper setting. The velocity signals are converted from analog to digital by an A/D converter, as specified in Section 4.1.3.

The damper settings are converted to analog signals by a D/A converter detailed in Section 4.1.5. The output of the D/A converter is changed from a voltage signal to a current signal in the voltage/current converter stage described in Section 4.1.6. This current signal drives the damper coils. The varying current through the coils changes the damping and affects the vehicle dynamics, which are then read by the sensors, closing the loop.

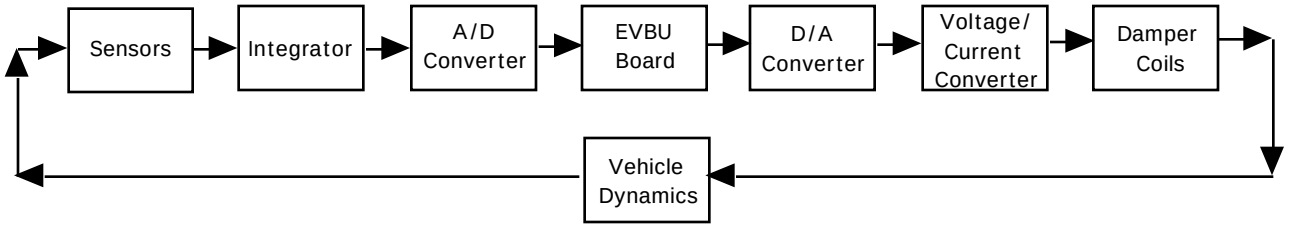

Figure 4.3. Controller Hardware Block Diagram.

4.1.1 Sensors

There are two accelerometers at each wheel location, one on the axle to measure the acceleration of the axle, and the other on the truck frame directly above the axle to measure the acceleration of the body. The output of these accelerometers is 0.1V/g. This can be increased by 10x or 100x with the signal conditioner that drives the accelerometers. The accelerometers used were PCB model 333A accelerometers, shown in Figure 4.4. The signal conditioner was a PCB 584, shown in Figure 4.5. The frequency range and shock loading are compatible with those expected to be encountered on the vehicle. The frequency range of the accelerometers is 1Hz-1KHz, while the frequencies of interest are 1Hz-15Hz. The shock limit of the sensors is 3500g. The shortcoming of these accelerometers is that they are intended for lab use and are not designed for extended outdoor usage.

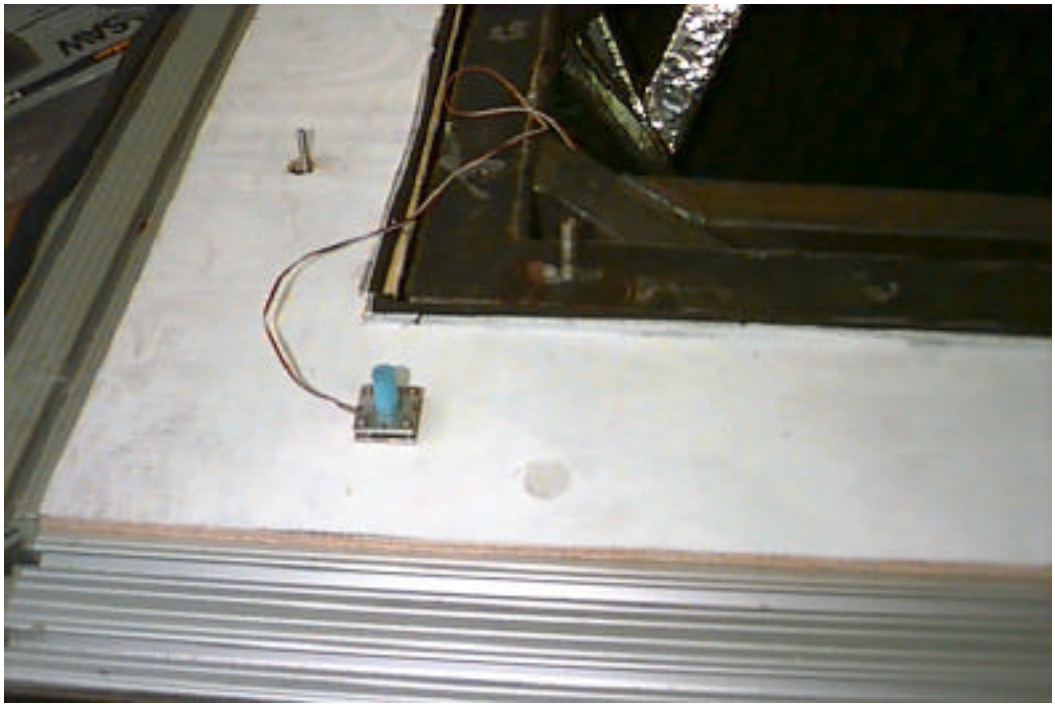

Figure 4.4. An Accelerometer in Its Mounting Bracket.

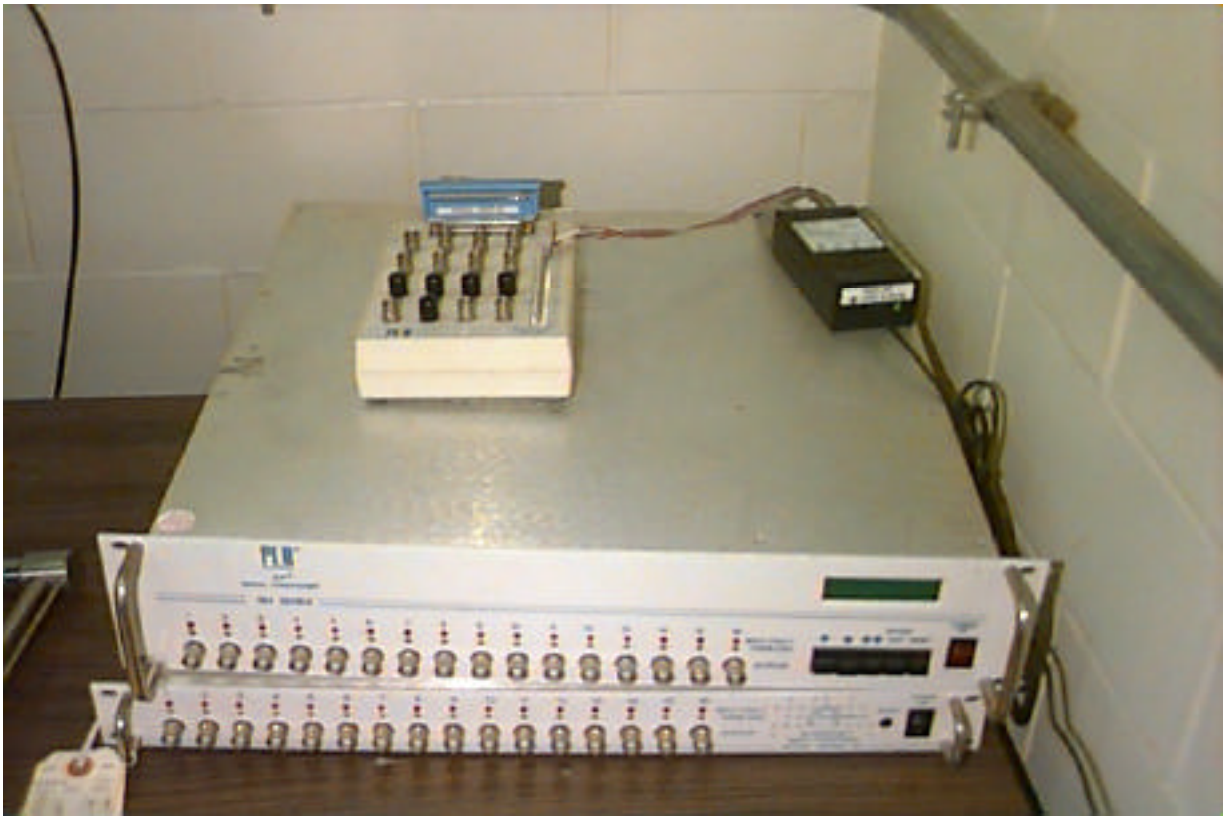

Figure 4.5. PCB Signal Conditioner.

4.1.2 Integrator

The accelerations are integrated to provide absolute velocity. The integration is performed using the op-amp circuit shown in Figure 4.6. This op-amp circuit is not a true integrator; the 10uF capacitor removes the DC component from the input signal and attenuates low frequency drift. The integrator also centers the velocity signal at 2.5V and limits it to 0-5V, which are the limits of the A/D converter chip in the next stage. This circuit is repeated for all eight of the accelerometers.

An integrator has the added benefit of removing high frequency noise by its nature. The frequency response shown in Figure 4.7 was chosen to cover the frequencies expected to be encountered in the vehicle.

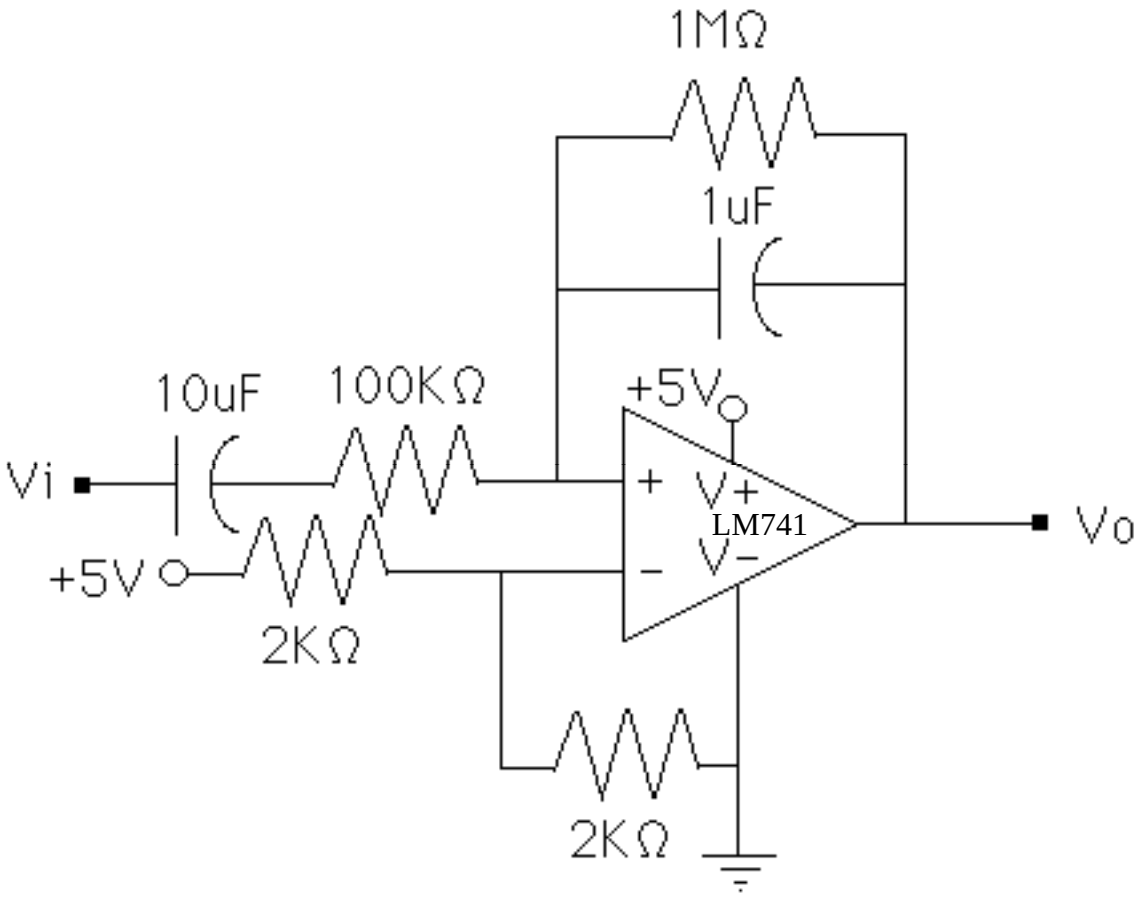

Figure 4.6. Integrator Circuit.

The transfer function of this circuit is given in Equation (4.1).

$$\frac{V_o}{V_i} = \frac{10s}{(s+1)^2} \qquad (4.1)$$

The frequency response of this circuit is shown in Figure 4.7, together with the frequency response of an ideal integrator. The blue line is the ideal integrator; while the green line is the actual circuit's frequency response.

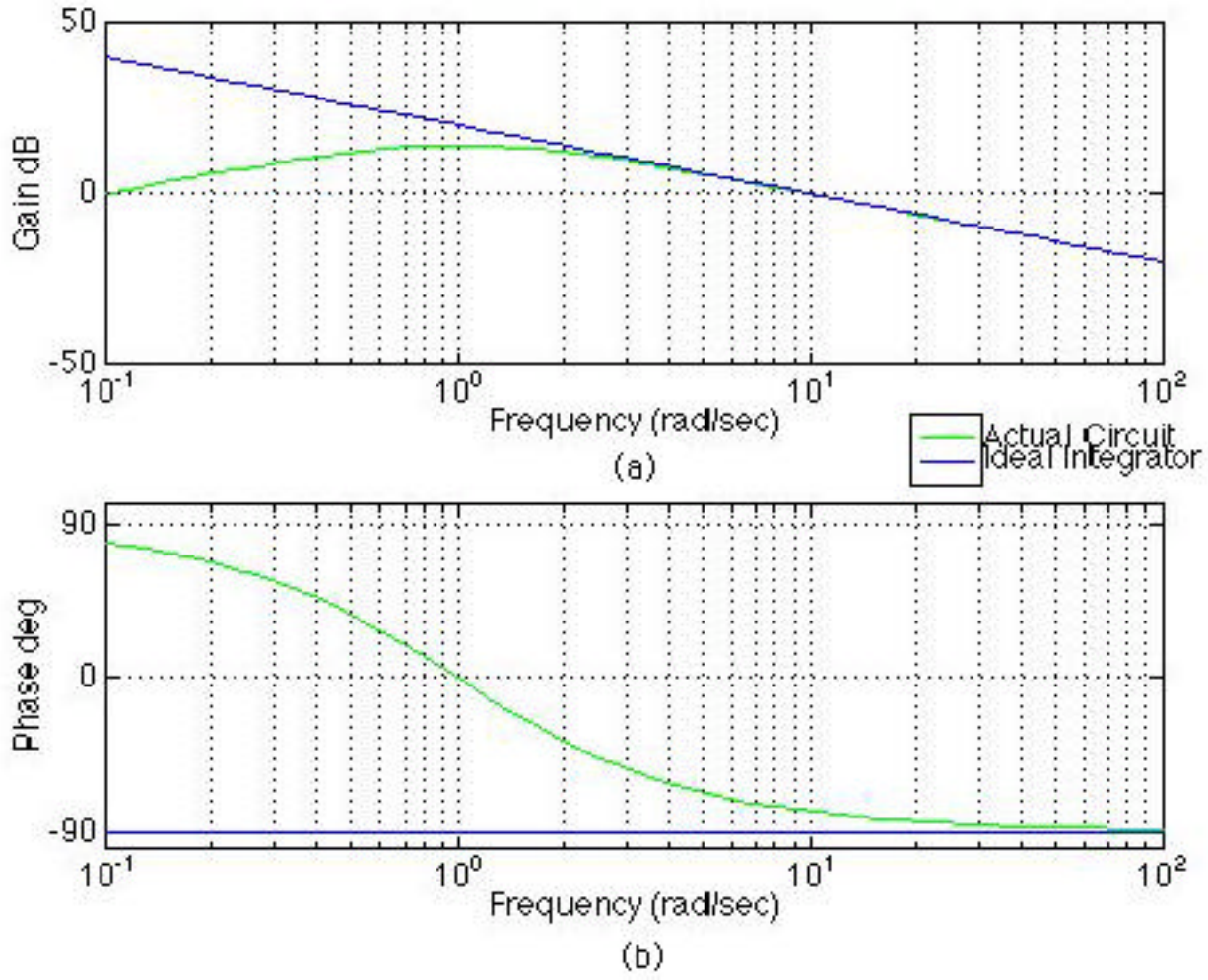

Figure 4.7. Integrator Frequency Response.

4.1.3 Analog-to-Digital Converter

An Analog-to-Digital (A/D) converter chip digitizes the analog velocity signals. The chip used was a National Semiconductor ADC0816CCN-ND.

The A/D chip can convert only one signal at a time. The signal to be converted is chosen by an analog multiplexor included on the chip. The EVBU (Evaluation Board Unit) microcontroller selects each velocity signal individually and commands the A/D chip to convert it. The A/D chip requires its own clock and notifies the EVBU board when it has completed converting the signal.

Although the EVBU board has built-in A/D channels, an external chip was used to provide more A/D channels. For the four wheels, only eight A/D channels were needed, which is the number of A/D channels built into the E9 chip, the chip that is the basis of the EVBU board. The architecture of the EVBU board, however, is such that one of the pins for these is unavailable; this pin is used to determine if the E9 should begin at internal ROM (BUFFALO) or EEPROM. Additionally, it was desired to design the system such that it might have the ability to control dampers for all six wheels on the three axles, or use the controller to receive additional sensors other than accelerometers. Therefore, the external A/D chip was implemented, allowing up to 16 channels.

Microcontrollers other than the 68HC11E9 that might have sufficient channels were sought, but nothing was found that was readily available. The A/D converter also has the benefit of having its own low pass filter, removing the DC component of the signal and centering it at 2.5V. This was useful

because the 2kΩ resistors in the integrators shown in Figure 4.6 are not exactly equal, so the true centering of the output is unknown.

While the A/D chip outputs an 8-bit signal, only the seven most significant bits are read by the microcontroller. This is because the least significant bit on PORT E of the microcontroller is used for other purposes (choosing between the internal ROM and EEPROM).

The A/D channels corresponding to the individual accelerometers are shown in Table 4.1.

Table 4.1. A/D Channel Assignments.

A/D Channel	Accelerometer
8	Left Front Frame
9	Left Front Axle
10	Right Rear Axle
11	Right Rear Body
12	Left Rear Body
13	Left Rear Axle
14	Right Front Axle
15	Right Front Body

4.1.4 Microcontroller

The end of conversion signal from the A/D chip causes an interrupt in the microcontroller. The microcontroller used was a Motorola 68HC11 EVBU board, shown in Figure 4.8. This EVBU board was chosen because of its ease of use in debugging and in testing different versions of the software.

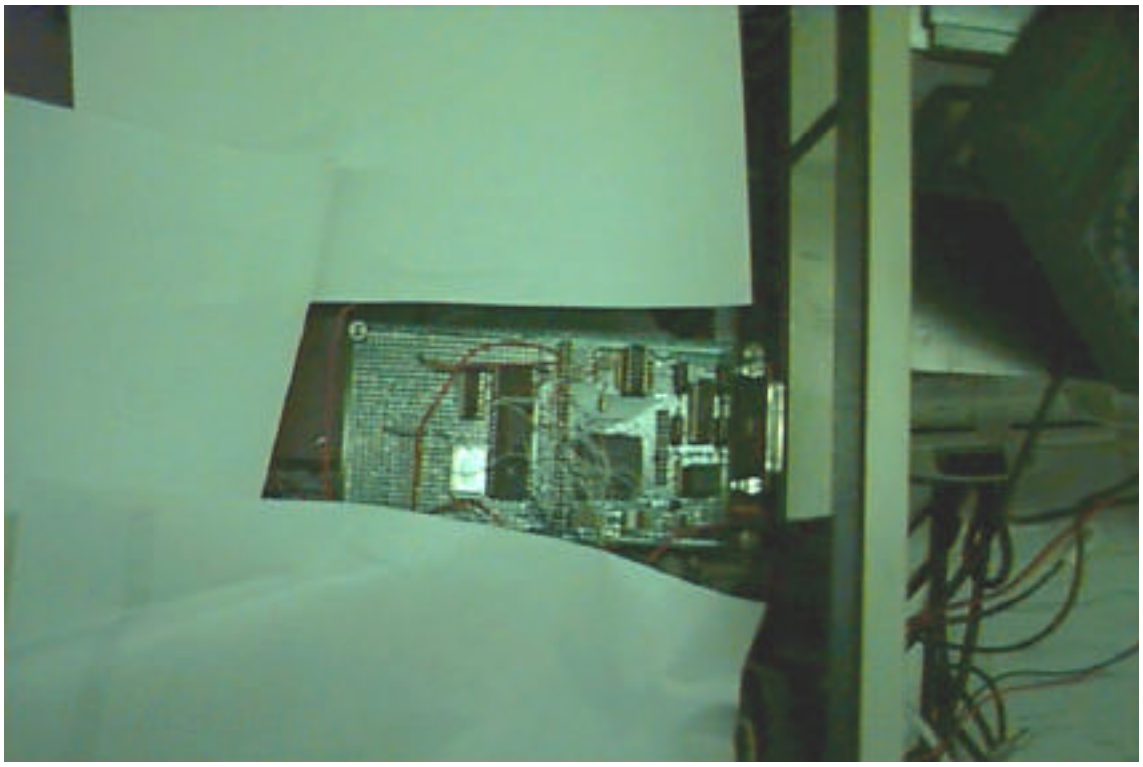

Figure 4.8. HC11 EVBU Board.

When the interrupt is triggered, the EVBU stores the current velocity value and then commands the A/D to begin converting the next signal. Between readings of the A/D, the EVBU uses the velocities to calculate the current output to the dampers. The EVBU uses the skyhook policy for this calculation, as will be

described in Section 4.2.2. The desired coil setting is sent to the D/A converter stage described in the next section. For more information on the EVBU, refer to [33].

The pin assignments are as follows:

PORTA

0 - Switch from Skyhook to Constant 3A Output

6 - A/D Address Latch

7- A/D Start Conversion

PORTB - D/A Output

PORTC

0-4 A/D Address

5-7 D/A Address

PORTD - Serial Communications

PORTE - A/D Data In

IRQ - End of A/D Conversion

The EVBU software is described in more detail in Section 4.2.

4.1.5 Digital-to-Analog Converter

The settings calculated by the EVBU are converted from digital to analog signals by a Digital-to-Analog (D/A) chip. The D/A chip used was a MAXIM MAX506BCPP-ND. There are three D/A converter chips in the controller. Each has four analog outputs, for a total of twelve outputs, so that the system can be expanded to all three axles. A demultiplexor selects between the three chips.

The D/A channels associated with particular damper coils are shown in Table 4.2 below.

Table 4.2. D/A Channel Assignments.

D/A Channel	Damper Coil
0	Left Rear
1	Right Rear
2	Right Front
3	Left Front
4	Unused
5	Unused
6	Left Rear
7	Right Rear
8	Left Front
9	Right Front
10	Unused
11	Unused

A D/A converter was chosen over a Pulse Width Modulation (PWM) scheme because it was more practical to have eight D/A channels than eight independent

PWM signals. It was judged that controlling eight PWM signals would consume too much of the microcontroller's time and memory, while the D/A converter approach would remove that burden, as well as provide a more straightforward implementation and ease of testing.

4.1.6 Voltage-to-Current Converter

The D/A output is converted from a voltage signal to a current signal. The voltage-to-current converter circuit is shown in Figure 4.9. The operational amplifier used was an APEX PA26. The transistor is needed because the op-amp by itself could not handle the power dissipation required. The transistor used was a Texas Instruments TIP120.

The current is, of course, the property that needs to be controlled. Converting the signal also means that the current would be independent of the resistance of the load. This is important because the coils themselves are of such low resistance (1Ω-4Ω) that connection resistances would be significant. In particular, the cables leading from the controller (placed in the cab) to the wheels would be long enough to add significant resistance.

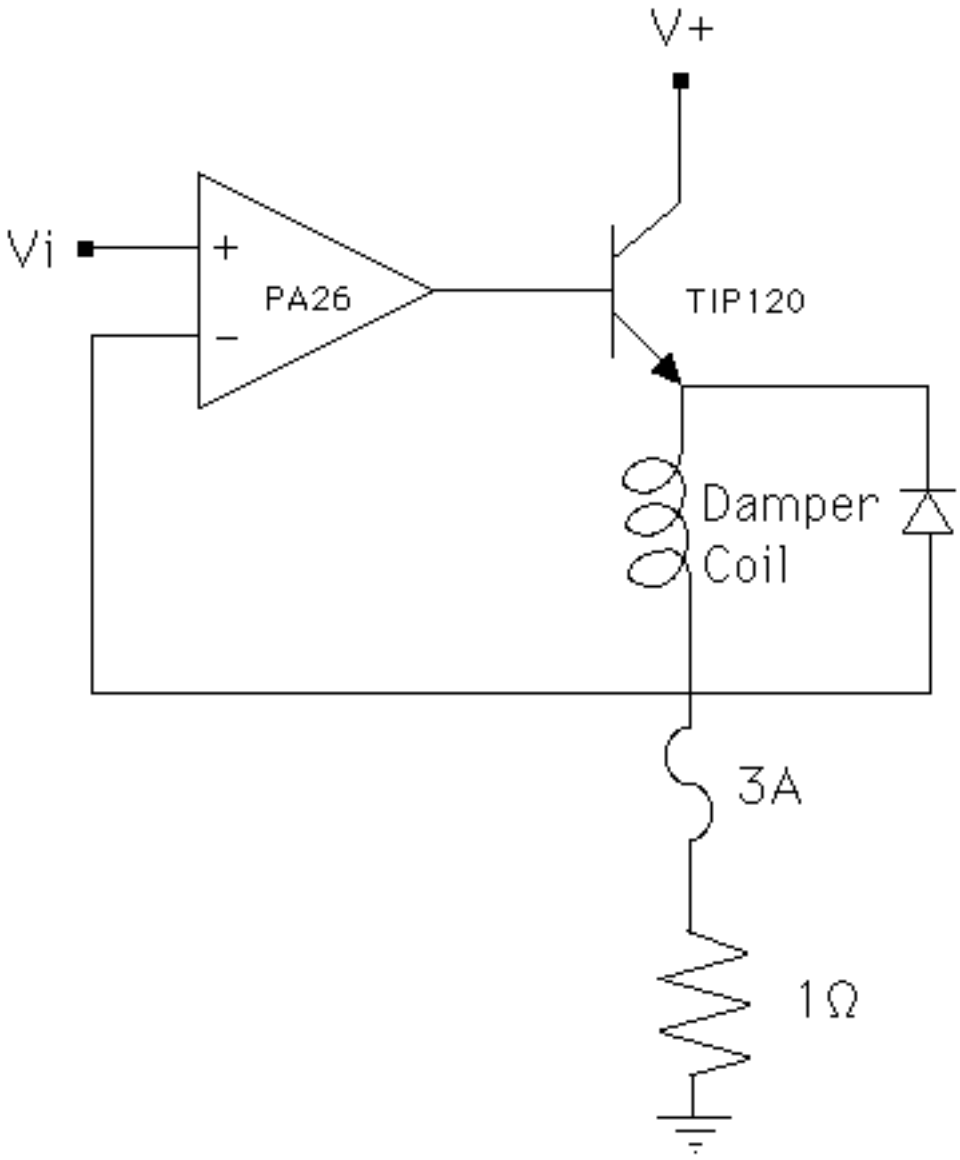

Figure 4.9. Voltage-to-Current Converter.

4.1.7 Damper Coils

The dampers each contain two coils. The lower coil is approximately 1.5Ω, while the upper coil is approximately 3.5Ω. The maximum current used to drive the coils is 3A. Another important consideration is that the coils are very much inductive loads, since they are intended to function as electromagnets. It was thus necessary to put flyback diodes in parallel with the coils. A fuse block with 3A fuses was added to make sure the current stayed below 3A.

4.1.8 Power Supplies

The controller uses five power supplies, as shown in Table 4.3. One 5V supply powers all the controller logic circuitry. The other four supplies drive the damper coils. Two 12V power supplies drive the 1.5Ω coils, while two 24V power supplies drive the 3.5Ω coils.

Table 4.3. Power Supplies.

Voltage	Maximum Current	Quantity	Purpose
5V	.5A	1	Controller Logic
12V	12.5A	2	Lower Coil Supply
24V	6.3A	2	Upper Coil Supply

4.2 Software

The software consists of three parts. One part controls the A/D converter chip and reads the data from it. Another implements the skyhook policy to determine the output current to the dampers. The third interfaces to the D/A converter. Each of these components is described in the following sections. A flowchart summarizing the program is shown in Figure 4.10.

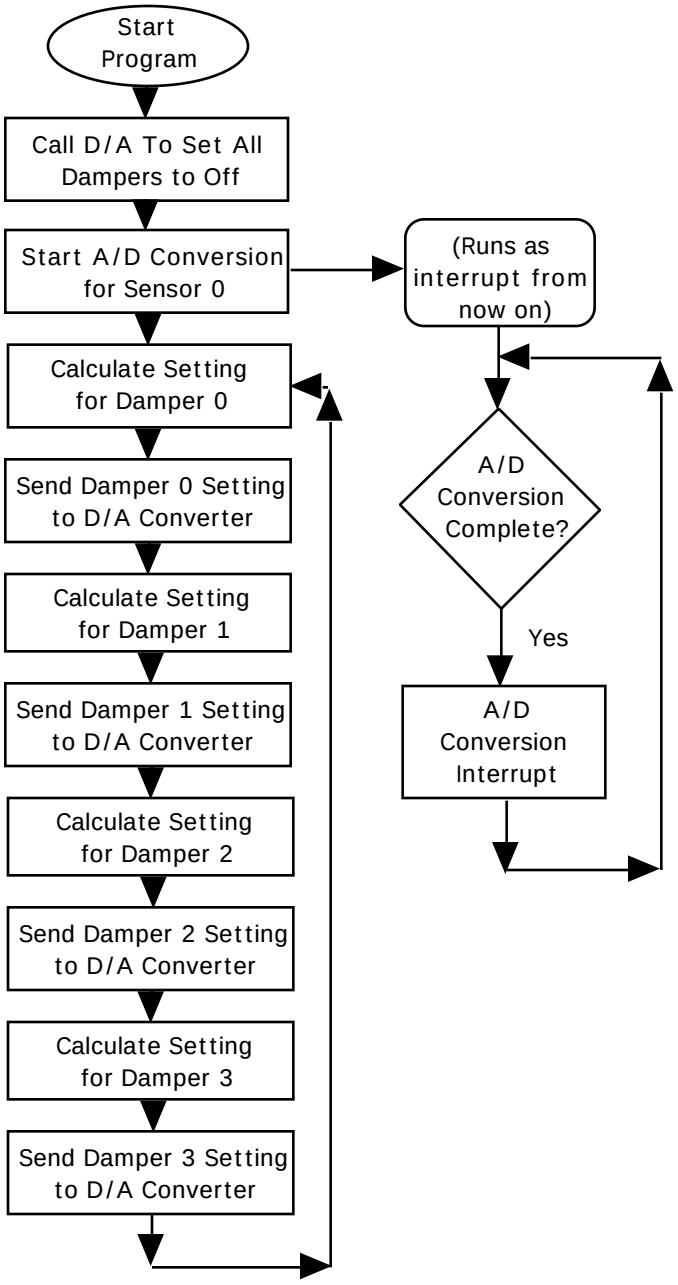

Figure 4.10. Controller Software Flowchart.

The dampers are updated approximately every 882µs. This gives a frequency of 1/882e-6=1.13KHz, which is well above the frequencies of interest (≤15Hz).

The complete controller software listing is included in Appendix C. What follows is a brief summary:

Constants:

DAMPMX - The maximum value for the damper setting, set to $9A or 3A.

Variables:

CSNS - The sensor currently being converted in the A/D converter

VEL1, VEL2, VEL3, VEL4, VEL5, VEL6, VEL7, VEL8 - The velocity at a particular accelerometer sensor ;see Table 3.1

Subroutines Labels:

LOOP - The main program loop

CALCDMP - Calculates the setting for a damper coil according to the skyhook procedure

SVCIRQ - Handles A/D conversion in response to an IRQ interrupt

WRITEDA - Handles D/A conversion, setting a particular damper to its desired setting

4.2.1 Main Program Loop

The main program loop performs two different tasks, depending on the setting of the pin Port A0. This pin is connected to a switch that is used to switch from a skyhook policy to a constant 3A. If the switch is set for 3A, then the main program loop calls the D/A conversion routine once for each damper coil to set them to 3A, and then waits for the switch to be set back to skyhook control. The A/D interrupt is also disabled while in the constant 3A mode.

If the switch is set to skyhook control, then the main loop calls the skyhook policy subroutine for each pair of body and axle accelerometers, sending the result to the D/A conversion subroutine for the appropriate damper. It then begins the process again. It is occasionally interrupted when the A/D conversion process completes.

The main program loop can be summarized as:

Main Program Loop

Label: LOOP

Input Registers: None

Input Ports:

Input Variables: VEL1, VEL2, VEL3, VEL4, VEL5, VEL6, VEL7, VEL8

Output Registers: None

Variables Affected: None

Ports Affected: None

Subroutines Called: CALCDMP, WRITEDA

4.2.2 Analog-to-Digital Converter Interface

The Analog-to-Digital (A/D) converter interface is interrupt driven. When the program first starts, it sends a start signal to the A/D chip to begin converting the first velocity signal. The microcontroller then continues with other tasks while waiting for the conversion to finish because the conversion process takes a considerable amount of time. When the conversion is finished the A/D chip sends a signal that triggers the interrupt. The A/D routine is triggered by the IRQ (interrupt request) interrupt. The microcontroller then stores the digital value from the A/D chip. It then selects the next velocity signal and commands the

A/D chip to begin the conversion. After this is completed, the microcontroller returns to the task it was performing prior to the interrupt. Figure 4.11 shows a flowchart of the A/D interrupt routine.

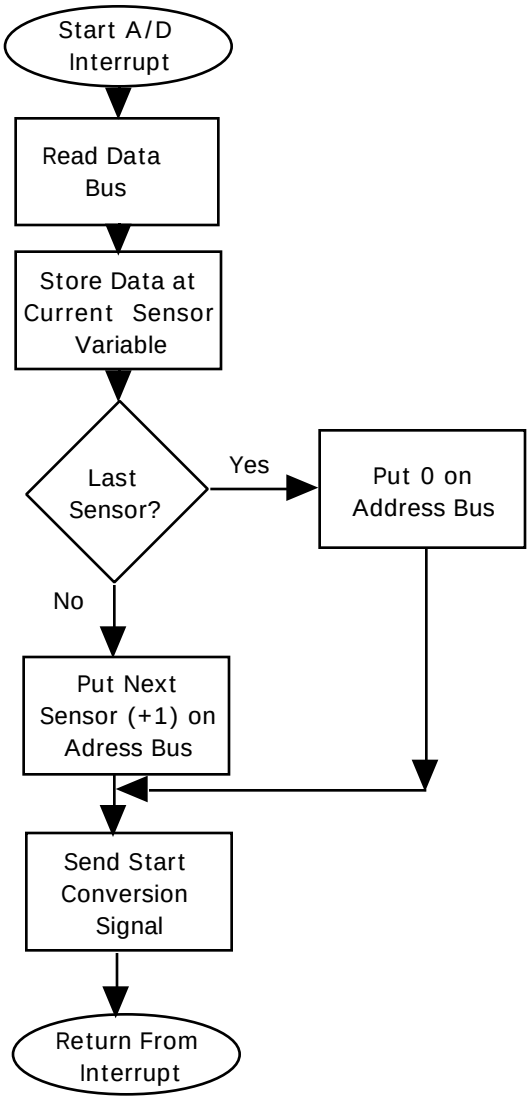

Figure 4.11. A/D Interrupt Flowchart.

The interrupt used is the IRQ interrupt. Although the IRQ interrupt cannot be disabled without disabling all interrupts, it did not cause any problems because no other interrupts were used.

The A/D interrupt only checks channels 8 through 15 of the A/D converter since these are the channels associated with the integrated acceleration. The channels are stored in variables ‘VEL1’ through ‘VEL8,’ with ‘VEL#’ containing the A/D conversion of channel #+7.

A summary of the A/D interrupt subroutine is as follows:

A/D Subroutine

Label: SVCIRQ

Called by: IRQ Interrupt

Input Registers: None

Input Ports: Port E [1..7]

Output Registers: None

Variables Affected: VEL1, VEL2, VEL3, VEL4, VEL5, VEL6, VEL7, VEL8

Ports Affected: PortA [??] PORTC [4..7]

4.2.3 Skyhook Control Implementation

The results from the A/D conversion are used in the skyhook routine. The skyhook routine implements the skyhook control policy in the controller. The relative velocity is calculated by subtracting the axle velocity from the body velocity. If they are of the same sign, then the damper coil current is turned on.

Otherwise, the damper coil current is off.

The skyhook subroutine is summarized below. A flowchart of the skyhook subroutine is shown in Figure 4.12.

Skyhook Subroutine:

Label: CALCDMP

Input Registers:

A- Body Velocity

B-Axle Velocity

Output Registers:

A - Desired Damper Setting

Variables Affected: None

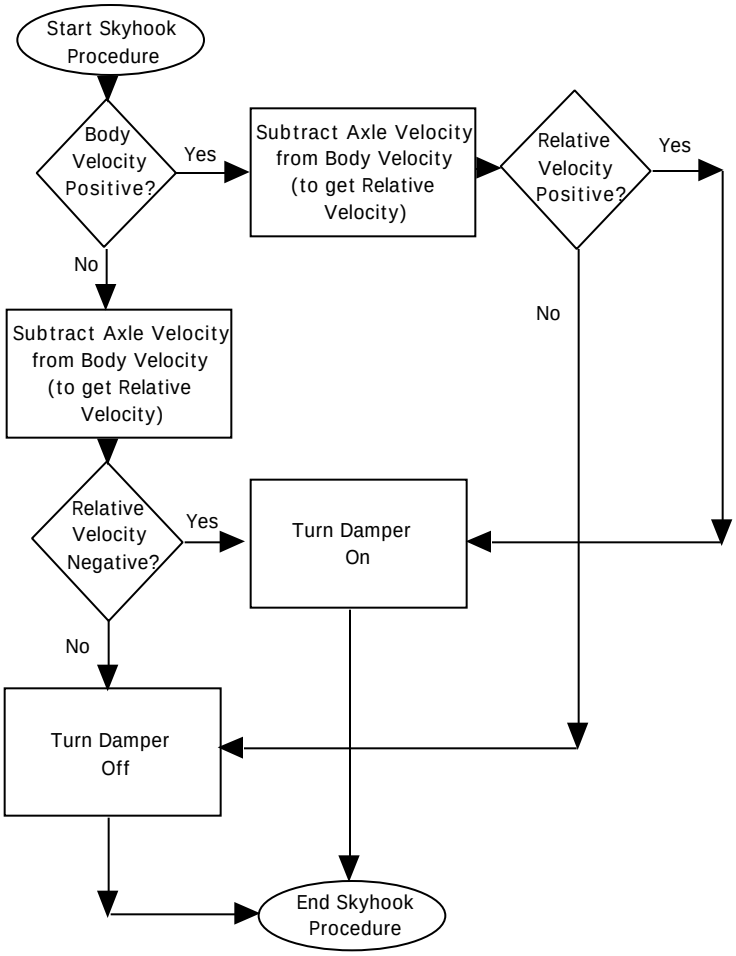

Figure 4.12. Skyhook Flowchart.

4.2.4 Digital-to-Analog Converter Interface

After the damper coil current setting is calculated, the Digital-to-Analog (D/A) converter interface is called. The setting is checked to ensure that it does not exceed 3A. The D/A setting corresponding to 3A is stored in the constant DAMPMX. This is $9A in hex (5*$9A/$FF≈3; 5A is the maximum current). The microcontroller sends the setting and address of the desired coil to the D/A chip. Next, the D/A write signal is sent, causing the D/A converter to adjust to the

appropriate value. The D/A converter interface is summarized below. A flowchart for the D/A subroutine is shown in Figure 4.13.

D/A Subroutine

Label: WRITEDA

Input Registers:

A- Desired Damper Setting

B[0..3] - Damper #

Input Ports: None

Output Registers: None

Variables Affected: None

Ports Affected: PortA [??] PortB [0..3] PortC[0..7]

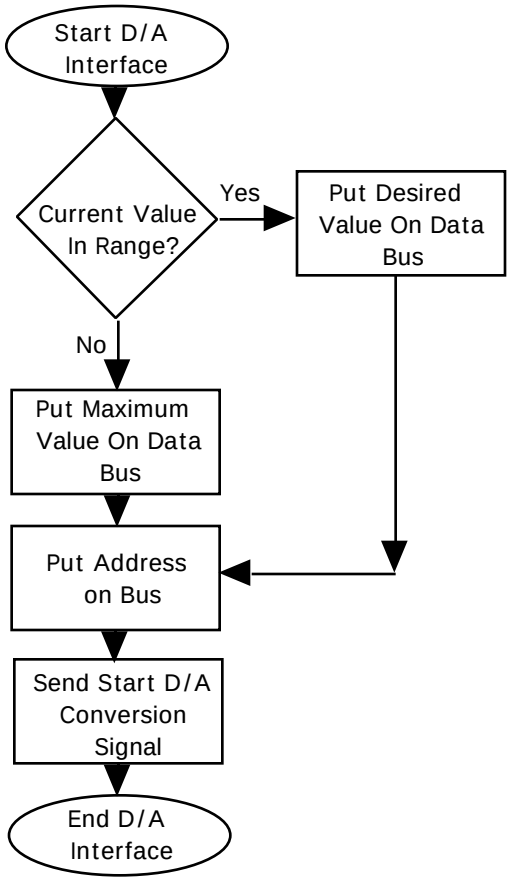

Figure 4.13. D/A Interface Flowchart.

4.3 Bench Testing and Debugging

Each of the components was tested individually before it was added to the overall controller. The complete circuit was also bench tested and debugged in the lab prior to installation on the vehicle.

4.3.1 Integrator Test

The integrator was tested by inputting various waveforms and checking that the output waveform was indeed the integral of the input. The integrator was found to integrate correctly in the frequency range of interest. For example, a square wave was input and found to integrate to a triangular waveform.

4.3.2 Analog-to-Digital Conversion

The A/D conversion was tested by inputting a variable voltage using a potentiometer. The digital value was output to a computer terminal and compared to the actual analog value. The conversion gave the correct values for the input voltages.

4.3.3 Digital-to-Analog Conversion

The D/A conversion was first tested by checking the voltage output compared to values entered on a computer terminal. It was then checked with the voltage/current converter added. The voltage/current converter was loaded with the actual damper coils and the current was measured. The current output was found to be sufficiently close to the specified current.

The interaction between the A/D and D/A converters was also tested by setting the D/A output to the same voltage as the A/D was reading in. The D/A converter was found to closely follow the input voltage.

4.3.4 Overall Controller

The complete system was bench tested in the laboratory by inputting various sinusoids out of phase with each other, and recording the inputs and the control signal for an individual coil. The results were then evaluated in MATLAB and compared to a MATLAB-generated skyhook control. Some results are shown in Figures 4.14-4.17. Figure 4.14 shows the acceleration inputs from the function generator. Figure 4.15 shows the theoretical velocity signals generated by the integrator circuit, and the theoretical relative velocity. Figure 4.16 shows the theoretical and actual control signals, normalized to ±3A, which are nearly identical, proving that the controller is working as intended. Figure 4.17 shows the functioning of the skyhook policy, demonstrating that the control signal is at the on current (3A) when the relative velocity and frame velocity are of the same sign, and is off when they are of opposite sign.

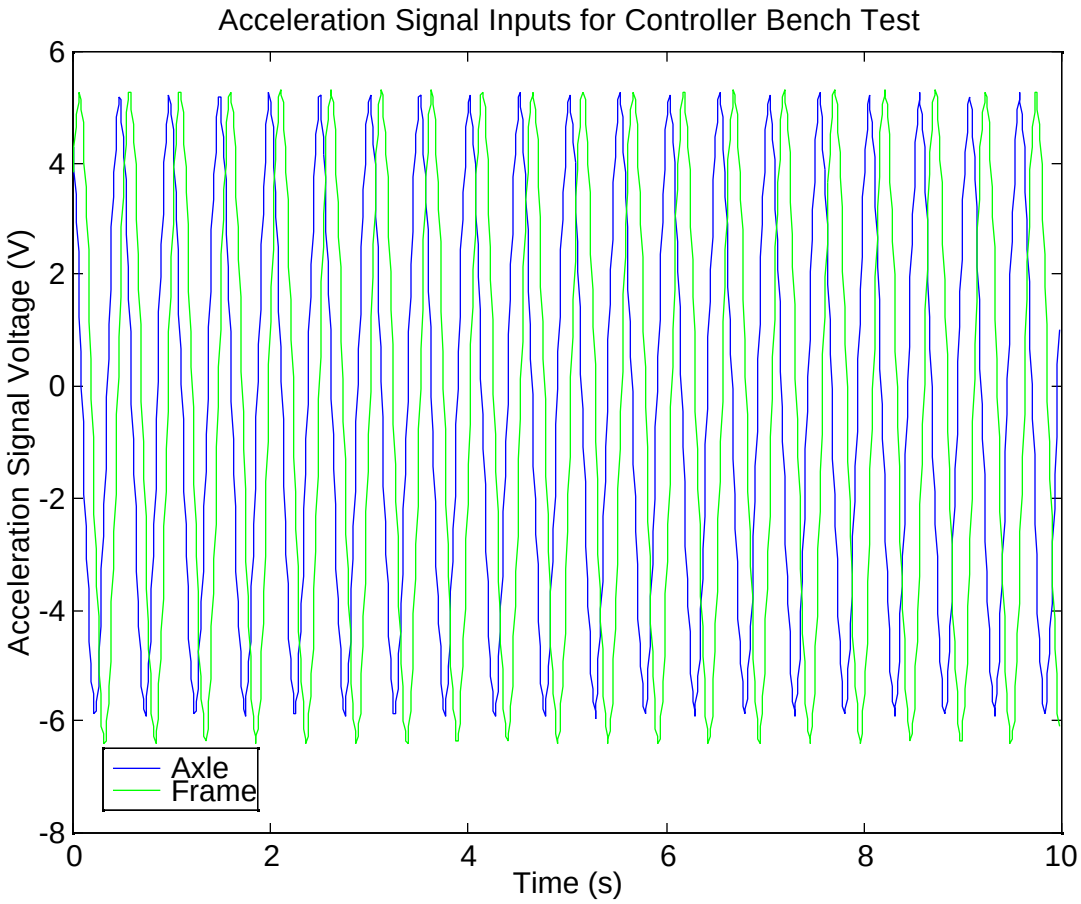

Figure 4.14. Acceleration Inputs for Controller Test.

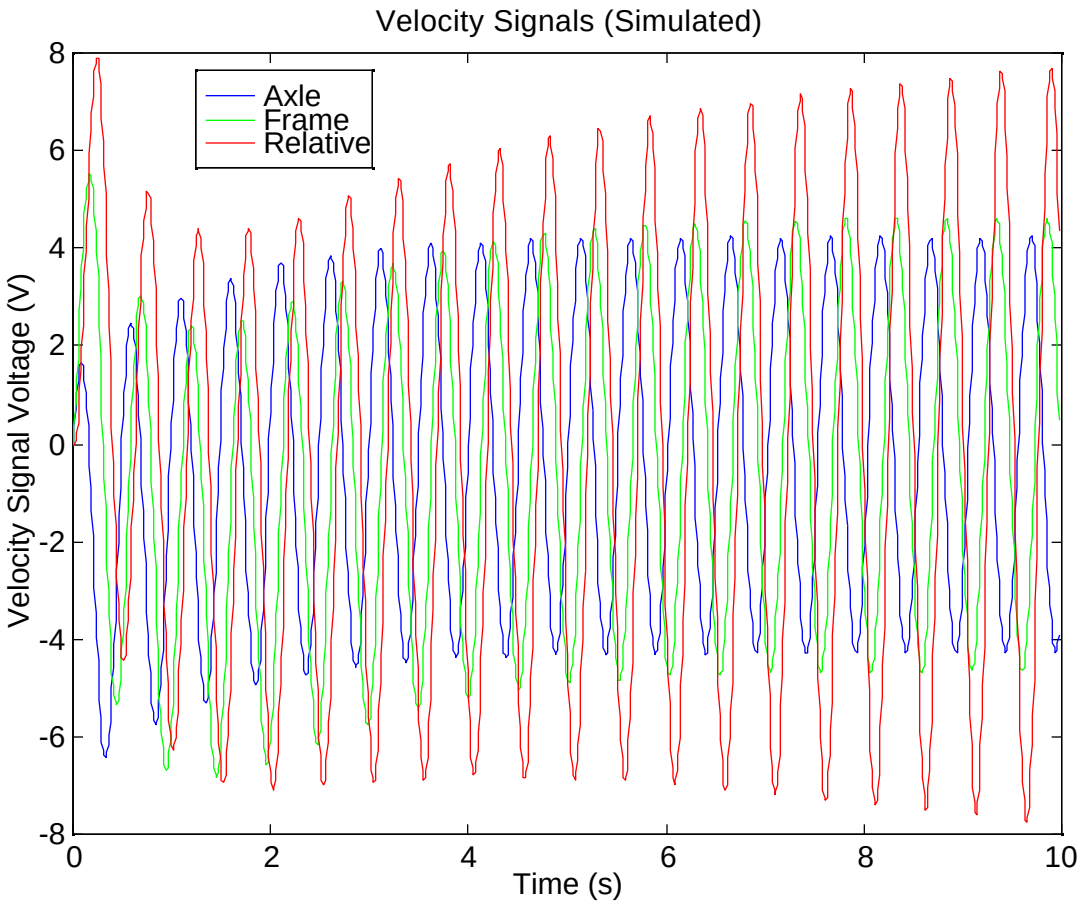

Figure 4.15. Simulated Velocity Signals.

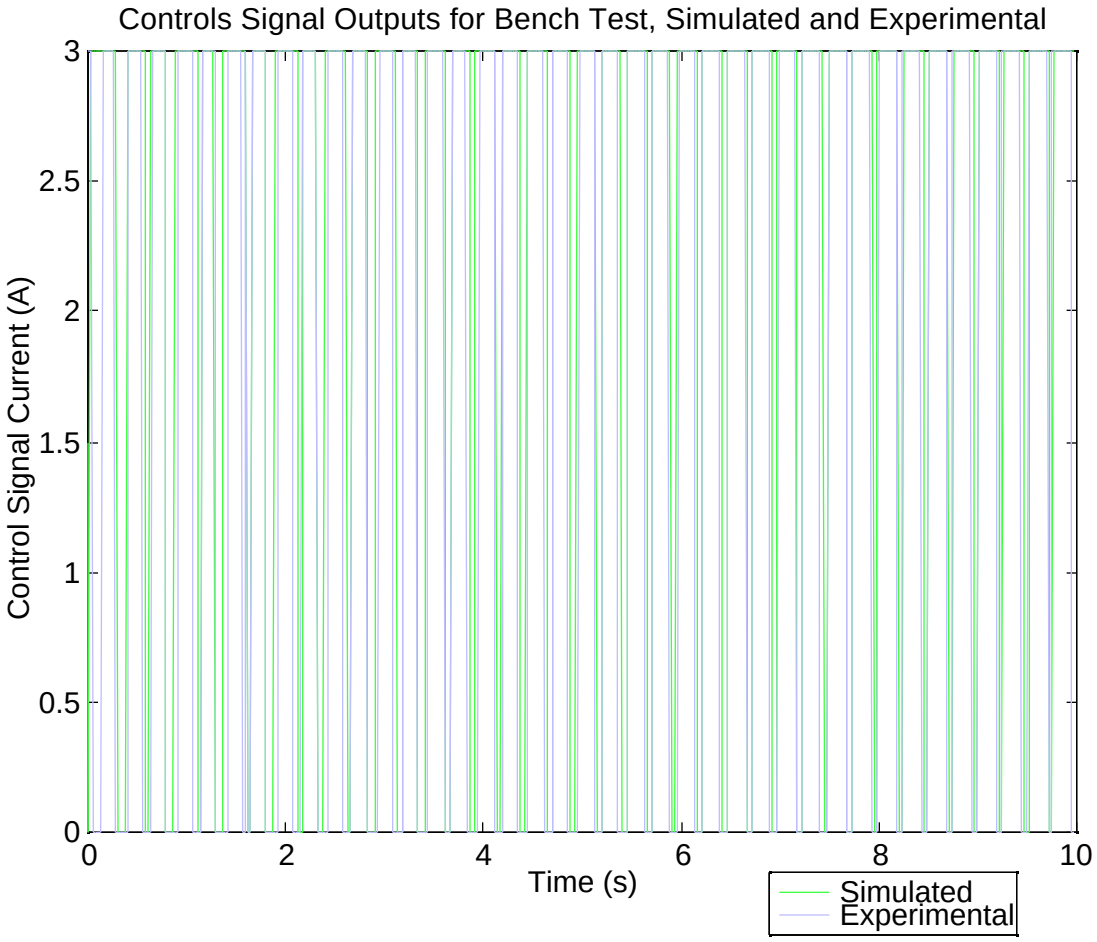

Figure 4.16 Simulated and Experimental Control Signal

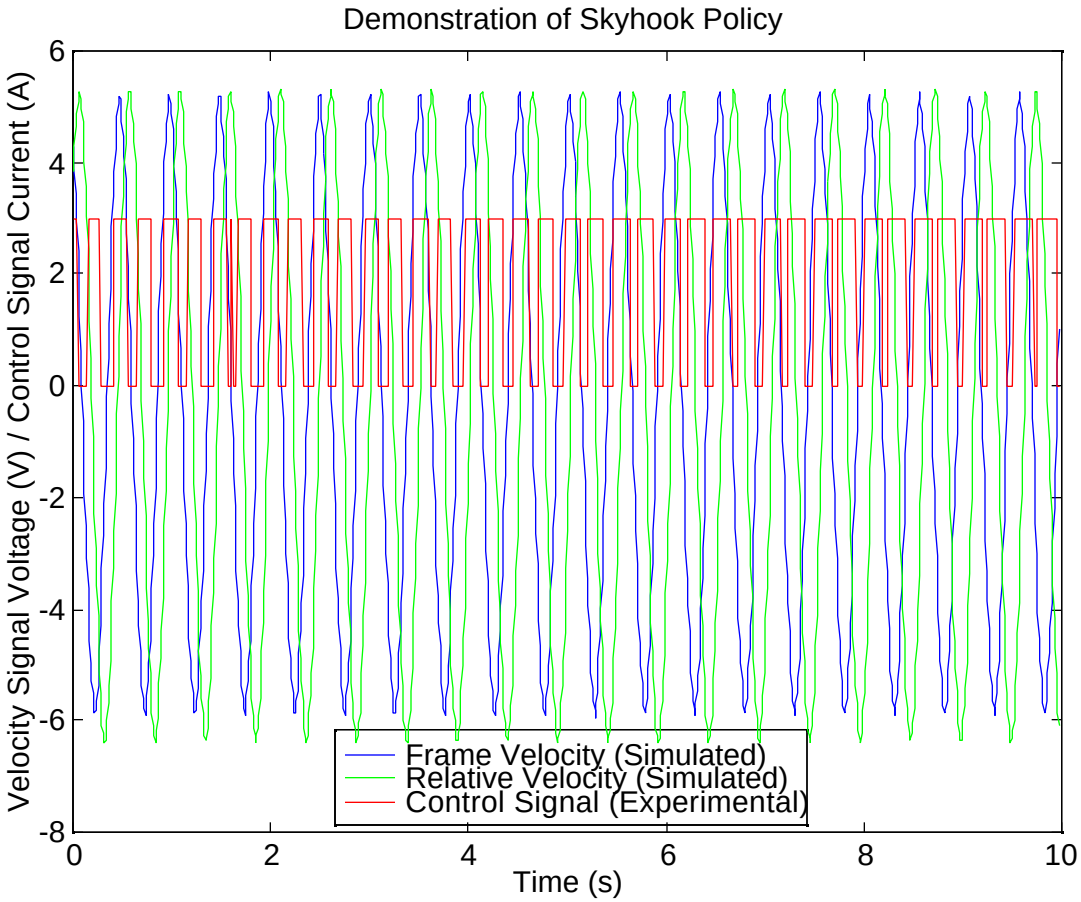

Figure 4.17. Demonstration of Skyhook Policy.

Chapter 5
Vehicle Testing

This chapter provides the testing of the semiactive primary suspension in which the real-time embedded controller described in earlier chapters was used. The installation of the system on a class 8 heavy truck, along with the results that were obtained from road testing, is presented. The test data are analyzed to establish the performance of the semiactive MR dampers, in comparison to a passive damper, for impulse disturbance response (hitting a speed bump), and frequency response to random road input (highway driving). The semiactive dampers were tested under three conditions: with the skyhook policy, with a constant 3A (full on), and with a constant 0A (full off). The full-on and full-off conditions were tested to provide a reference to verify that the semiactive case was different from them and that the data acquisition set-up was operating correctly.

5.1 System Installation

The completed system was installed on the vehicle for testing. The magneto-rheological dampers were installed on the front axle and rear axle of the cab, replacing the passive dampers. The stock passive dampers were left in place on the middle axle. Two accelerometers were placed near each of the four wheels with semiactive dampers, one on the axle, and one on the frame above it. Figure

5.1 shows an installed damper and the placement of its associated accelerometers. The accelerometers were connected to the signal conditioner that drives them, and the acceleration outputs of the signal conditioner were connected to the controller. The outputs of the controller were connected to dampers.

Figure 5.1. Installed Semiactive Damper and Accelerometers.

5.2 Data Acquisition Setup

The data was recorded on a SONY DAT (Digital Audio Tape) recorder, shown in Figure 5.2. The data recorded consisted of the eight accelerometers used by the controller, and three additional accelerometers placed on a triaxial mount inside the cab, as shown in Figure 5.3. For the placement of the wheel accelerometers,

refer back to Figure 5.1. Table 5.1 summarizes the placement of the accelerometers and the corresponding channels they were recorded to on the DAT recorder. Figure 5.4 shows the placement of all accelerometers. A block diagram summarizing the relationships of the test set-up components is shown in Figure 5.5.

Figure 5.2. Sony DAT Recorder.

Figure 5.3. Cab Triaxial Mount Accelerometers.

Table 5.1. DAT Channel Assignments.

DAT Channel	Corresponding Accelerometer
1	Driver's Side Front Frame
2	Driver's Side Front Axle
3	Passenger's Side Front Frame
4	Passenger's Side Front Axle
5	Driver's Side Rear Frame
6	Driver's Side Rear Axle
7	Passenger's Side Rear Frame
8	Passenger's Side Rear Axle
9	Cab Horizontal Acceleration (Roll)
10	Cab Vertical Acceleration
11	Cab Forward Acceleration

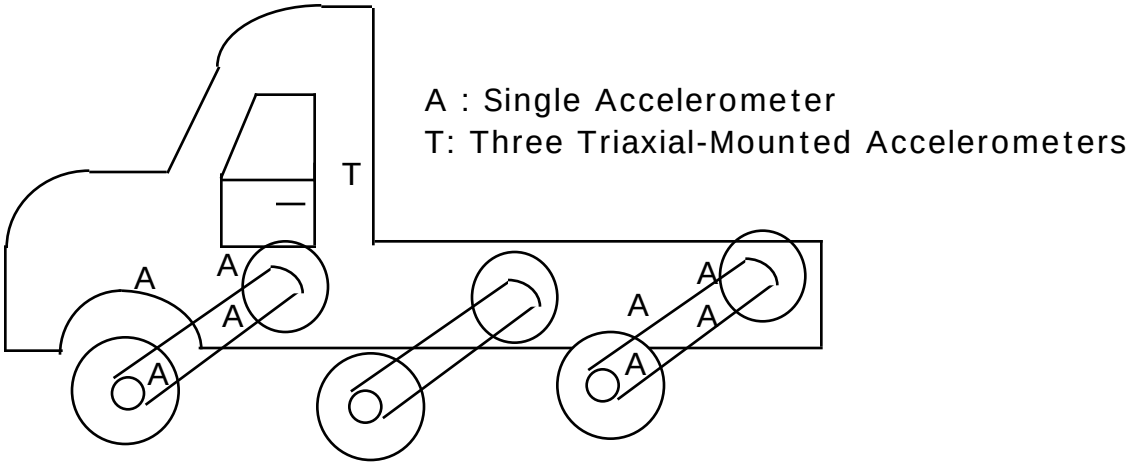

Figure 5.4. Placement of Accelerometers.

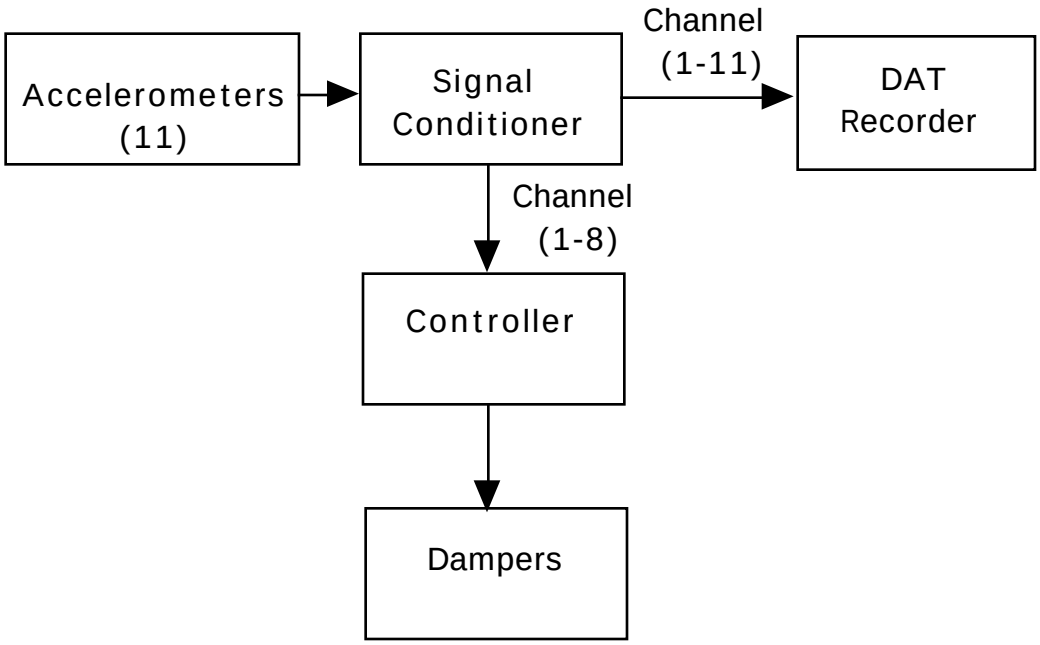

Figure 5.5. Installation Block Diagram.

5.3 Test Conditions

The tests consisted of driving over a speed bump, providing impulse response data, and highway driving, providing random input response data. The speed

bump was hit at a speed of 5mph, while the highway driving was at 65mph. The speed bump was approximately 3" in height. The highway driving was on Route 460 between the Prices Fork and Southgate Drive exits in Blacksburg, VA, as shown in Figure 5.6.

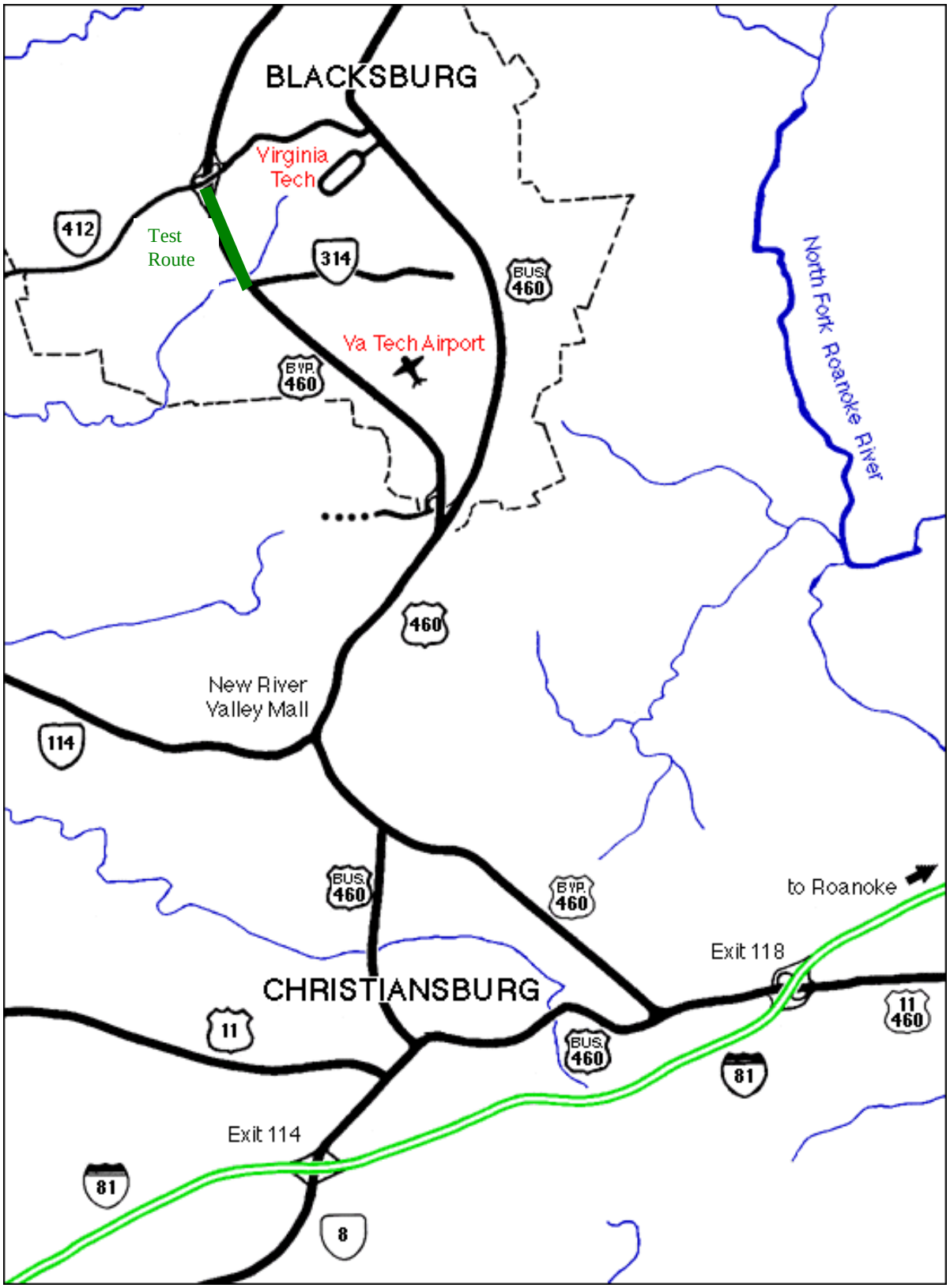

Figure 5.6. Highway Test Route [34].

Data were taken for four different operating conditions: the semiactive controller operating a skyhook policy with the magneto-rheological dampers; the controller providing a constant 3A to the magneto-rheological dampers; the controller off, with the magneto-rheological dampers still installed; and the original passive dampers.

The data were downloaded from the DAT recorder to a computer for analysis in 10s increments. The data sets analyzed are summarized in Table 5.2 below.

Table 5.2. Data Sets Analyzed.

Data Set	Test Condition
1-9	Semiactive Speed Bump
10	Semiactive Highway
11	Constant 3A Highway
12-17	Constant 3A Speed Bump
18-23	Constant 0A Speed Bump
24-30	Original Passive Dampers Speed Bump
31	Original Passive Dampers Highway

5.4 Speed Bump Data

The four operating conditions tested for hitting a speed bump were semiactive, constant 3A, constant 0A, and original passive dampers. The speed bump was hit multiple times for each case. The data recorded on the DAT recorder were downloaded to a computer for analysis in MATLAB in 10s increments, centered around each hit of the speed bump.

5.4.1 Data Filtering

The acceleration data for the speed bump hits contained both large low frequency drift and high frequency noise that made it difficult to analyze; an example of the raw data is shown in Figure 5.7. The acceleration was put through a digital filter in MATLAB. The frequency response of the filter is shown in Figure 5.8. The filter was chosen to bandpass 1Hz through 15 Hz, this being the range of frequencies representing the important truck dynamics.

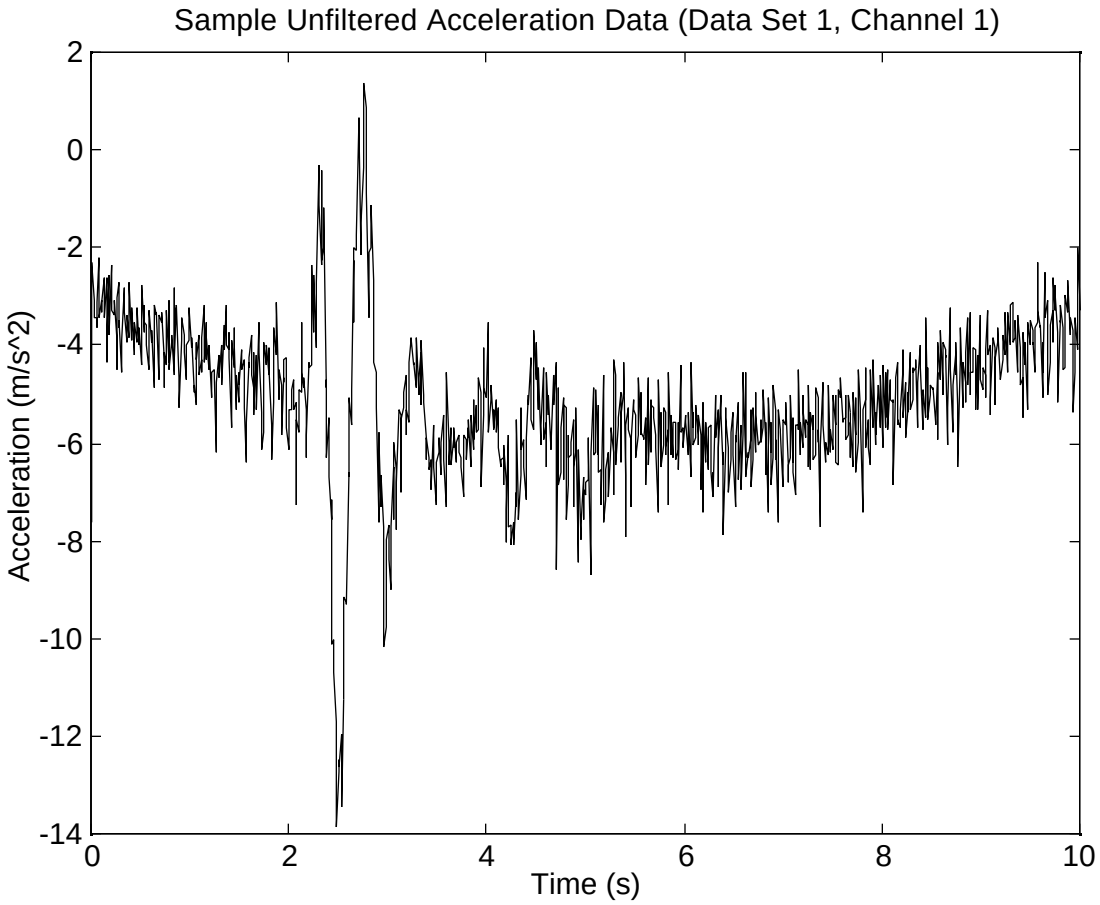

Figure 5.7. Sample Unfiltered Acceleration Data.

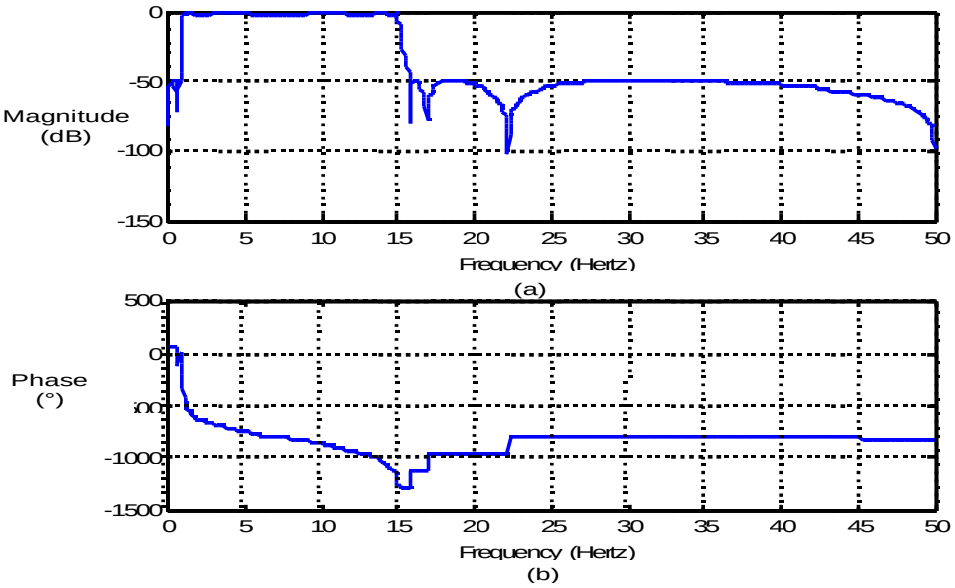

Figure 5.8. Data Filter.

A typical time trace of acceleration, after filtering, is shown in Figure 5.9.

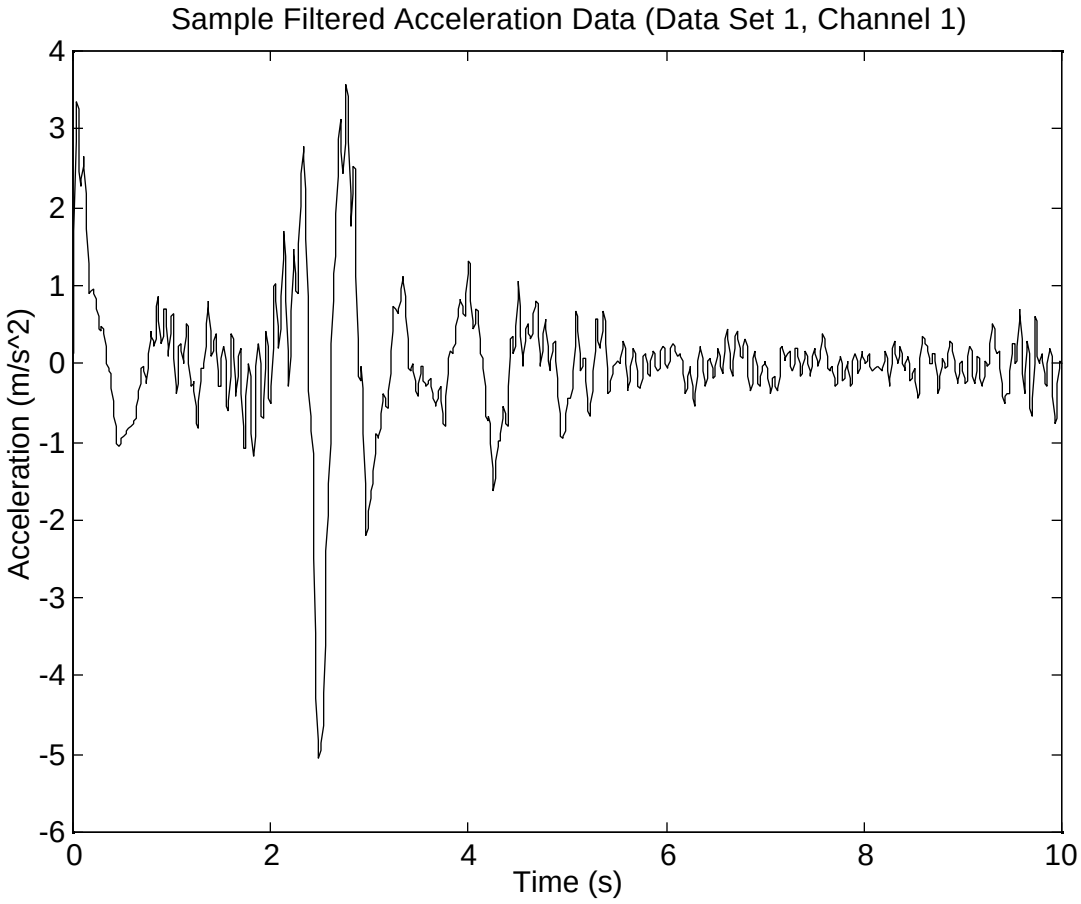

Figure 5.9. Sample Filtered Acceleration Data.

5.4.2 Acceleration Data

Because of the large volume of data collected, the analysis was automated. A Matlab m-file was written to automatically collect various characteristics of the acceleration data: the maximum positive value, the minimum negative value, the slope between the maximum positive value and the next peak, and the RMS from 1.5s before to 1.5s after the maximum positive peak. The maximum and

minimum peaks were chosen to provide a measure of the maximum force transmitted. The minimum peak was also subtracted from the maximum peak to measure the maximum peak-to-peak magnitude of the acceleration. The slope measures the decay rate of the transient response to the impulse disturbance. The RMS would provide a measure of the total energy of the vibration during the speed bump hit. For each of the four operating conditions, the average of each channel for each measure was calculated. The results are shown in Figures 5.10-5.14. The exact numerical values are given in Tables 5.3-5.7.

The RMS acceleration of the semiactive system was higher for most channels than the passive damping for the corresponding channel. Although it was expected that the skyhook policy would increase wheelhop as it did for channels 2,4,6, and 8, it was hoped that the frame RMS would be reduced. The RMS at the frame was less for semiactive than passive damping at the rear wheels (channels 5 and 7), but at the more important front two wheels, the RMS at the frame (channels 1 and 3) for the semiactive damping was greater than for the passive damping. As for the cab, which could be most directly related to driver comfort, the semiactive damping was worse than passive damping in all three directions, roll, pitch, and yaw (channel 9,10, and 11).

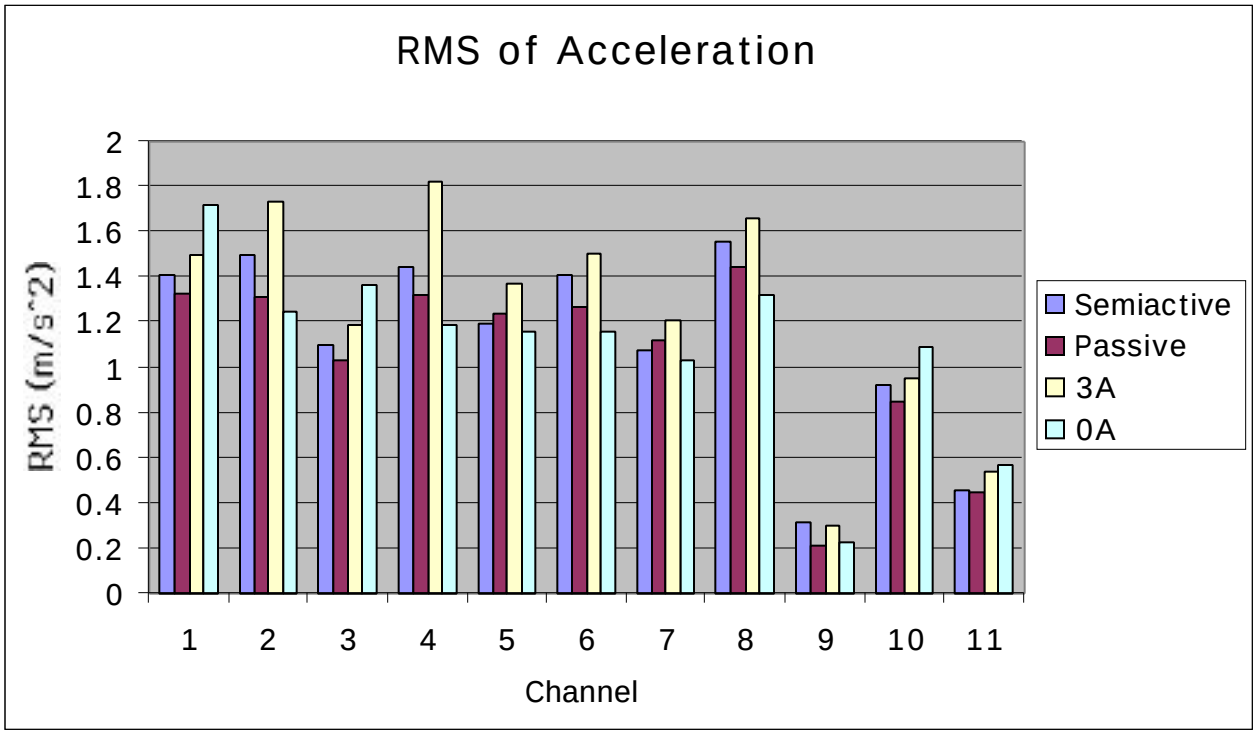

Figure 5.10. Average RMS for Acceleration.

Table 5.3. Average Acceleration RMS.

Channel	Semiactive	Passive	3A	0A
1. Front Driver's Side Frame	1.4089	1.3303	1.4973	1.7194
2. Front Driver's Side Axle	1.4946	1.3103	1.7342	1.2480
3. Front Passenger's Side Frame	1.0972	1.0334	1.1895	1.3641
4. Front Passenger's Side Axle	1.4445	1.3221	1.8242	1.1873
5. Rear Driver's Side Frame	1.1935	1.2430	1.3761	1.1620
6. Rear Driver's Side Axle	1.4126	1.2674	1.5033	1.1619
7. Rear Passenger's Side Frame	1.0740	1.1214	1.2083	1.0363
8. Rear Passenger's Side Axle	1.5574	1.4461	1.6581	1.3187
9. Horizontal Cab (Roll)	0.31494	0.21254	0.30623	0.22998
10. Vertical Cab	0.92542	0.84610	0.95247	1.0954
11. Forward Cab	0.45412	0.44817	0.54099	0.56830

The front wheels appear to have larger slopes (and therefore better) at the frame (channel 1 and 3). It would seem as if these larger slopes should correlate to lower RMS, but Table 5.3 shows that they did not. It is difficult to make sense of some of these values, for instance, how channel 5 shows the most improvement of semiactive damping over passive damping, while channel 7 (the opposite rear wheel), being worse for semiactive damping than passive damping. However, it does seem that there were improvements at the cab due to the semiactive suspension for channels 9 and 10 (roll and vertical motion, respectively). Channels 9 and 10 have larger slopes for semiactive damping than passive damping, although this again does not correlate to lower RMS in Table 5.3.

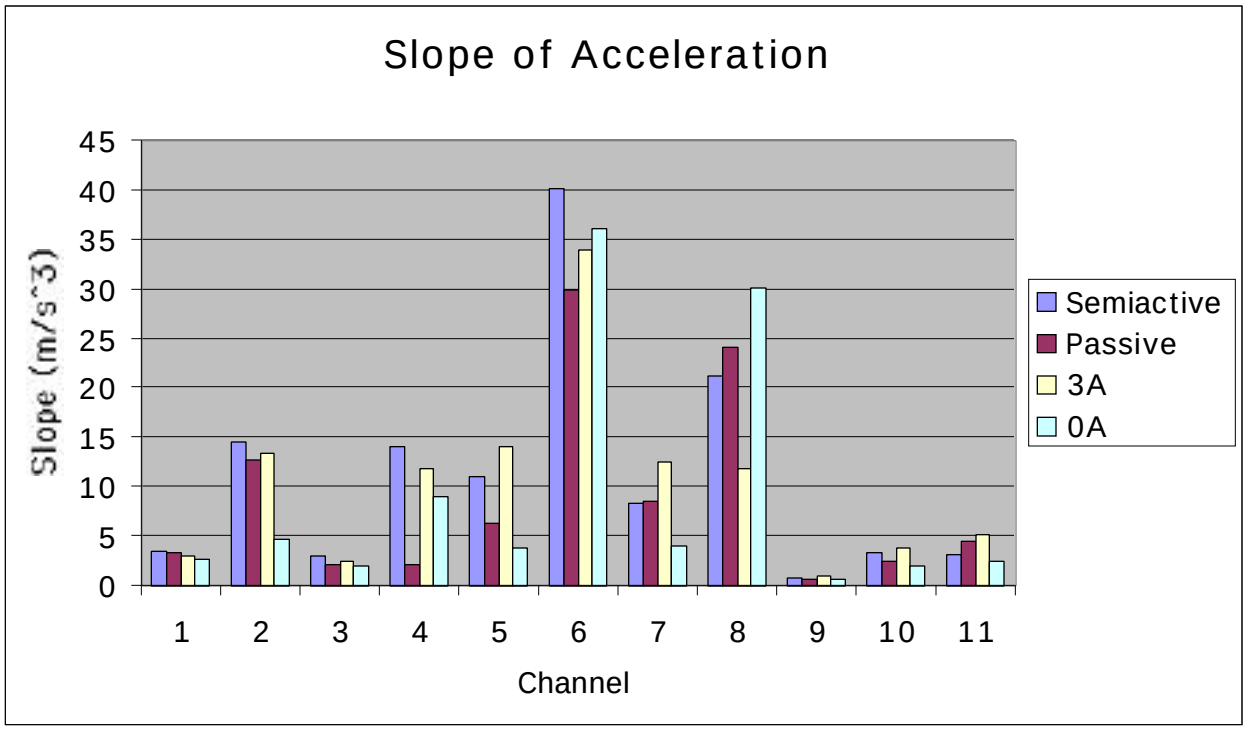

Figure 5.11. Average Slope for Acceleration.

Table 5.4. Average Slope for Acceleration.

Channel	Semiactive	Passive	3A	0A
1. Front Driver's Side Frame	3.5632	3.4079	3.0469	2.7128
2. Front Driver's Side Axle	14.509	12.751	13.345	4.6898
3. Front Passenger's Side Frame	3.0172	2.2537	2.4365	1.9331
4. Front Passenger's Side Axle	14.120	2.1072	11.880	9.1022
5. Rear Driver's Side Frame	11.019	6.3674	14.083	3.7820
6. Rear Driver's Side Axle	40.188	29.906	33.992	36.130
7. Rear Passenger's Side Frame	8.2846	8.5200	12.610	3.9328
8. Rear Passenger's Side Axle	21.271	24.170	11.887	30.057
9. Horizontal Cab (Roll)	0.82584	0.64144	0.99533	0.61206
10. Vertical Cab	3.3005	2.5864	3.7668	2.0308
11. Forward Cab	3.2039	4.5288	5.1160	2.5053

In all but one case, the minimum peaks of the semiactive damping channels are greater in magnitude than the corresponding channel for the passive damping

tests. The peculiar exception is channel 11, probably the least relevant measure as it is likely to be affected by the acceleration and deceleration of the vehicle.

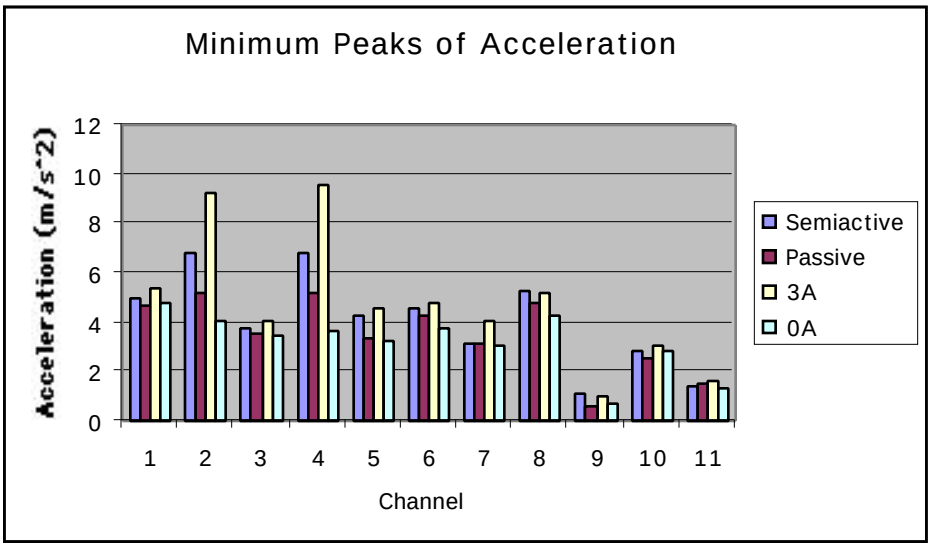

Figure 5.12. Average Minimum Peaks for Acceleration.

Table 5.5. Average Minimum Peaks for Acceleration.

Channel	Semiactive	Passive	3A	0A
1. Front Driver's Side Frame	4.9446	4.6274	5.4185	4.7352
2. Front Driver's Side Axle	6.7889	5.1863	9.2452	4.0953
3. Front Passenger's Side Frame	3.7620	3.5166	4.0400	3.4410
4. Front Passenger's Side Axle	6.8135	5.2263	9.5626	3.6330
5. Rear Driver's Side Frame	4.2236	3.4034	4.6003	3.2973
6. Rear Driver's Side Axle	4.5328	4.3010	4.8190	3.7654
7. Rear Passenger's Side Frame	3.1738	3.1296	4.0385	3.0545
8. Rear Passenger's Side Axle	5.3281	4.7389	5.2176	4.2310
9. Horizontal Cab (Roll)	1.1490	.63094	1.0040	.67936
10. Vertical Cab	2.8951	2.5463	3.0839	2.8457
11. Forward Cab	1.4263	1.5725	1.6014	1.3548

Table 5.6 and Figure 5.13 show all channels to have greater (and therefore worse) maximum peaks for the semiactive damping case than for the passive damping case.

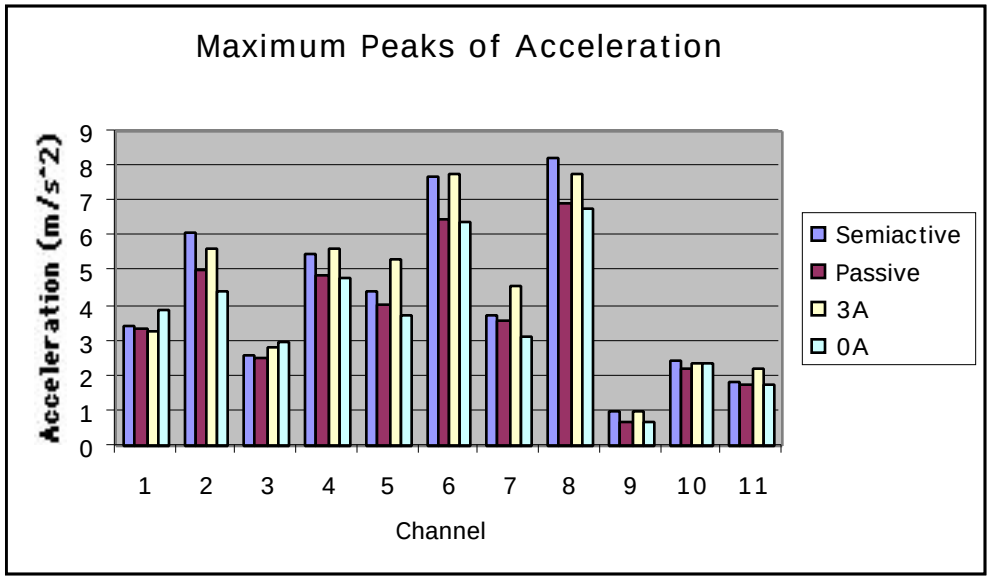

Figure 5.13. Average Maximum Peaks of Acceleration.

Table 5.6. Average Maximum Peaks for Acceleration.

Channel	Semiactive	Passive	3A	0A
1. Front Driver's Side Frame	3.3946	3.3791	3.2629	3.9021
2. Front Driver's Side Axle	6.1285	5.0307	5.6215	4.4253
3. Front Passenger's Side Frame	2.6146	2.5147	2.8045	2.9688
4. Front Passenger's Side Axle	5.5021	4.8520	5.6277	4.7804
5. Rear Driver's Side Frame	4.3996	4.0672	5.3111	3.7301
6. Rear Driver's Side Axle	7.7072	6.4796	7.7723	6.4272
7. Rear Passenger's Side Frame	3.7598	3.5907	4.5967	3.1187
8. Rear Passenger's Side Axle	8.2448	6.9160	7.7911	6.8186
9. Horizontal Cab (Roll)	0.97640	0.69719	0.98486	0.69547
10. Vertical Cab	2.4193	2.2370	2.3293	2.3928
11. Forward Cab	1.8540	1.7893	2.2155	1.7804

The peak-to-peak magnitude shown in Figure 5.14 is the difference between the minimum and maximum peaks of Figures 5.12 and 5.13. The semiactive is higher than the passive for all channels, which is expected since both the minimum and maximum magnitudes were higher for semiactive.

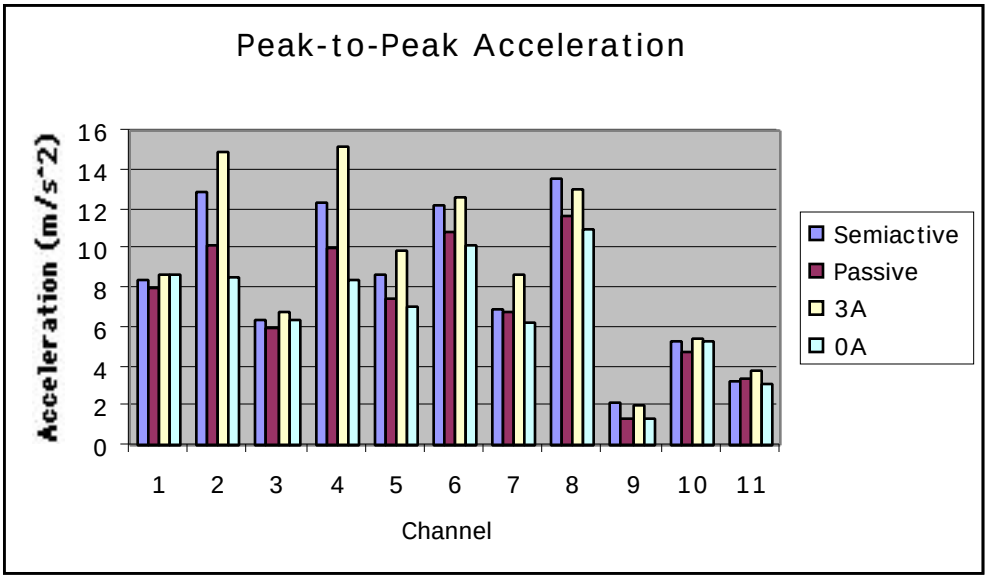

Figure 5.14. Peak to Peak Acceleration

Table 5.7. Peak-to-Peak Acceleration.

Channel	Semiactive	Passive	3A	0A
1. Front Driver's Side Frame	8.3392	8.0065	8.6814	8.6373
2. Front Driver's Side Axle	12.9174	10.217	14.8667	8.5206
3. Front Passenger's Side Frame	6.3766	6.0313	6.8445	6.4098
4. Front Passenger's Side Axle	12.3156	10.0783	15.1903	8.4134
5. Rear Driver's Side Frame	8.6232	7.4706	9.9114	7.0274
6. Rear Driver's Side Axle	12.24	10.7806	12.5913	10.1926
7. Rear Passenger's Side Frame	6.9336	6.7203	8.6352	6.1732
8. Rear Passenger's Side Axle	13.5729	11.6549	13.0087	11.0496
9. Horizontal Cab (Roll)	2.1254	1.32813	1.98886	1.37483
10. Vertical Cab	5.3144	4.7833	5.4132	5.2385
11. Forward Cab	3.2803	3.3618	3.8169	3.1352

5.4.3 Displacement Data

The acceleration data were also integrated twice to provide absolute displacement. In order to obtain meaningful displacement data, this integrated signal was passed through the filter of Figure 5.8 a second time to further reduce the low frequency drift. The same four measures were taken as for the acceleration: max and min peaks; RMS; and slope from max peak to next peak. Each of these values was then averaged for each data set as for the acceleration. The results are shown in Figures 5.15-5.19, with Tables 5.8-5.12 giving the numerical values.

The RMS displacement appears to be slightly better for the semiactive than the passive for the frame channels. The RMS displacement is equal or worse on the axle channels as we would expect from the theory that skyhook control should increase wheelhop. The improved frame RMS unfortunately does not seem to cause the cab RMS to improve, as channels 9 and11are higher than the semiactive, while channel 10 is approximately equal.

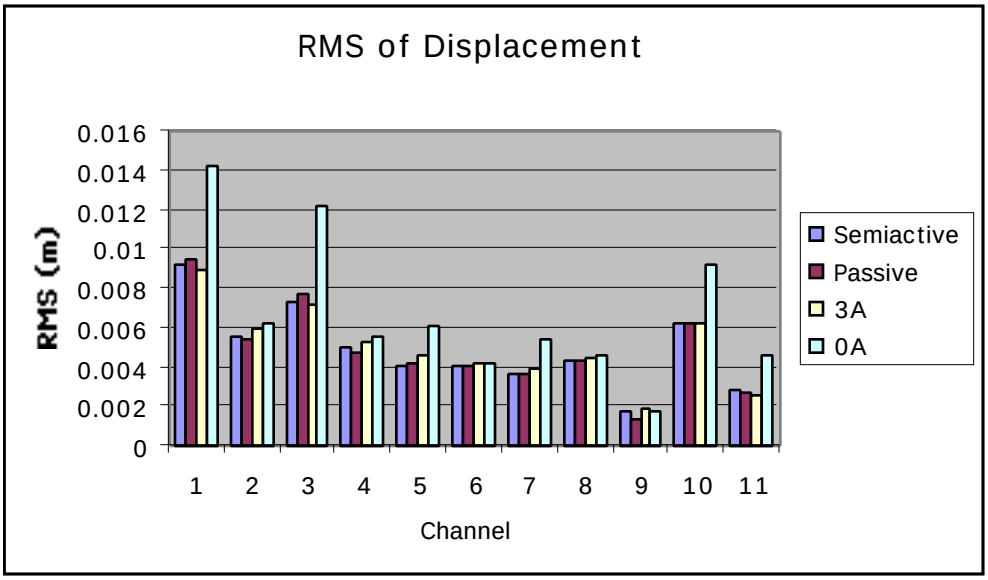

Figure 5.15. Average RMS of Displacement.

Table 5.8 Average RMS of Displacement.

Channel	Semiactive	Passive	3A	0A
1. Front Driver's Side Frame	0.0092	0.0095	0.0090	0.0142
2. Front Driver's Side Axle	0.0055	0.0054	0.0060	0.0062
3. Front Passenger's Side Frame	0.0073	0.0077	0.0072	0.0122
4. Front Passenger's Side Axle	0.0050	0.0048	0.0053	0.0055
5. Rear Driver's Side Frame	0.0041	0.0042	0.0046	0.0061
6. Rear Driver's Side Axle	0.0041	0.0041	0.0042	0.0042
7. Rear Passenger's Side Frame	0.0036	0.0037	0.0039	0.0054
8. Rear Passenger's Side Axle	0.0043	0.0044	0.0045	0.0046
9. Horizontal Cab (Roll)	0.0018	0.0014	0.0019	0.0018
10. Vertical Cab	0.0062	0.0062	0.0063	0.0092
11. Forward Cab	0.0028	0.0027	0.0026	0.0046

The slope of the displacement seems larger and therefore better for the semiactive damping compared to the passive damping for every channel, except channel 7 (rear passenger side frame). It is similar to the slope of the

acceleration from Figure 5.11 and Table 5.4, where seven again has a lower slope for semiactive damping than for passive damping, when all the other frame accelerometers (channels 1,3, and 5) show that the slope for the semiactive damping was higher than for passive damping. Improvements in the cab (channel 9-11) are quite noticeable.

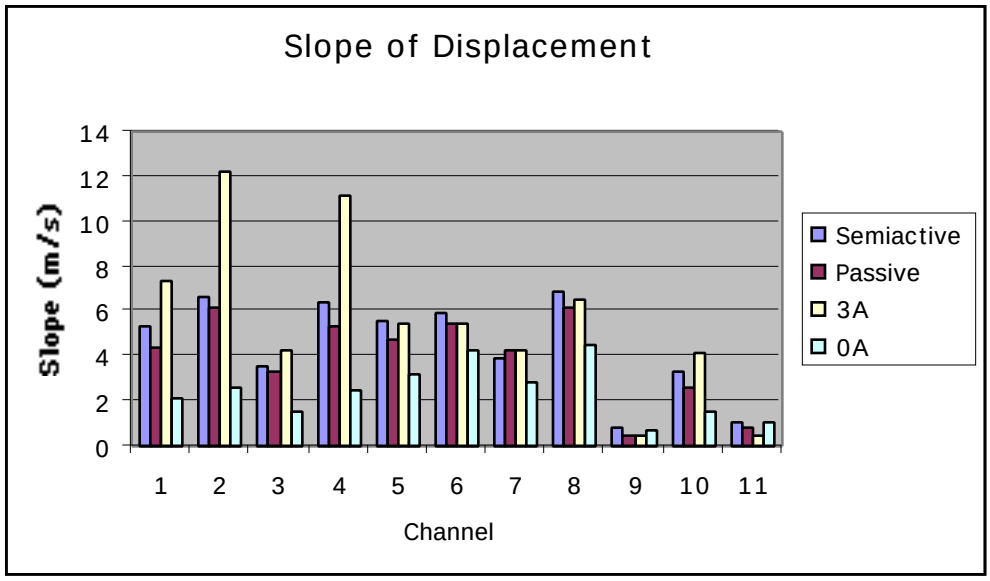

Figure 5.16. Average Slope of Displacement.

Table 5.9. Average Slope of Displacement.

Channel	Semiactive	Passive	3A	0A
1. Front Driver's Side Frame	5.2971	4.3400	7.3257	2.1074
2. Front Driver's Side Axle	6.5948	6.1537	12.1846	2.6117
3. Front Passenger's Side Frame	3.5626	3.3706	4.2449	1.5990
4. Front Passenger's Side Axle	6.4405	5.2907	11.1801	2.4664
5. Rear Driver's Side Frame	5.5350	4.7402	5.4992	3.2252
6. Rear Driver's Side Axle	5.9510	5.4306	5.4339	4.3118
7. Rear Passenger's Side Frame	3.8740	4.3068	4.2933	2.8703
8. Rear Passenger's Side Axle	6.8230	6.2216	6.5193	4.5666
9. Horizontal Cab (Roll)	0.8355	0.4574	0.4757	0.7241
10. Vertical Cab	3.2828	2.6233	4.1023	1.5832
11. Forward Cab	1.0118	0.8257	0.5206	1.0253

The magnitudes of the minimum peaks for displacement are slightly smaller and therefore better for some of the semiactive damping channels when compared to the passive damping. The frame channels 1, 3, 5, and 7 all have lower magnitudes for semiactive than passive. The axle channels 2, 4, 6, and 8 are all greater for semiactive damping than passive damping as we expect due to increased wheelhop. The lower frame magnitudes, however, do not seem to help in the cab, as channels 9,10, and 11 all show the semiactive damping having higher magnitudes.

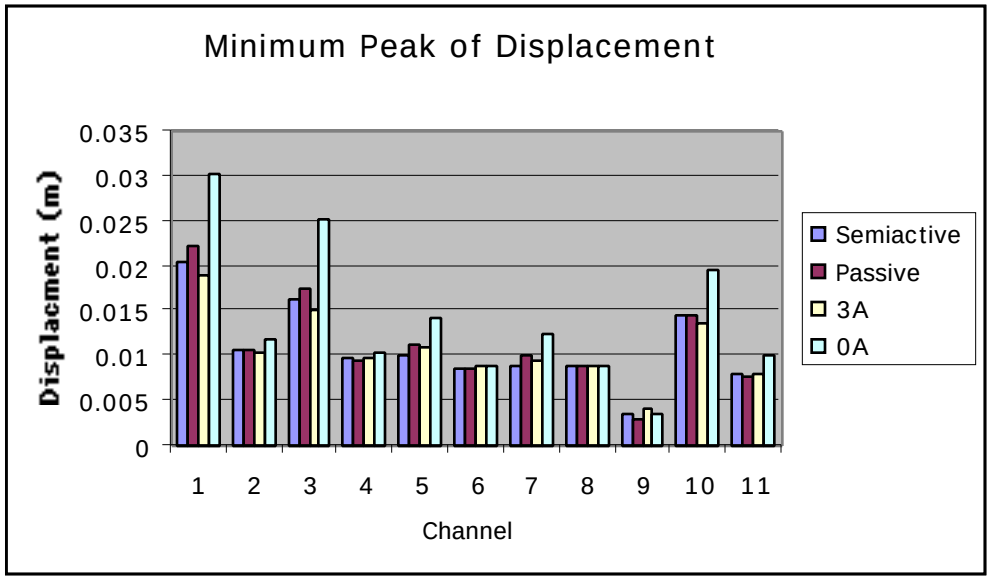

Figure 5.17. Average Minimum Peaks of Displacement.

Table 5.10. Average Minimum Peaks of Displacement.

Channel	Semiactive	Passive	3A	0A
1. Front Driver's Side Frame	0.0204	0.0222	0.0189	0.0302
2. Front Driver's Side Axle	0.0108	0.0106	0.0105	0.0118
3. Front Passenger's Side Frame	0.0164	0.0176	0.0151	0.0251
4. Front Passenger's Side Axle	0.0097	0.0095	0.0099	0.0103
5. Rear Driver's Side Frame	0.0101	0.0113	0.0109	0.0141
6. Rear Driver's Side Axle	0.0086	0.0087	0.0088	0.0088
7. Rear Passenger's Side Frame	0.0088	0.0102	0.0094	0.0126
8. Rear Passenger's Side Axle	0.0088	0.0088	0.0090	0.0090
9. Horizontal Cab (Roll)	0.0036	0.0030	0.0041	0.0036
10. Vertical Cab	0.0145	0.0144	0.0137	0.0195
11. Forward Cab	0.0079	0.0078	0.0081	0.0102

The maximum peaks for semiactive damping is higher for some channels and lower for others. This implies that the semiactive damping did little to improve this measure. It definitely did not lower the magnitude in the cab, where

the roll (channel 9) has a much higher magnitude for semiactive damping than passive damping.

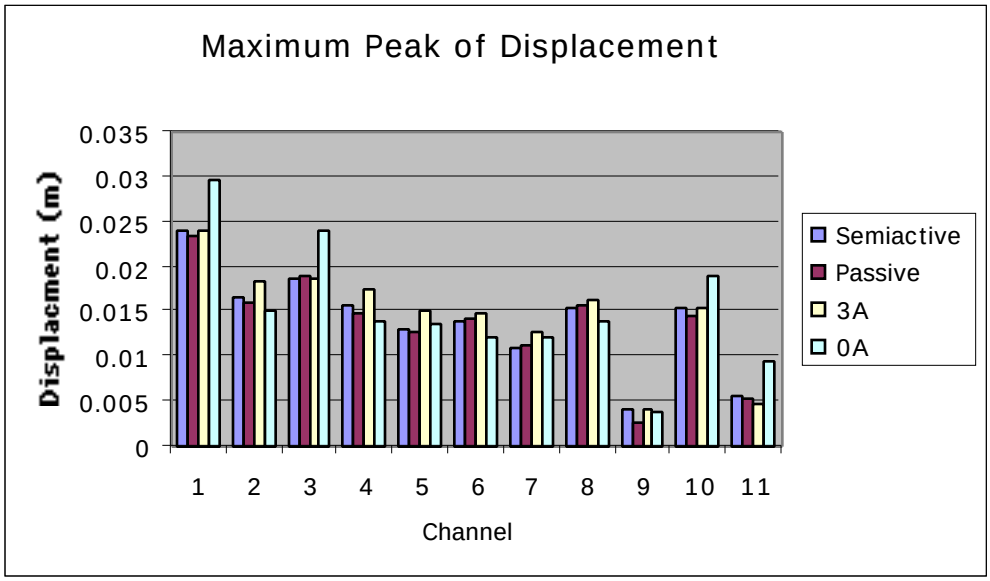

Figure 5.18. Average Max Peaks of Displacement.

Table 5.11. Average Maximum Peaks of Displacement.

Channel	Semiactive	Passive	3A	0A
1. Front Driver's Side Frame	0.0240	0.0234	0.0241	0.0298
2. Front Driver's Side Axle	0.0167	0.0160	0.0184	0.0151
3. Front Passenger's Side Frame	0.0188	0.0190	0.0187	0.0241
4. Front Passenger's Side Axle	0.0156	0.0148	0.0175	0.0138
5. Rear Driver's Side Frame	0.0130	0.0128	0.0151	0.0137
6. Rear Driver's Side Axle	0.0138	0.0141	0.0147	0.0122
7. Rear Passenger's Side Frame	0.0111	0.0113	0.0129	0.0121
8. Rear Passenger's Side Axle	0.0154	0.0156	0.0163	0.0138
9. Horizontal Cab (Roll)	0.0043	0.0028	0.0043	0.0038
10. Vertical Cab	0.0155	0.0146	0.0154	0.0191
11. Forward Cab	0.0057	0.0054	0.0048	0.0094

The peak-to-peak displacement shown in Figure 5.19 is the difference between the minimum and maximum peaks from Figures 5.17 and 5.18. It shows

more definite trend than Figure 5.18. It shows the total displacement to be lower for the semiactive damping than the passive damping at the frame for every wheel (channels 1,3,5, and 7). There is, however, no improvement at the cab (channels 9,10, and 11).

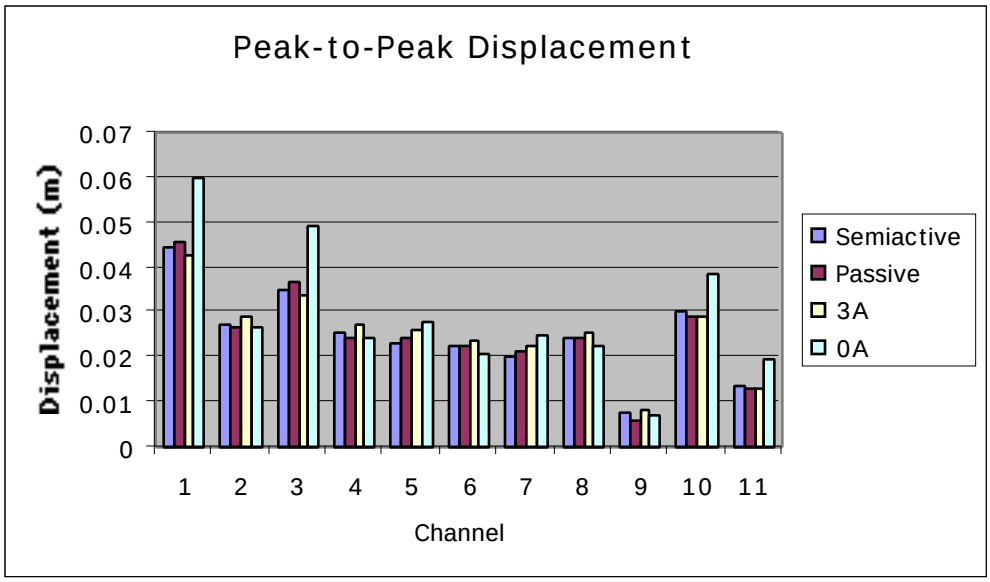

Figure 5.19. Peak-to-Peak Displacement.

Table 5.12. Peak-to-Peak Displacement.

Channel	Semiactive	Passive	3A	0A
1. Front Driver's Side Frame	0.0444	0.0456	0.043	0.06
2. Front Driver's Side Axle	0.0275	0.0266	0.0289	0.0269
3. Front Passenger's Side Frame	0.0352	0.0366	0.0338	0.0492
4. Front Passenger's Side Axle	0.0253	0.0243	0.0274	0.0241
5. Rear Driver's Side Frame	0.0231	0.0241	0.026	0.0278
6. Rear Driver's Side Axle	0.0224	0.0228	0.0235	0.021
7. Rear Passenger's Side Frame	0.0199	0.0215	0.0223	0.0247
8. Rear Passenger's Side Axle	0.0242	0.0244	0.0253	0.0228
9. Horizontal Cab (Roll)	0.0079	0.0058	0.0084	0.0074
10. Vertical Cab	0.03	0.029	0.0291	0.0386
11. Forward Cab	0.0136	0.0132	0.0129	0.0196

5.4.4 Summary of Road Data

The slopes were improved for the semiactive damping, although the peak amplitudes were generally not improved. The RMS was also unimproved. This implies that the initial magnitudes of the disturbance were higher for the semiactive damping(hence the higher peaks), but the transients died out faster. The RMS was worse because the increase in magnitude of the initial disturbance more than cancelled out the effect of the increased slope. That the displacement results were slightly better than the acceleration results is also indicative that the semiactive damping caused the transients to decay faster.

5.5 Highway Data

The highway data sets were downloaded to a computer for analysis in Matlab in 10s increments. Each data set was made into five data sets, each consecutive one beginning 12 elements (2ms) after the previous, that is:

Array1=OriginalDataSet

Array2=Array1(12..length(Array1))

Array3=Array2(12..length(Array2))=Array1(24..length(Array1))

Etc...

This was done so that the FFTs (Fast Fourier Transform) could be averaged to remove noise. Each of these five arrays was decimated by 60, lowering the sampling frequency from 6kHz to 100Hz, which would speed up the FFT. A 1024-point FFT was taken for each of the five decimated arrays. The magnitudes of these five FFTs were averaged to provide an auto power spectrum. Figures 5.20-5.39 show the auto power spectra of each channel.

Figure 5.20 shows that the constant 3A has increased the transmissibility of all frequencies. Every following figure that includes the constant 3A data has the same characteristics, so I will not comment on them further. They are only included to show that the 3A does indeed increase vibration for every channel.

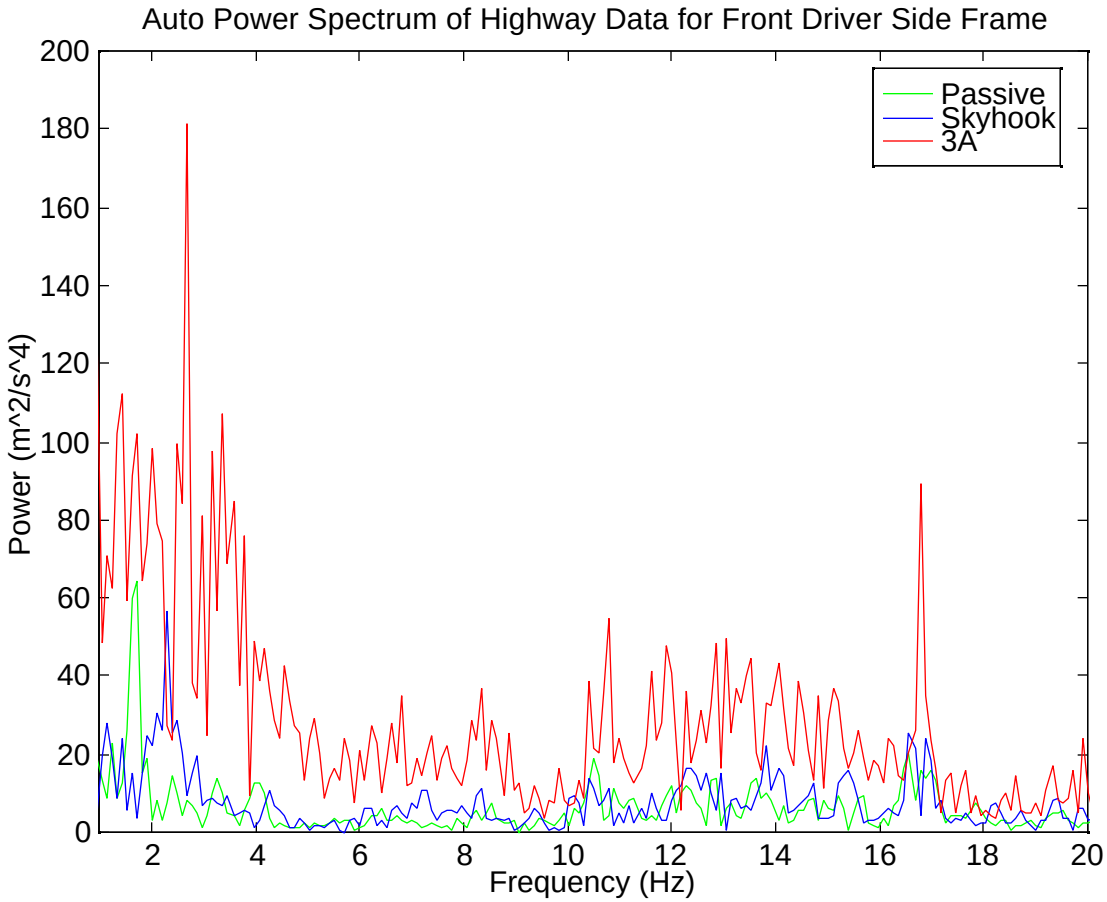

Figure 5.20. Auto Power Spectrum of Highway Data for Front Driver Side Frame (Passive, S/A, 3A).

The data in Figure 5.21 are difficult to characterize, other than to say that they are inconclusive. There is no definite frequency where one can say that the response has been increased or decreased from passive damping to semiactive damping.

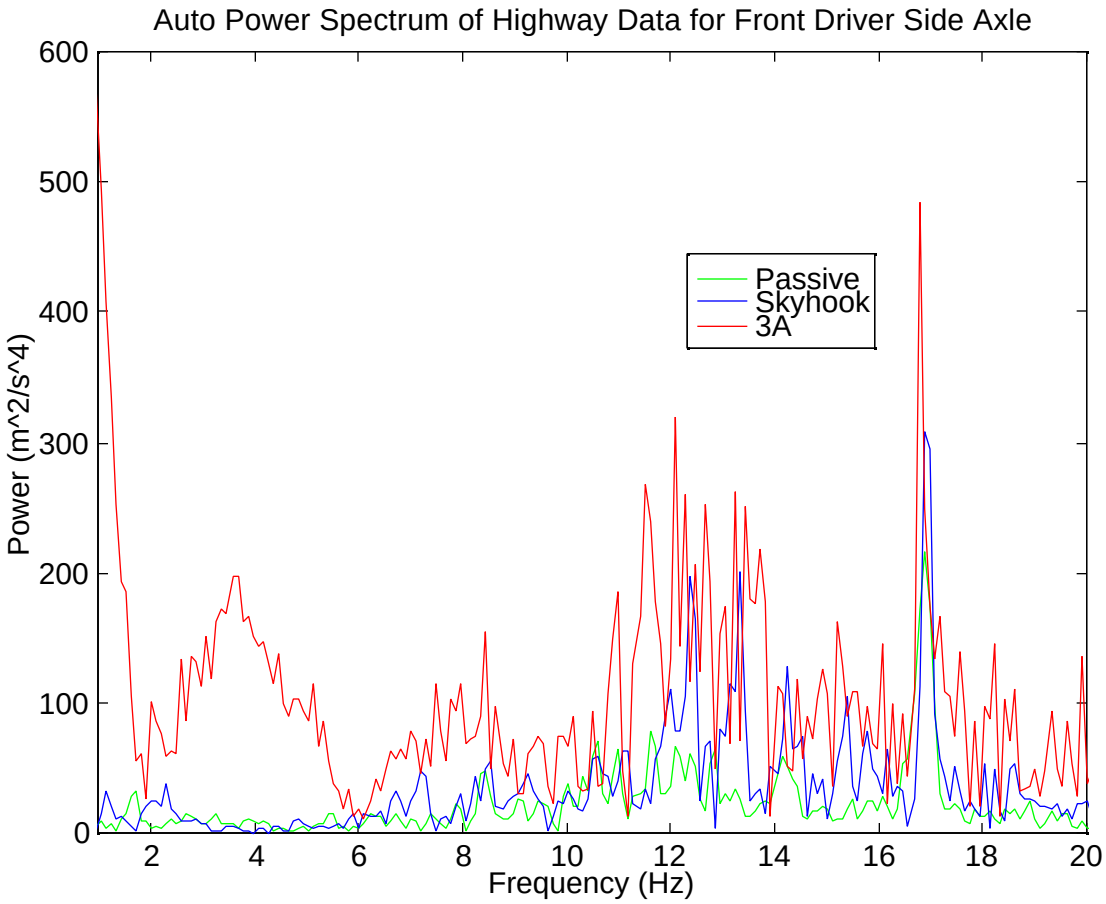

Figure 5.22. Auto Power Spectrum of Highway Data for Front Driver Side Axle (Passive, S/A, 3A).

In Figure 5.23 the semiactive damping seems to have more activity in the higher frequencies.

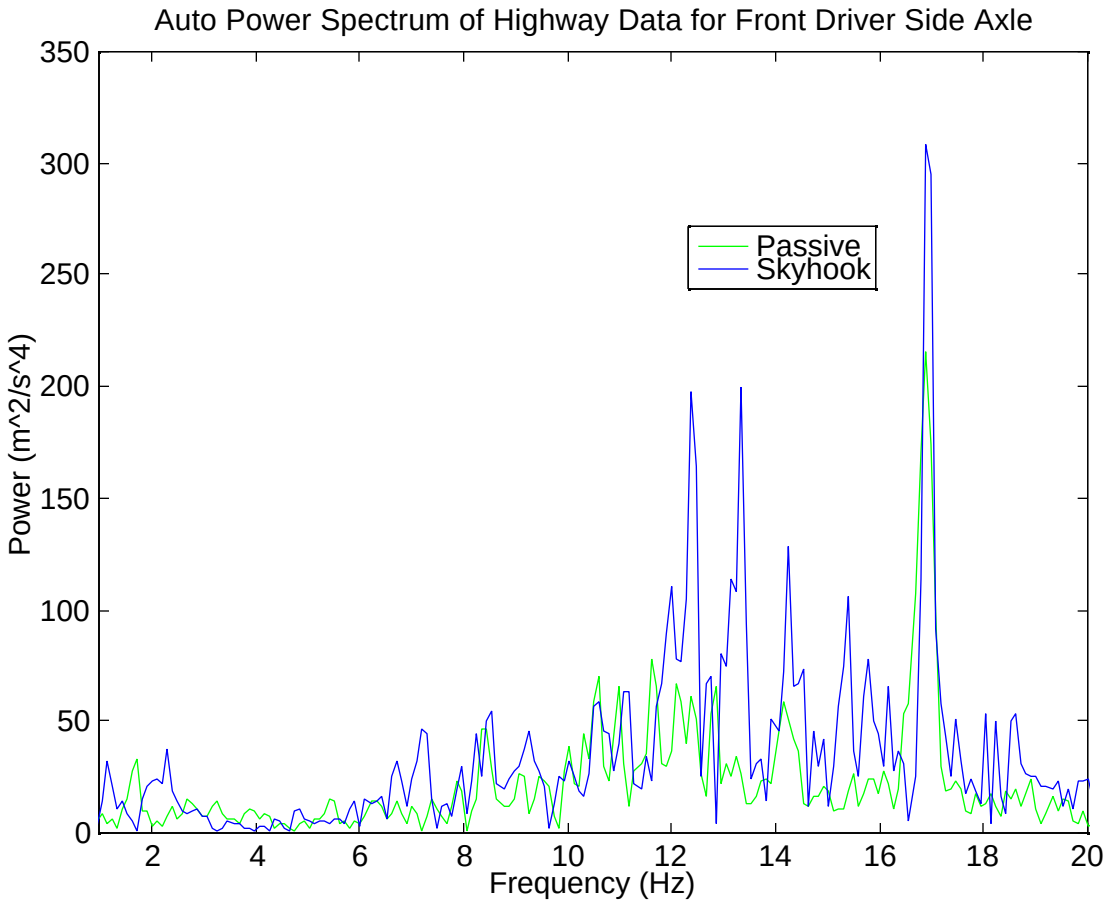

Figure 5.23. Auto Power Spectrum of Highway Data for Front Driver Side Axle (Passive, S/A).

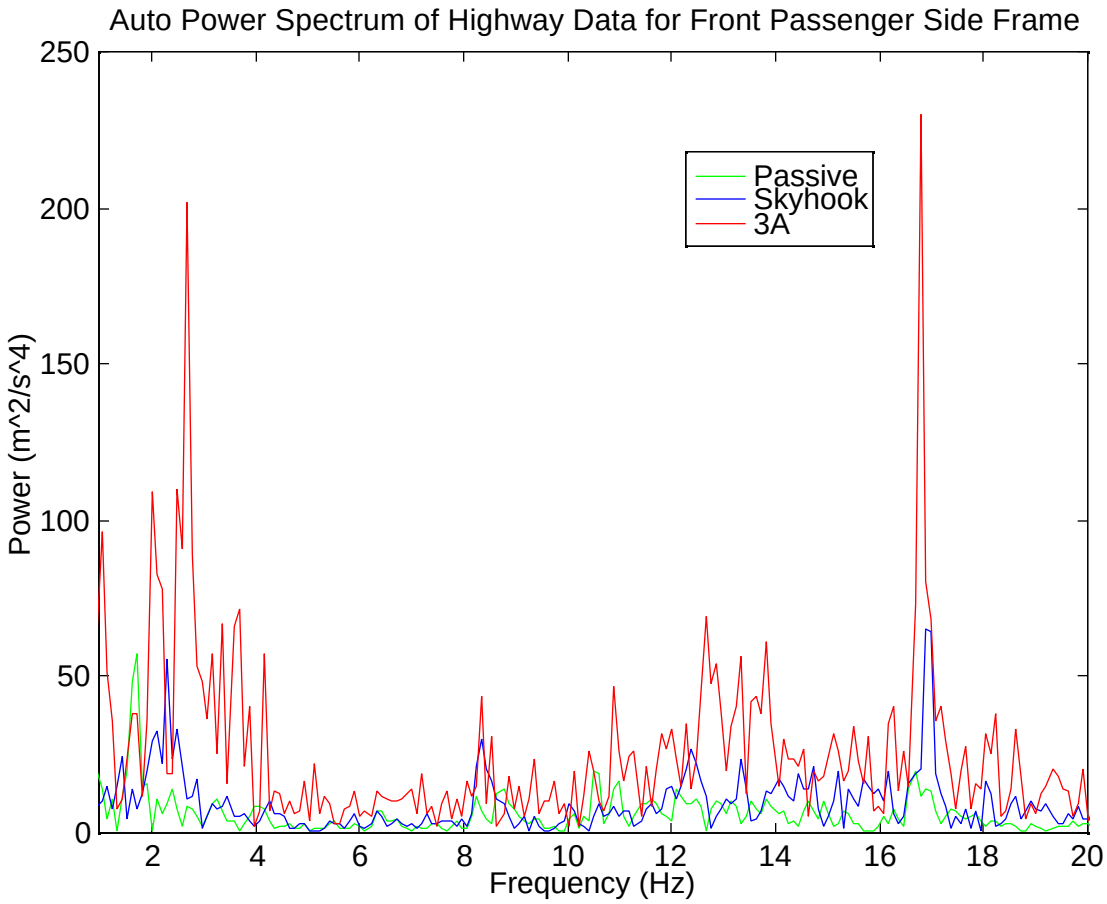

Figure 5.24. Auto Power Spectrum of Highway Data for Front Passenger Side Frame (Passive, S/A, 3A).

Compare Figure 5.25 to Figure 5.21. Note how we see the same peaks for passive near 2Hz and a peak for the semiactive near 2.5 Hz. The semiactive seems to have additional activity in the higher frequencies.

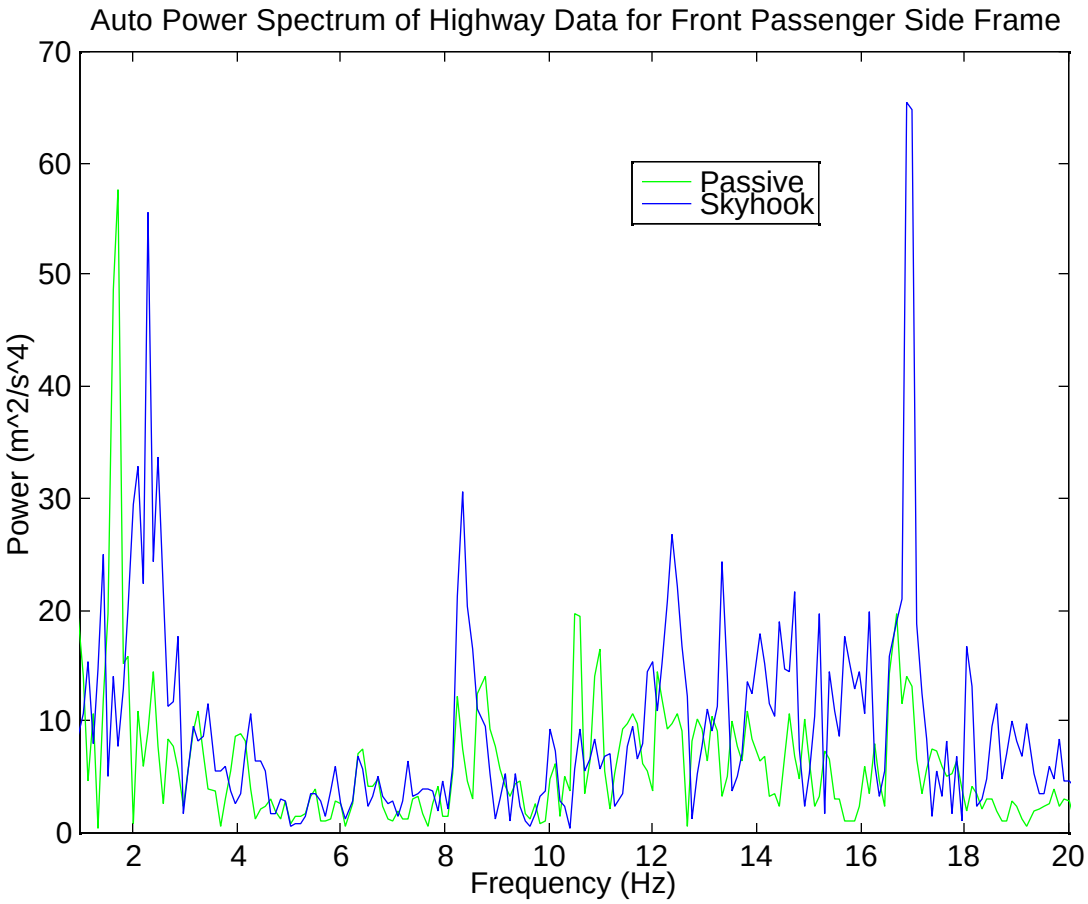

Figure 5.25. Auto Power Spectrum of Highway Data for Front Passenger Side Frame (Passive, S/A).

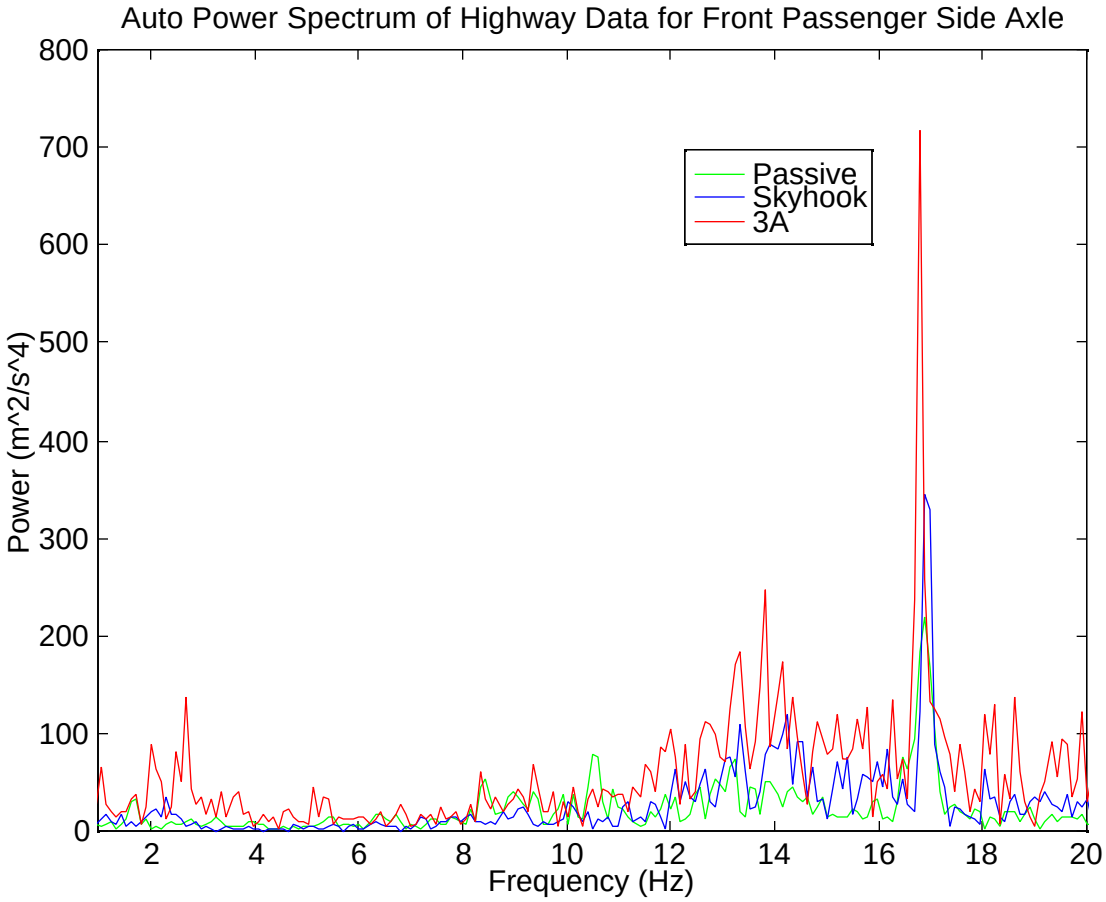

Figure 5.26. Auto Power Spectrum of Highway Data for Front Passenger Side Axle (Passive, S/A, 3A).

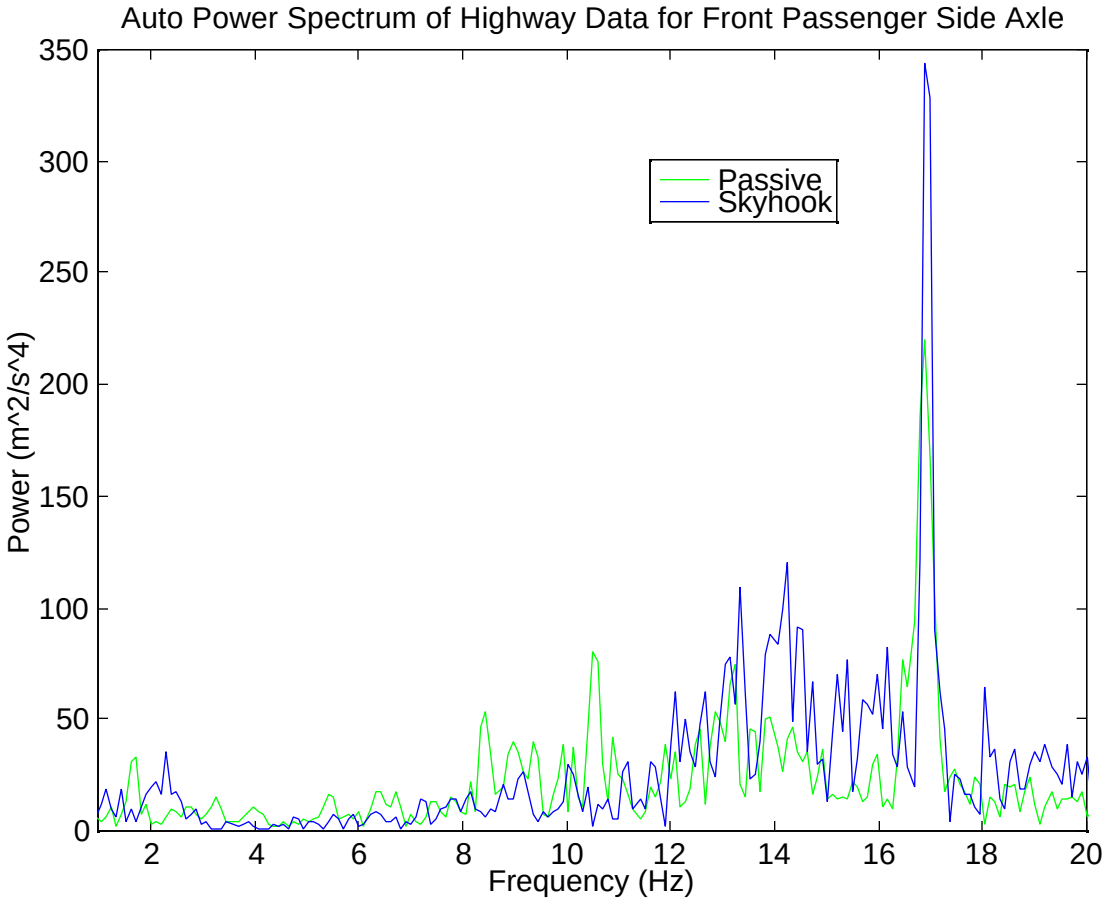

Figure 5.27. Auto Power Spectrum of Highway Data for Front Passenger Side Axle (Passive, S/A).

As in Figure 5.23, Figure 5.27 shows that the semiactive damping seems to have increased activity at the higher frequencies.

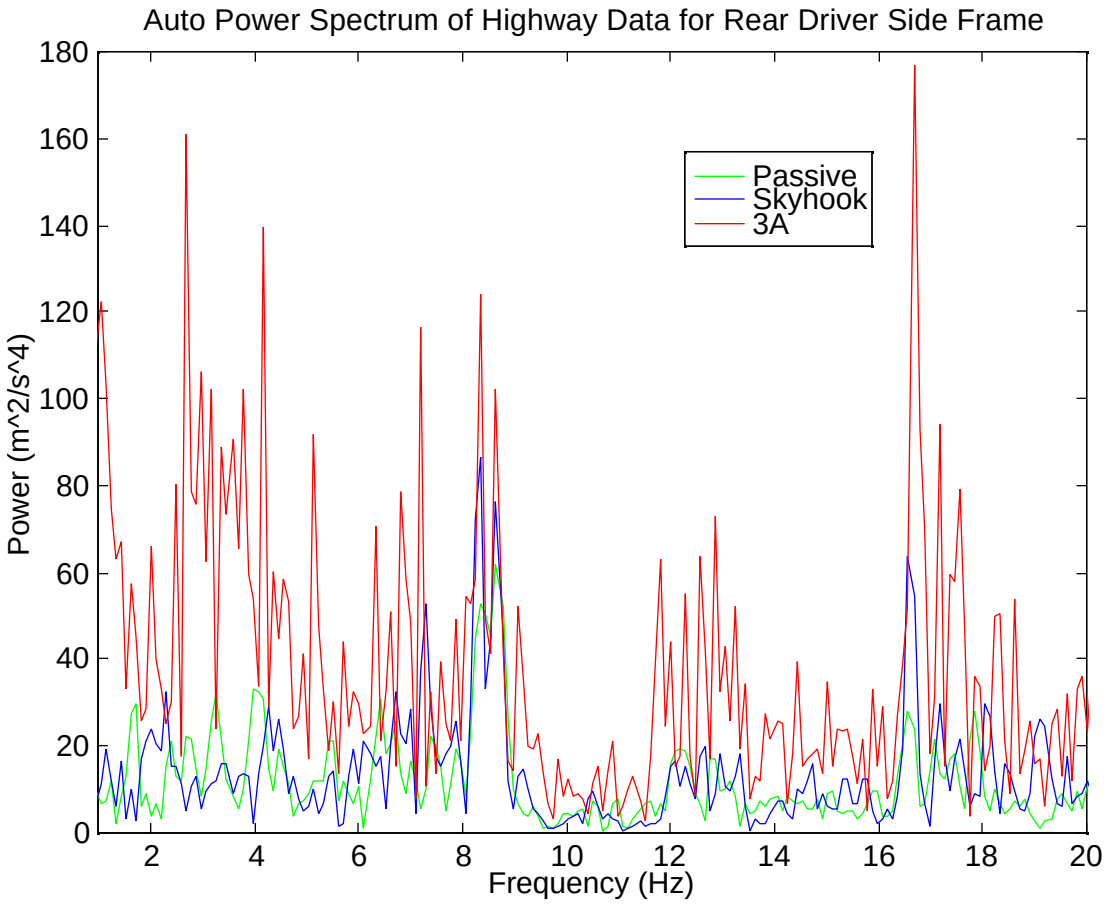

Figure 5.28. Auto Power Spectrum of Highway Data for Rear Driver Side Frame (Passive, S/A, 3A).

Figure 5.29 shows the passive damping and semiactive dampingto be comparable on this channel, with the semiactive being a little bit worse, with higher magnitudes at the peaks, and an extra peak at 7Hz.

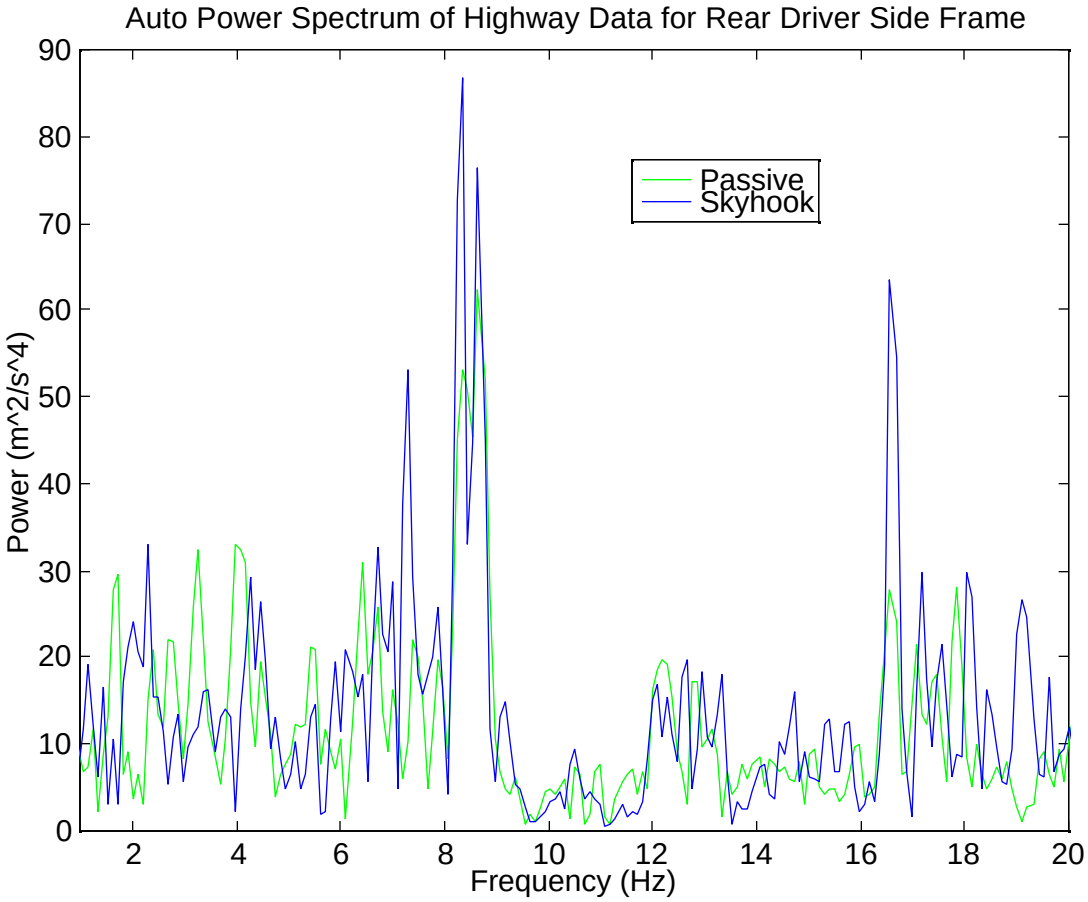

Figure 5.30. Auto Power Spectrum of Highway Data for Rear Driver Side Frame (Passive, S/A).

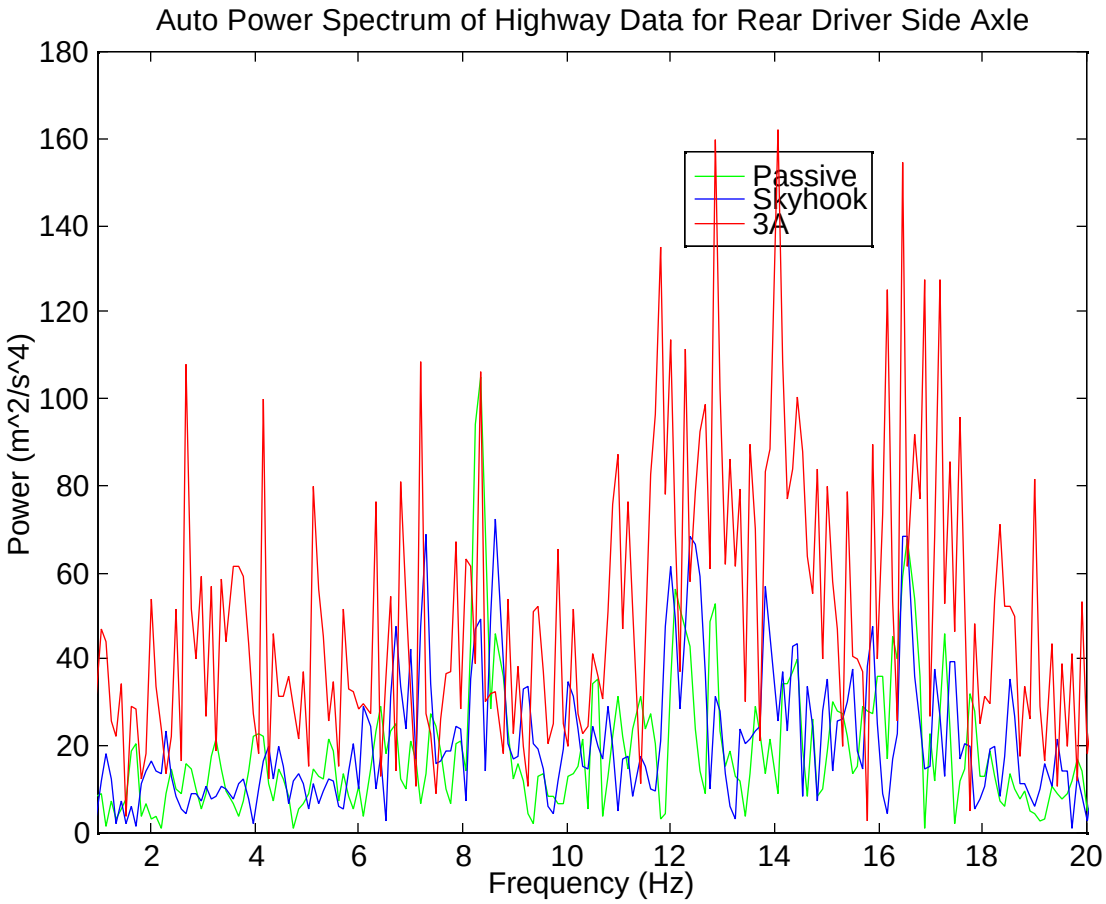

Figure 5.30. Auto Power Spectrum of Highway Data for Rear Driver Side Axle (Passive, S/A, 3A).

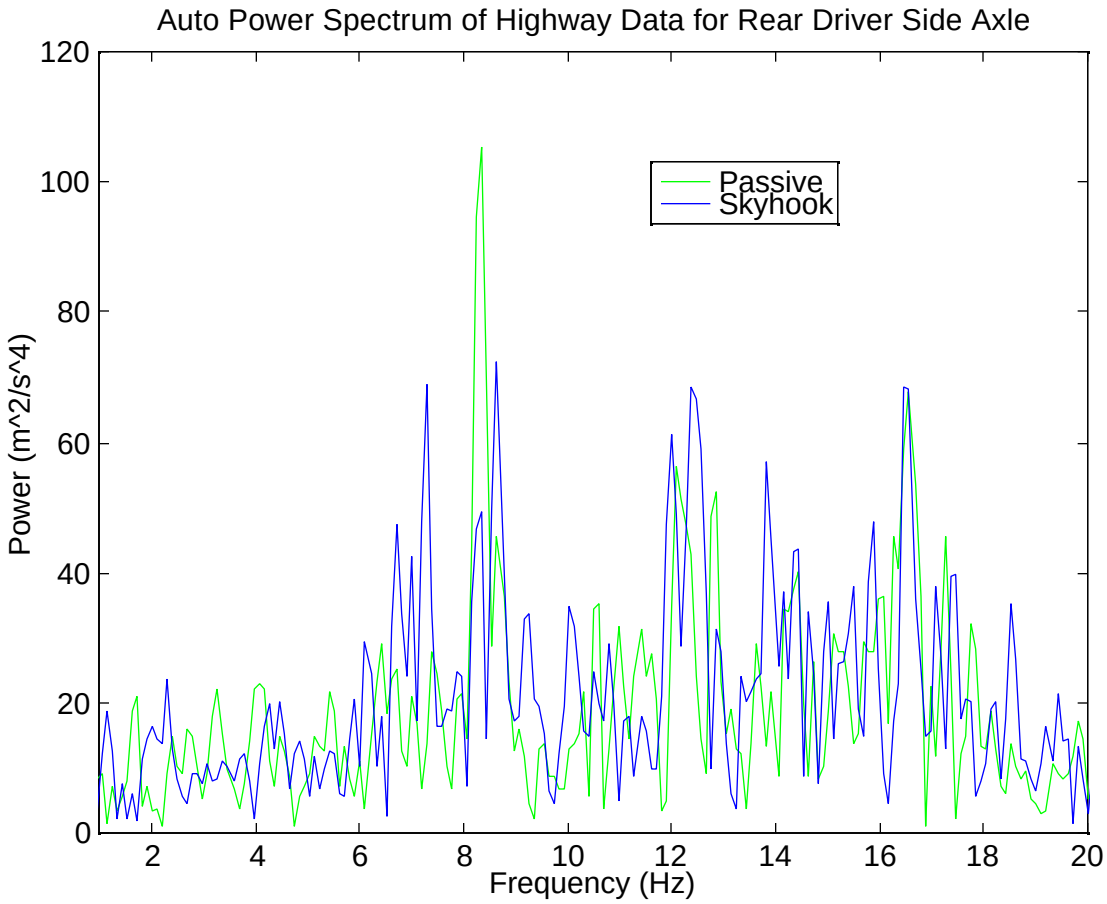

Figure 5.31. Auto Power Spectrum of Highway Data for Rear Driver Side Axle (Passive, S/A).

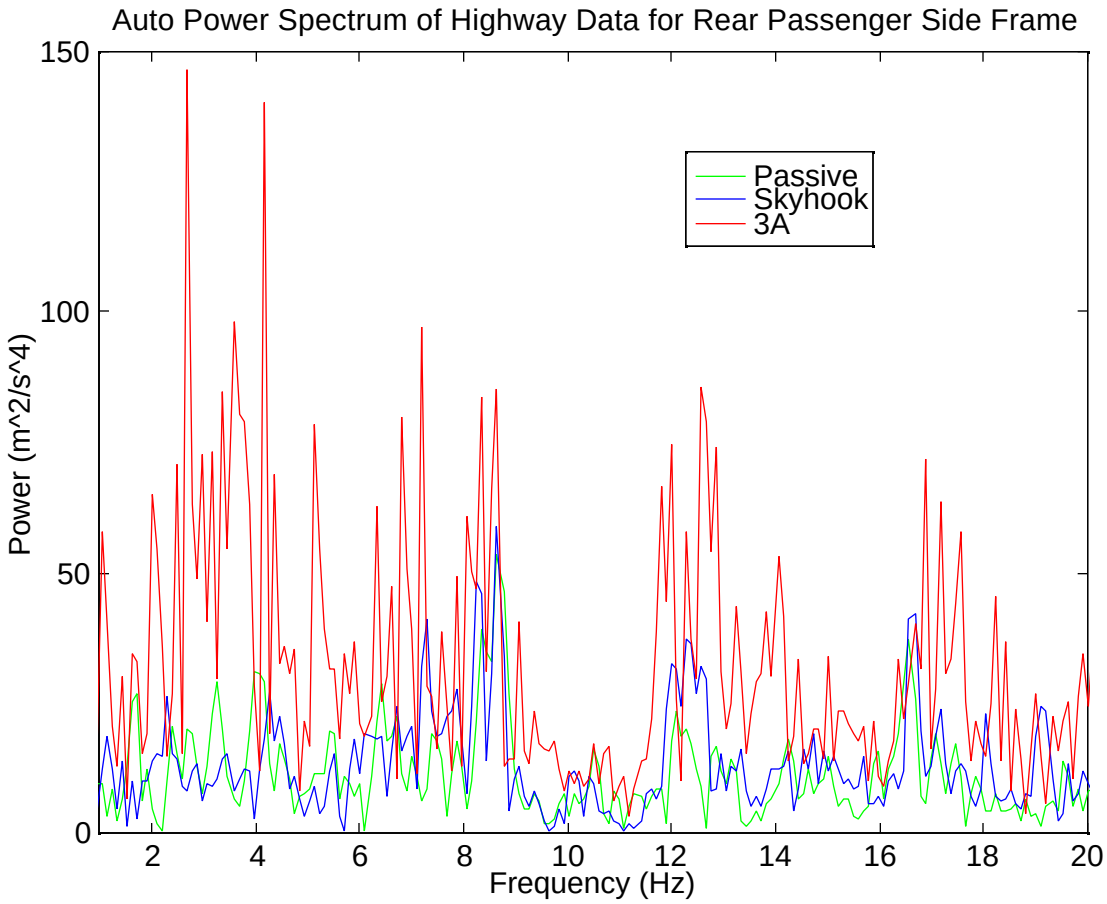

Figure 5.32. Auto Power Spectrum of Highway Data for Rear Passenger Side Frame (Passive, S/A).

Compare Figure 5.33 to Figure 5.29. Again, the passive and semiactive damping closely follow each other, with the magnitudes of the semiactive damping being slightly worse. Also, the semiactive suspension again has an extra peak at approximately 7Hz.

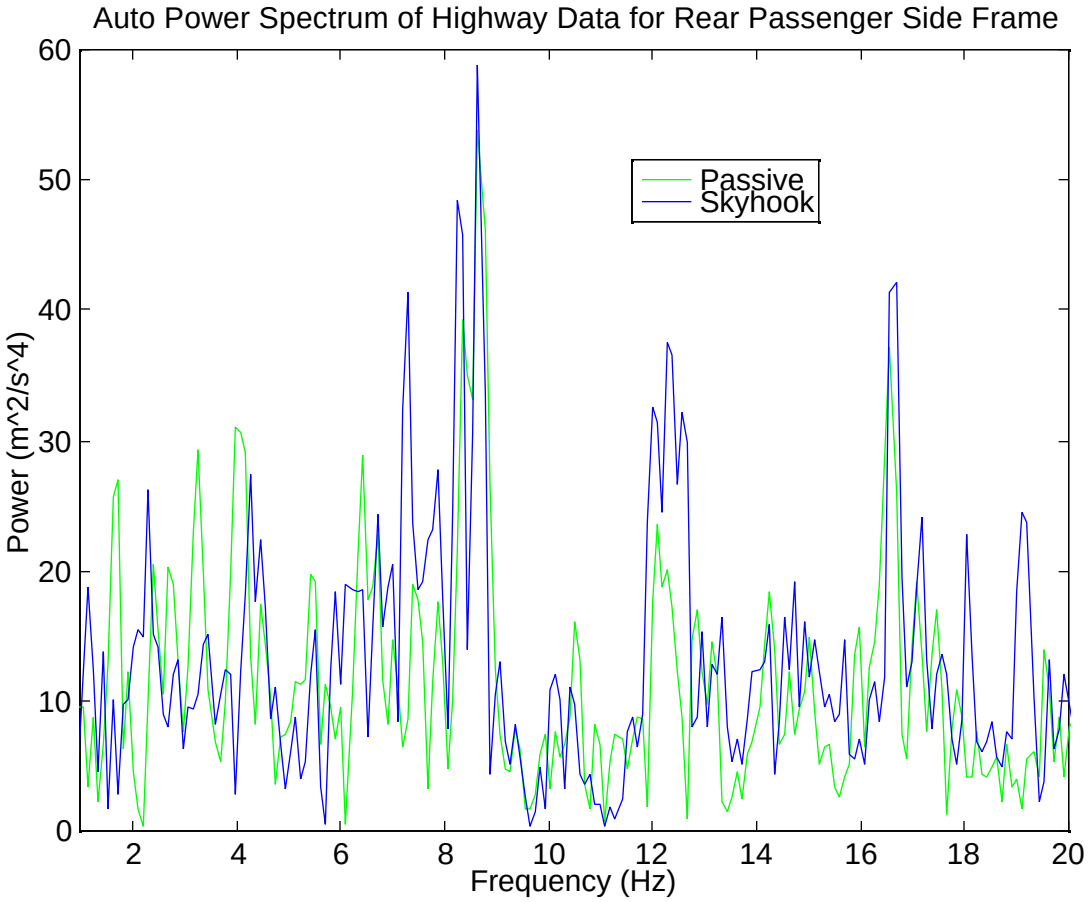

Figure 5.33. Auto Power Spectrum of Highway Data for Rear Passenger Side Frame (Passive, S/A).

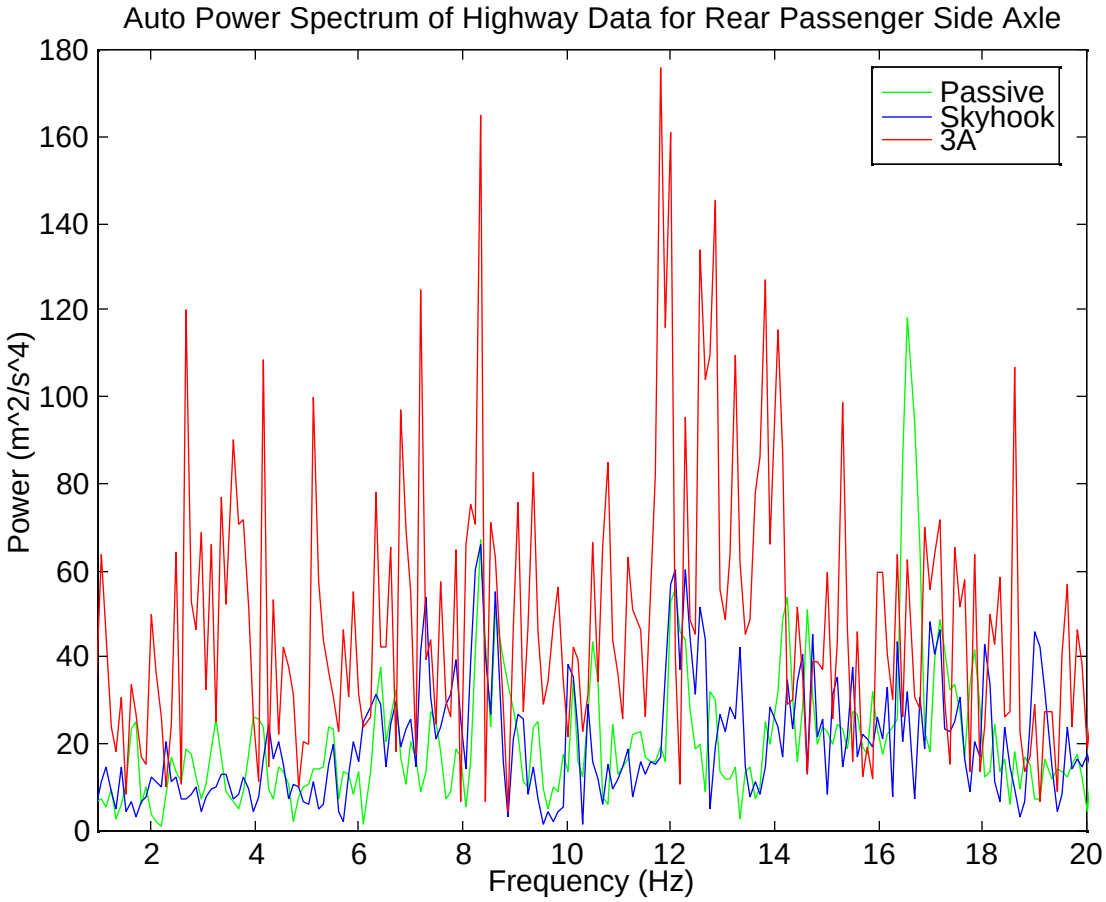

Figure 5.34. Auto Power Spectrum of Highway Data for Rear Passenger Side Axle (Passive, S/A, 3A).

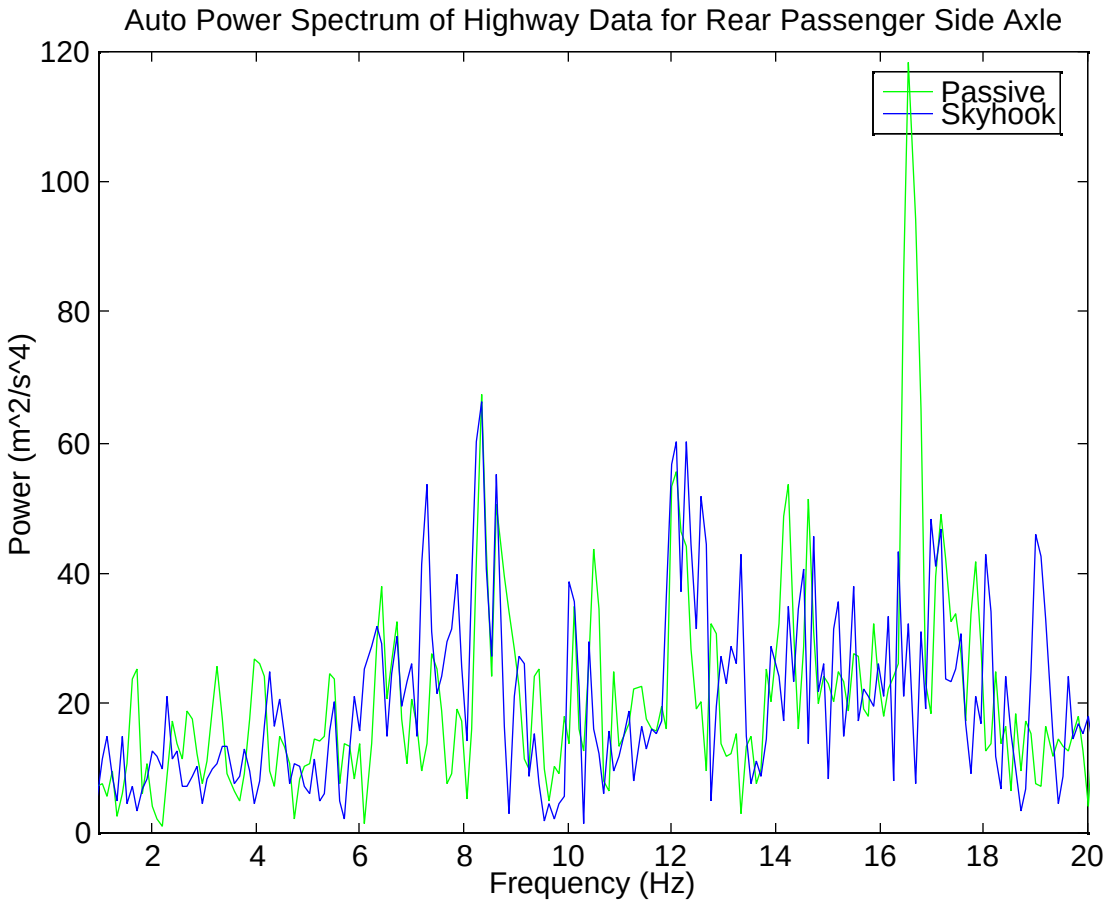

Figure 5.35. Auto Power Spectrum of Highway Data for Rear Passenger Side Axle (Passive, S/A).

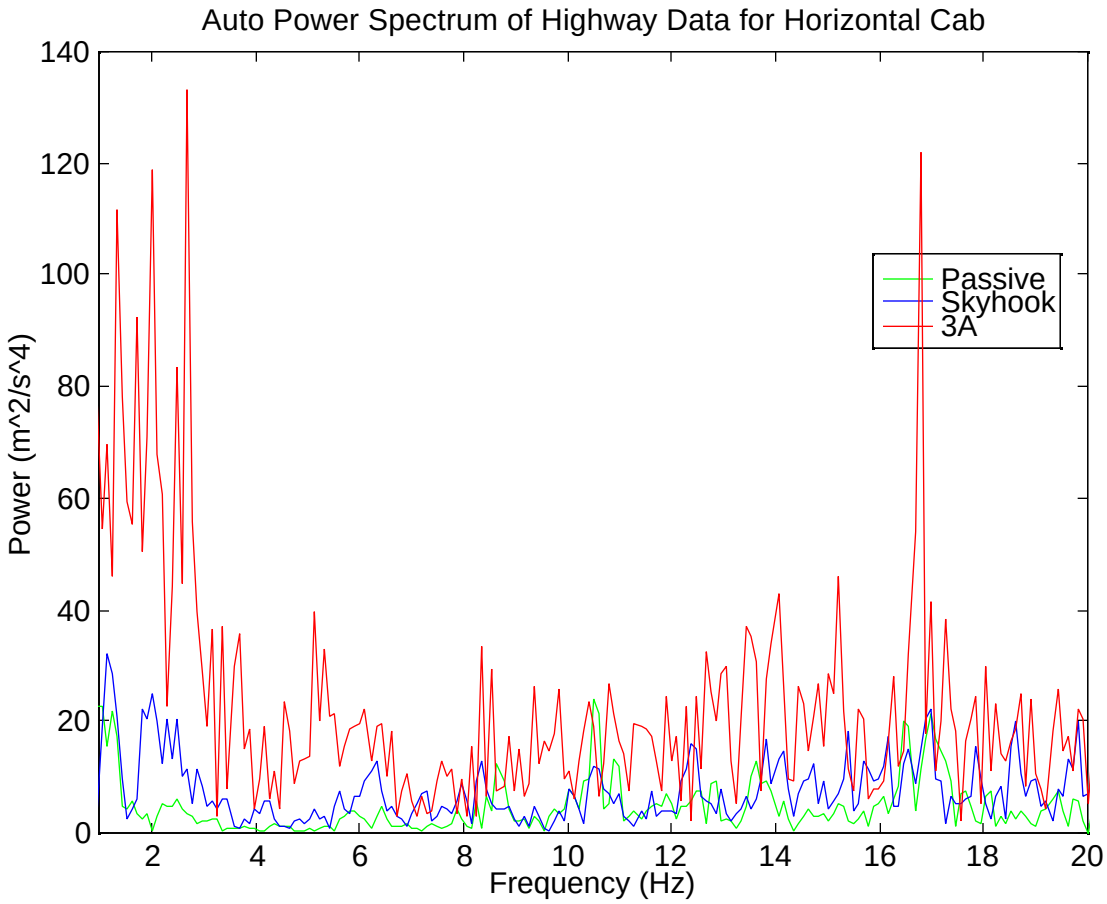

Figure 5.36. Auto Power Spectrum of Highway Data Horizontal Cab (Passive, S/A, 3A).

The channel shown in Figure 5.37 measures roll of the cab. This figure shows the semiactive suspension to be worse for almost the entire frequency range of interest.

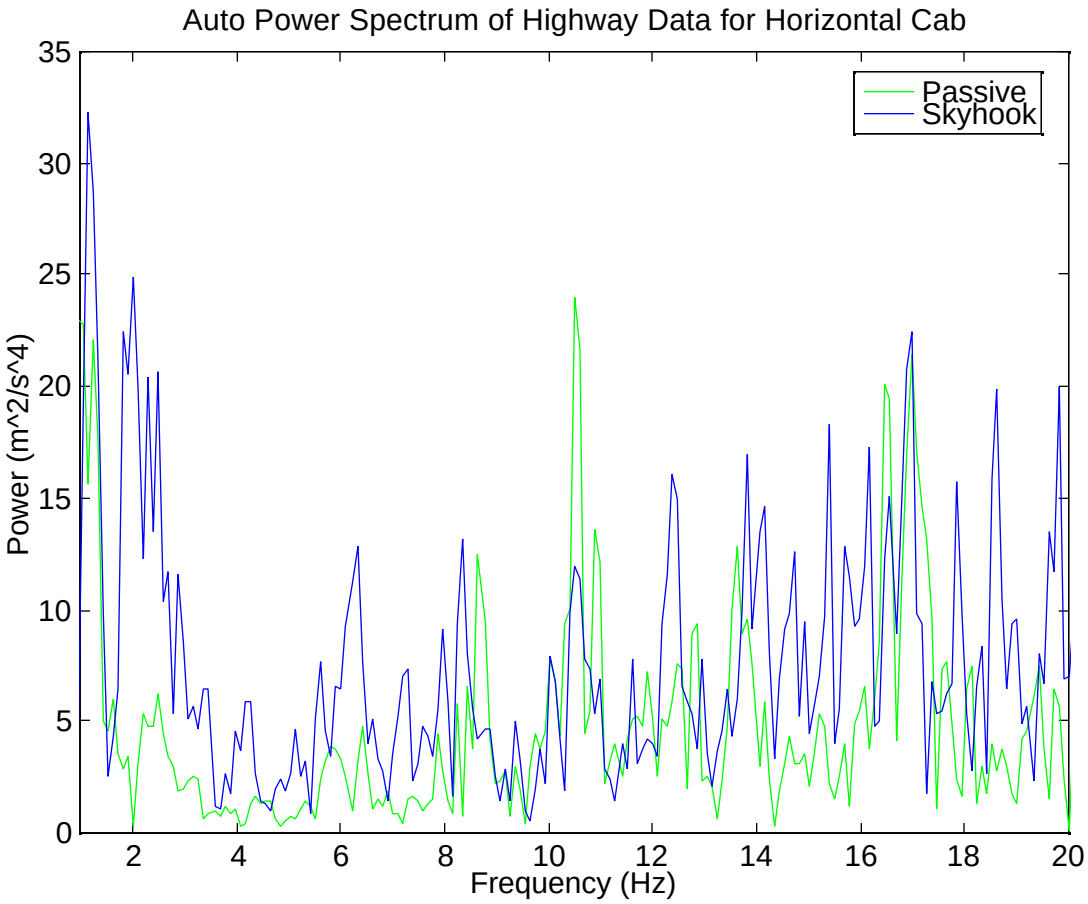

Figure 5.37. Auto Power Spectrum of Highway Data Horizontal Cab (Passive, S/A).

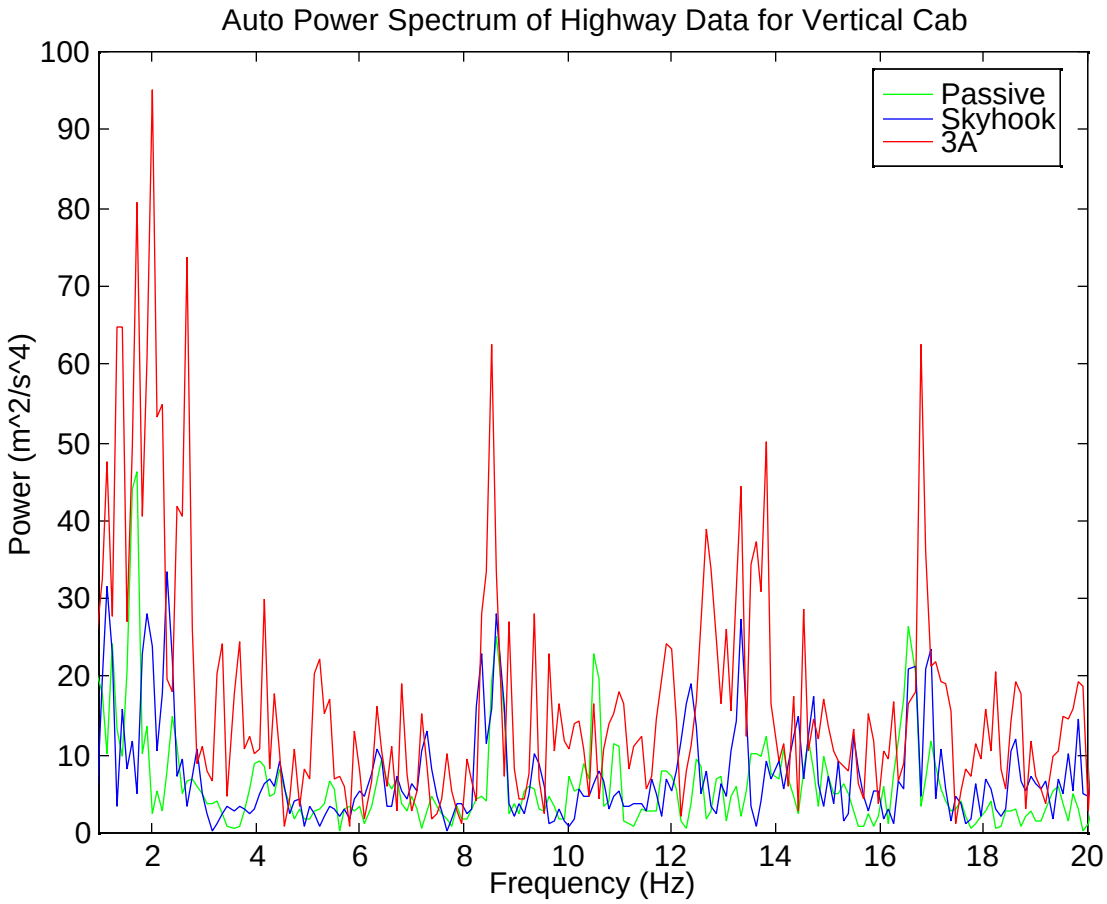

Figure 5.38. Auto Power Spectrum of Highway Data Vertical Cab (Passive, Semiactive, 3A).

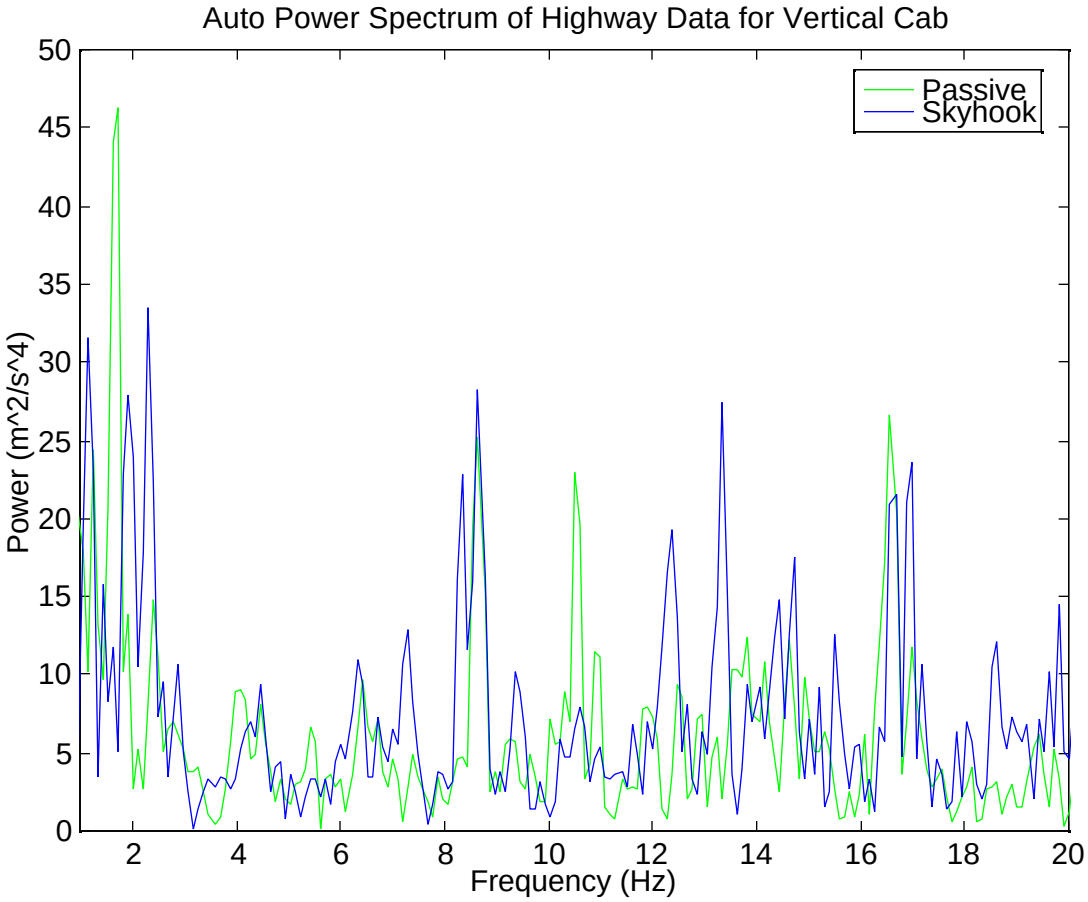

Figure 5.39. Auto Power Spectrum of Highway Data Vertical Cab (Passive, S/A).

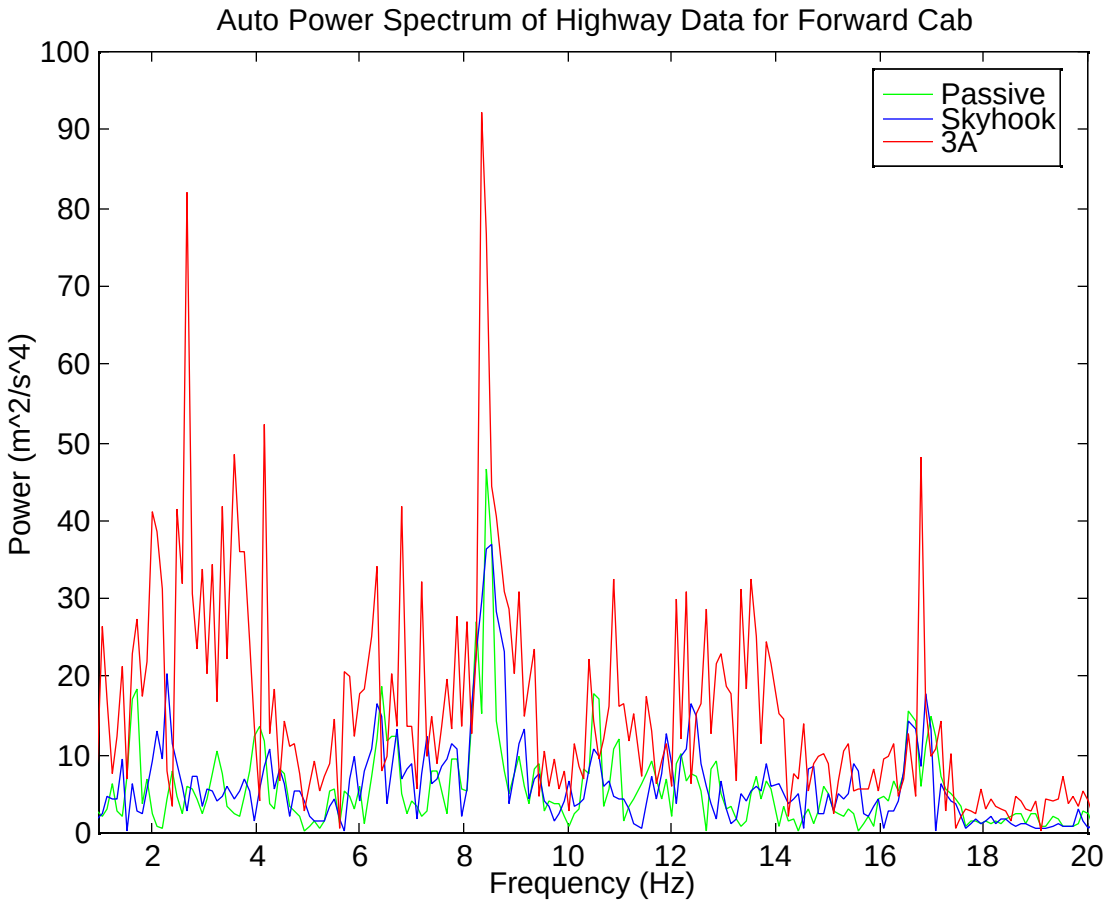

Figure 5.40. Auto Power Spectrum of Highway Data Forward Cab (Passive, S/A, 3A).

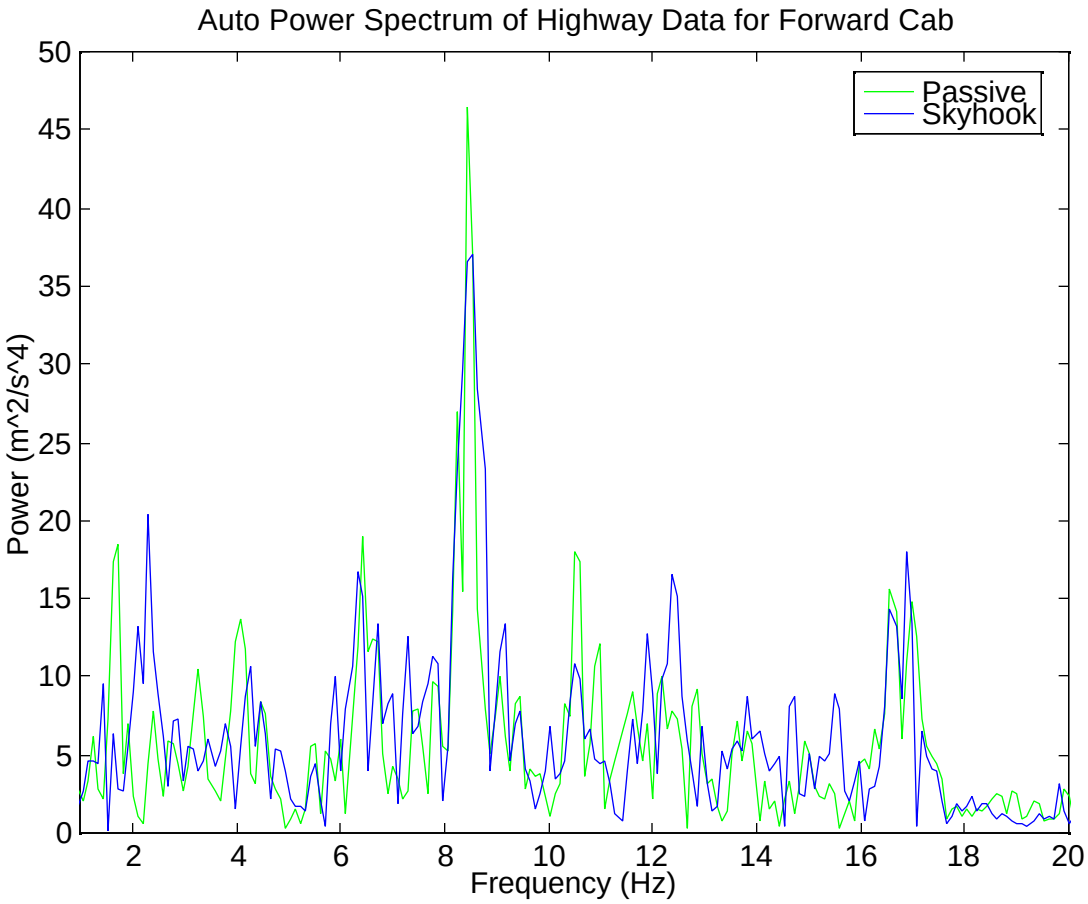

Figure 5.41. Auto Power Spectrum of Highway Data Forward Cab (Passive, S/A).

5.5.1 Summary of Highway Test Results

While a few points can be pointed out on the above figures, the data are primarily inconclusive. The semiactive suspension seems to have moved the peaks around, but not out of the area of concern (1Hz-10Hz). The only certainty is that the semiactive suspension did not improve the ride as much as had been hoped.

5.5.2 Subjective Feel

Since part of the motivation of the semiactive suspension is to improve comfort, it is appropriate to mention here how the ride felt as a passenger. The difference between the 0A ride and 3A ride was very noticeable. The 3A ride was harsh and jolting, as we would expect, while the 0A ride was bouncy, taking a long time to settle out, again as we would expect. The passive and semiactive suspensions provided a much more comfortable ride than the 0A or 3A, being neither too harsh nor too bouncy. However, as for differences between the passive and semiactive suspensions, none was noticeable.

Chapter 6
Conclusions

This chapter is intended to summarize the work that was performed throughout this research. It is also intended to provide recommendations for future research studies involving the testing of magneto-rheological dampers with a real-time embedded controller.

6.1 Summary

This study involved the design, prototyping, and testing of a real-time embedded controller for semiactive MR dampers. The controller was designed such that it is capable of driving six magneto-rheological dampers installed on a vehicle, such as a class 8 truck, in real time.

A prototype of the controller was fabricated at the Advanced Vehicle Dynamics Laboratory at Virginia Tech. The controller was initially bench tested in the laboratory for debugging, and later installed on a Volvo VN class 8 truck, along with four MR twin-tube dampers, for road testing. A series of tests were conducted on roads in Blacksburg, Virginia to establish the benefits of the MR dampers and to compare their performance with passive dampers. Eleven channels of data were recorded in the field for further analysis in the lab.

The analysis of the test results in the lab unfortunately did not indicate any clear trend regarding the benefits of MR dampers. The results proved, at best, to be inconclusive, highlighting the need for further system tuning and field testing. The system tuning would include further tuning of the MR dampers, further verification of proper functioning of the controller, implementation of continuous skyhook control, and verification of proper functioning of the data acquisition system.

Overall, it is believed that even though no conclusive results regarding the performance of the MR semiactive primary suspension were obtained, the research highlighted several important issues regarding the tuning and field testing of such systems for future research studies. These "lessons learned" should prove quite invaluable for the research team at Virginia Tech, as well as for others who are interested in this topic. Some of our recommendations for future research are stated in the following section.

6.2 Recommendations

As alluded to earlier, more work is needed to completely overcome the challenges of field testing a system such as the one that studied here on a complex dynamic system such as a heavy truck. The specific recommendations that follows this research are:

1. Consider implementing continuously-variable MR semiactive damping, as opposed to the on/off semiactive damping that was road tested in this study.
2. Conduct further testing with different levels of on-state damping. It is believed that the on-state damping that was adopted here may have been too high to provide desirable body dynamics. Lower levels of on-state damping may provide lower levels of body acceleration for semiactive dampers without significantly increasing wheelhop.
3. Implement alternative semiactive control policies, such as those recommended by Ahmadian [18] that might provide a more desirable performance of the suspension system.
4. Use the experience from this study to evaluate the performance of the MR semiactive suspensions in reducing the dynamic loading onto the pavement, as suggested by the groundhook control policy recommended by Ahmadian [21].
5. Use the controller developed in this study to evaluate the combined effect of semiactive secondary suspensions (i.e., cab and seat suspensions) and primary suspensions on traveler and cargo comfort, as well as other issues, such as wheelhop, roll stability, and pavement dynamic loading.

The author is confident that the above recommended research will lead to even more recommendations for future research studies which hopefully will

advance the MR semiactive suspension technology toward a successful hardware implementation and commercialization.

References

1. Crosby, M. J. and Karnopp, D. C., “The Active Damper - A New Concept for Shock and Vibration Control”, The Shock and Vibration Bulletin, vol. 43(4), pp. 119-133, June 1973.

2. Karnopp, D. C., “Active and Semi-Active Vibration Isolation,” Journal of Mechanical Design, Vol. 117, pp. 177-185, June 1995.

3. http://www.lordcorp.com/b.mech.html

4. Carlson, J. D., Catanzarite, D. M., and St. Clair, K. A., “Commercial Magneto-Rheological Fluid Devices,” Lord Library of Technical Articles, n. LL-8001, July 1995.

5. Barak, P., “Magic Numbers in Design of Suspension for Passenger Cars”, SAE Technical Papers Series, n. 878, pp.53-88, July 1991.

6. “Measurement of Whole Body Vibration of the Seated Operator of Off-Highway Work Machines”, SAE J1013, Society of Automotive Engineers, Warrendale, PA, 1992.

7. Krasnicki, E. J., “Comparison of Analytical and Experimental Results for a Semi-Active Vibration Isolator”, The Shock and Vibration Bulletin, v. 50, pp. 69-76, September1980.

8. Krasnicki, E. J. , “The Experimental Performance of an ‘On-Off’ Active Damper,” The Shock and Vibration Bulletin, vol. 51, pp. 125-131, November1980.

9. McMichael, S. C, “The Simulation and Spectral Analysis of A Motorcycle Model with a Semiactive On-Off rear Shock Absorber,” Ph. D. Thesis, University of California, Davis, CA, 1981.

10. Boonchanta, P., “Comparisons of Active, Passive, and Semiactive Suspensions for Ground Vehicles,” Ph. D. Thesis, University of California, Davis, CA, 1982.

11. Boonchanta, P., and Krasnicki, E. J., “Fluid Control Means for Vehicle Suspension System,” U. S. patent 4,491,207, 1985.

12. Miller, L. R., and Nobles, C. M., “The Design and Development of a Semi-Active Suspension for a Military Tank,” SAE Technical Paper Series No. 881133, 1985.

13. Ahmadian, M., “Ride Evaluation of A Class 8 Truck With Semiactive Suspensions”, DSC, Vol. 52, pp. 21-26, 1993.

14. Reichert, B. A., “Application of Magnetorheological Dampers for Vehicle Seat Suspensions,” Master’s Thesis, Virginia Tech, Blacksburg, Virginia (December 1997).

15. Miller, L. R., and Nobles, C. M., “Methods for Eliminating Jerk and Noise in Semi-Active Suspensions,” Truck and Bus Meeting and Exposition, Detroit, Michigan, November 1990.

16. Cai , Y., and Chen, S. S., “Control of Maglev Suspension Systems,” Journal of Vibration and Control, vol. 2, pp. 349-368, August 1996.

17. Margolis, D. L., “A Procedure for Comparing Passive, Active, and Semiactive Approaches to Vibration Isolation,” Journal of the Franklin Institute, vol. 15, no. 4, pp. 225-238, April 1983.

18. Margolis, D. L., “The Approximate Frequency Response of Semiactive Systems Requiring No Computer,” Journal of the Franklin Institute, vol. 316, no. 3, pp. 261-271, September 1983.

19. Ahmadian, M., Reichert, B., Song, X., “Harmonic Analysis of Semiactive Suspensions,” Proceedings of the Sixteenth Biennial Conference on Mechanical Vibration, ASME Design Technical Conference, Sacramento, CA, September 1997.

20. Ahmadian, M., “Semiactive Control of Multiple Degree of Freedom Systems,” Proceedings of Design Engineering Technical Conferences, September 1997.

21. Ahmadian, M., “A Hybrid Semiactive Control For Secondary Suspension Applications,” Proceedings of Sixth ASMA Symposium on Advanced Automotive Technologies, November 1997.

22. Kimbrough, S., “Bilinear Modelling and Regulation of Variable Component Suspensions,” ASME Monograph AMD-vol. 80, DSC-vol. 2, 1986

23. Hrovat, D., Margolis, D. L., and Hubbard, M., “An Approach Toward the Optimal Semi-Active Suspension,” Journal of Dynamic Systems, Measurement, and Control, vol. 110, pp. 288-296, September 1988.

24. Yi, K., and Hedrick, K., “Dynamic Tire Force Control by Semiactive Suspensions,” Journal of Dynamic Systems, Measurement, and Control, vol. 115, pp. 465-474, September 1993.

25. Khulief, Y. A., and Sun, S. P., “Finite Element Modeling and Semiactive Control of vibrations in Road Vehicles,” Journal of Dynamic Systems, Measurement, and Control, vol. 111, pp. 521-527, September 1989.

26. Tibaldi, M., and Zattoni, E., “Robust Control of Active Suspensions for High Performance Vehicles,” Proceedings of the lEEE lnternational Symposium on lndustrial Electronics, pp. 242-247, June 1996.

27. Redfield, R. C., “Performance of Low-Bandwidth, Semi-Active Damping Concepts for Suspension Control,” Vehicle System Dynamics, vol. 20, pp. 245-267, January1991.

28. Bellizi , S., and Bouc, R., “Adaptive Sub-Optimal Parametric Control for Non-Linear Stochastic Systems. Application to Semi-Active Isolators,” Probabilistic Methods in Applied Physics, pp. 401, 223-238, January 1995.

29. Shulman, Z. P., Kordonsky, V. I., Zaltsgendler, E. A., Prokhorov, I. V., Khusid, B. M., and Demchuk, S. A. , “Structure, Physical Properties and Dynamics of Magnetorheological Suspensions,” International Journal of Multiphase Flow, vol. 12, no. 6, pp. 935-955, November 1986.

30. Popplewell, J., and Rosensweig, R. E., “Magnetorheological Fluid Composites,” Journal of Physics D, vol. 29, pp. 2297-2303, January 1996.

31. Lukianovich, G., Ashour, O., Thurston, W., Rogers, C., and Chaudhry, Z., “Electrically-Controlled Adjustable Resistance Exercise Equipment Employing Magnetorheological Fluid”, SPIE, vol. 2721, pp. 283-291, April1996.

32. Ashour, O., Rogers, C. A., and Kordonsky, W., “Magnetorheological Fluids: Materials, Characterization, and Devices,” Journal of Intelligent Material Systems and Structures, Vol. 7, pp.123-130, March 1996.

32. Gleb, V. K., and Kuz’min, V. A., “Electro- and Magnetorheological Viscometers,” Heat Transfer - Soviet Research, vol. 17, no. 1, pp. 90-95, January-February 1985.

33. “M68HC11 Reference Manual”, Motorola Inc., No. M68HC11RM/AD, 1991.

34. http://www.physics.vt.edu/map2.html

Appendix A
Parts List

Part	Manufacturer	Supplier	Suppl. Part #	Qty	Appr. $ ea.
HC11 EVBU (Microcontroller)	Motorola	Motorola	S68HC11EVBU	1	$68.11
LM741 (Op-Amp)	National Semiconductor	Digikey	LM741CN-ND	8	$0.91
1MΩ Resistors	?	Radio Shack	271-1356	8	$1.00/5
100kΩ Resistors	?	Radio Shack	271-1131	8	$1.00/5
1uF Capacitors	?	Radio Shack	272-1055	8	$0.49
10uF Capacitors	?	Radio Shack	272-999	8	$0.49
2kΩ Resistors	Yageo	Digikey	2.0KW-1-ND	2	$0.27
ADC0816CCN (A/D Chip)	National Semiconductor	Digikey	ADC0816CCN-ND	1	$25.43
MX045 (Clock Oscillator)	CTS	Digikey	CTX150-ND	1	$4.08
74LS04N (Hex Inverter)	National Semiconductor	Digikey	DMLS04N-ND	1	$0.53
74HCT138E (Decoder)	Harris	Radio Shack	276-2829	1	$1.50
MAX506BCPP (D/A Chip)	MAXIM	Digikey	MAX506BCPP-ND	3	$12.74
PA26 (Power Op Amp)	APEX	APEX	PA26	4	$8.65
TIP120 (Transistor)	Texas Instruments	Radio Shack	276-2068	8	$1.70
276-1368 (Heat Sink)	?	Radio Shack	276-1368	8	$1.50
YAGEO-554 (1Ω Resistor)	YAGEO	Digikey	1.0W-10-ND	8	$0.60
1N4934GI (Diode)	Diodes Incorporated	Digikey	1N4934CT-ND	8	$0.25
5V Power Supply	ASTEC	HOSFELT Elect.	40-143	1	$39.95
12V Power Supply	TOKO	Digikey	TS9980-ND	2	$208.02

24V Power Supply	TOKO	Digikey	TS9982-ND	2	$208.02
40 Pin IC Socket	Assman	Digikey	AE7140-ND	1	$4.74
20 Pin IC Sockets	Assman	Digikey	AE7120-ND	3	$2.37
16 Pin IC Socket	Assman	Digikey	AE7116-ND	1	$1.89
14 Pin IC Sockets	Assman	Digikey	AE7114-ND	2	$1.65
8 Pin IC Sockets	Assman	Digikey	AE7108-ND	8	$0.96
Fuse Block	?	Radio Shack	270-742	2	$2.39
3A Fuses	?	Radio Shack	270-1009	8	$1.29
Protoboard 8”x6”	?	Radio Shack	276-1396	3	$3.49

Suppliers

APEX
5980 North Shannon Road
Tucson, AZ 85741
Phone: (520) 690-8601

DigiKey
701 Brooks Ave. South
Thief River Falls, MN 56701-0677
Phone: 1-800-344-4539

HOSFELT Electronics
2700 Sunset BLVD
Steubenville, OH 43952-1158
Phone: 1-800-524-5414

Motorola University Support
505 Barton Springs Road
Suite 100
Austin, Texas 78704
Phone: ?
(To get the HC11 EVBU, you must send them a photocopy of your student ID.)

Newark Electronics
217 Wilcox Avenue
Gaffney, SC 29340
Phone: 1-800-4NEWARK

Radio Shack
Gables Shopping Center
118 Country Club Dr. SW
Blacksburg, VA 24060
Phone: (540)951-8954

Appendix B
Schematic

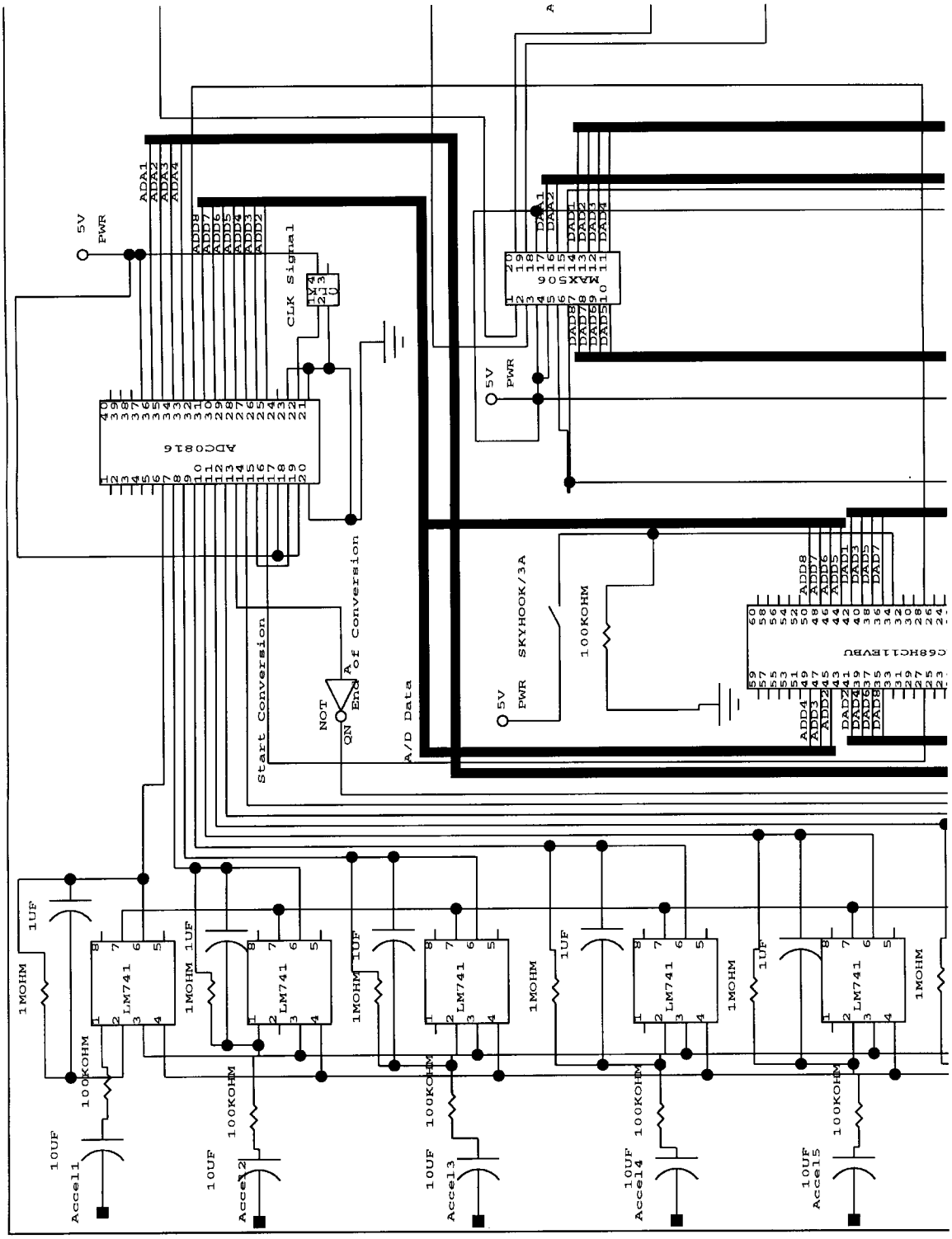
5V
PWR
ADA1
ADA2
ADA3
ADA4
ADD8
ADD7
ADD6
ADD5
ADD4
ADD3
ADD2
CLK Signal
ADC0816
Start Conversion
End of Conversion
NOT
A/D Data
SKYHOOK/3A
100KOHM
DAA1
DAA2
DAD1
DAD2
DAD3
DAD4
DAD5
DAD6
DAD7
DAD8
LM741
1MOHM
1UF
10UF
100KOHM
Accel1
Accel2
Accel3
Accel4
Accel5

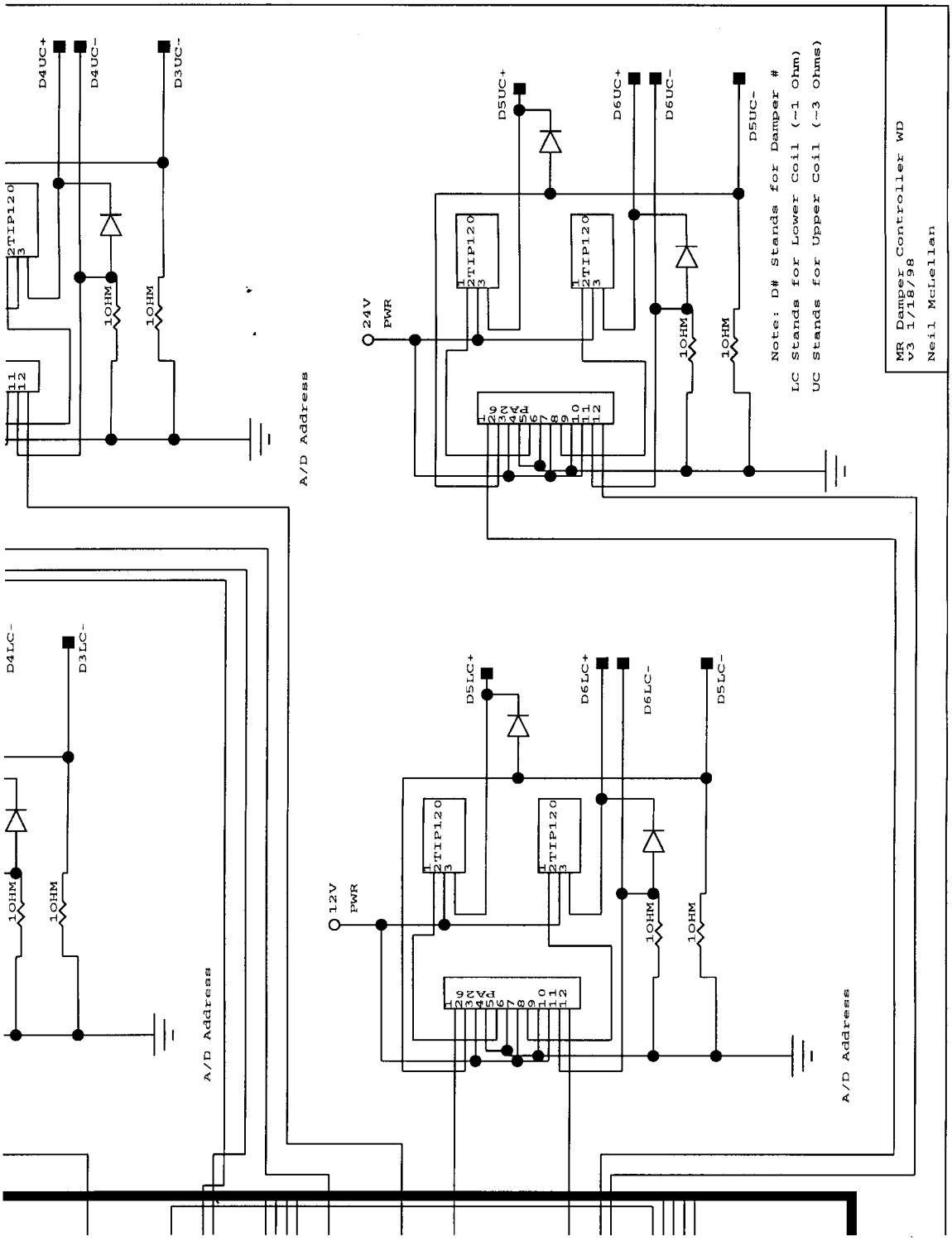
MR Damper Controller WD
v3 1/18/98
Neil McLellan
Note: D# Stands for Damper #
LC Stands for Lower Coil (~1 Ohm)
UC Stands for Upper Coil (~3 Ohms)
D4UC+
D4UC-
D3UC-
D5UC+
D6UC+
D6UC-
D5UC-
D4LC-
D3LC-
D5LC+
D6LC+
D6LC-
D5LC-
2TIP120
10HM
24V
PWR
12V
PWR
A/D Address

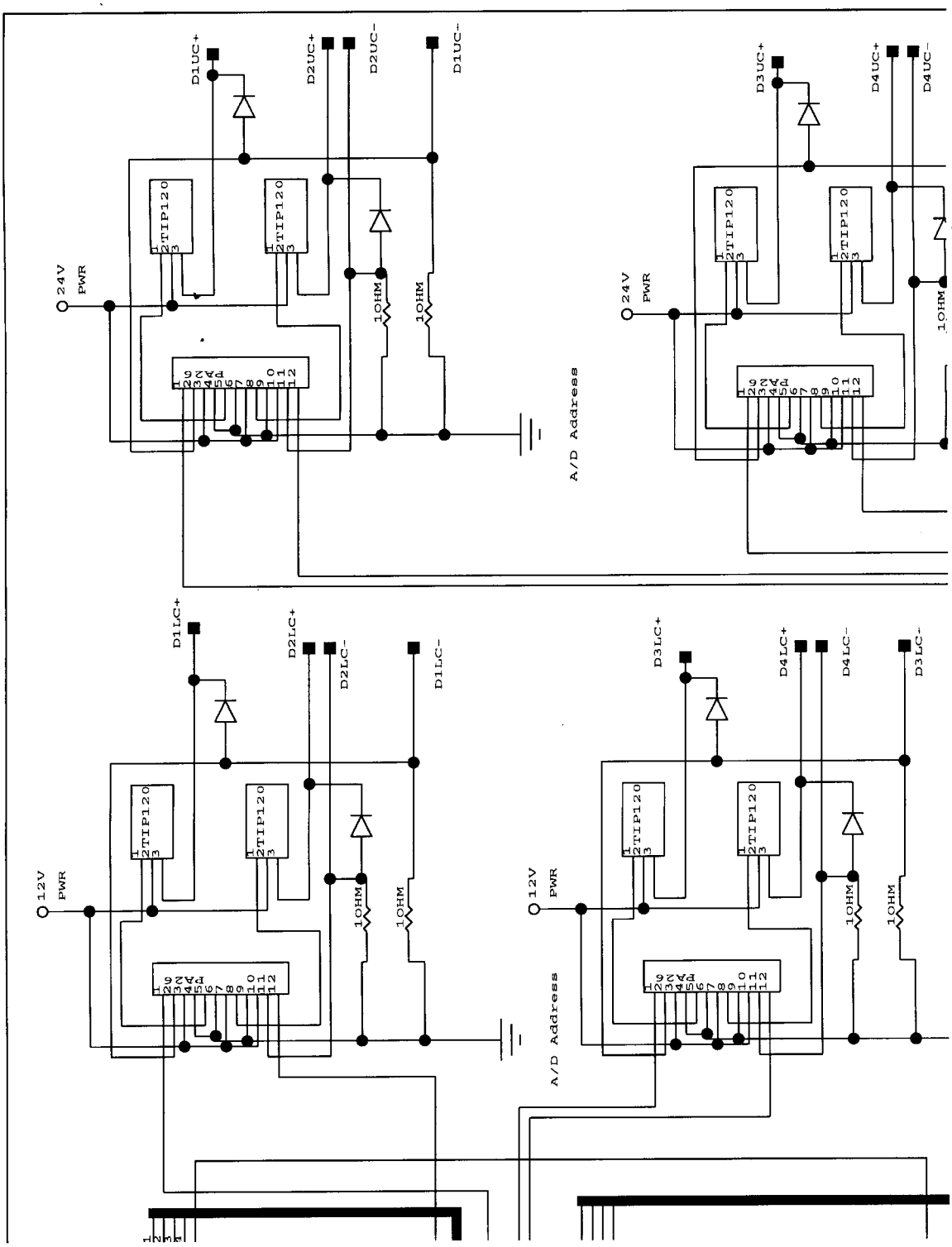
D1UC+
D2UC+
D2UC-
D1UC-
D3UC+
D4UC+
D4UC-
24V
PWR
2TIP120
1OHM
A/D Address
D1LC+
D2LC+
D2LC-
D1LC-
D3LC+
D4LC+
D4LC-
D3LC-
12V
PWR

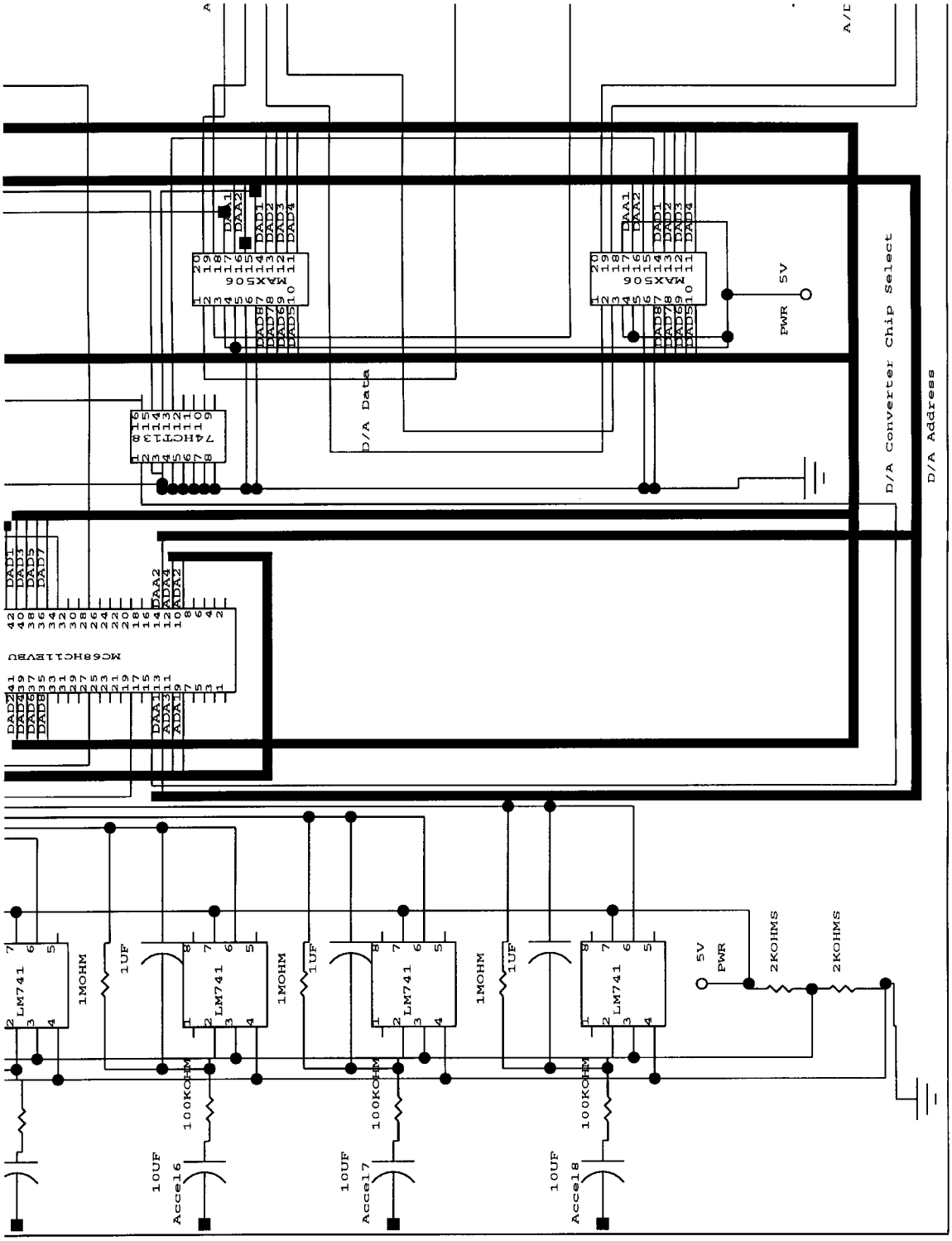
D/A Converter Chip Select
D/A Address
D/A Data
MAX506
74HCT14
MC68HC11EVBU
LM741
1MOHM
1UF
100KOHM
10UF
Accel6
Accel7
Accel8
5V
PWR
2KOHMS

Appendix C
Microcontroller Code Listing

```
*** Dampers.ASM
*** Neil McLellan
*** Created 3/25/97
*** Modified 3/26/97, ?
*** 5/27/97, 5/29/97, 6/3/97, 6/12/97, 7/20/97
*** 8/20/97, 8/21/97, 12/4/97

*Pseudovector adresses
PVIRQ EQU $00EE
PVSCI EQU $00C4
PVTOC EQU $00D0
PVOC3 EQU $00D9

*Register adresses
PORTA EQU $1000
PIOC EQU $1000
PORTC EQU $1003
PORTB EQU $1004
PORTCL EQU $1005
DDRC EQU $1007
PORTD EQU $1008
DDRD EQU $1009
PORTE EQU $100A
CFORC EQU $100B
TOC3 EQU $101A
TCNT EQU $100E
TCTL1 EQU $1020
TMSK1 EQU $1022
TFLG1 EQU $1023
TMSK2 EQU $1024
TFLG2 EQU $1025
PACTL EQU $1026
SPCR EQU $1028
SPSR EQU $1029
SPDR EQU $102A
BAUD EQU $102B
SCCR1 EQU $102C
SCCR2 EQU $102D
SCSR EQU $102E
```

```
SCDR EQU $102F
BPROT EQU $1035
OPTION EQU $1039
COPRST EQU $103A
PPROG EQU $103B
HPRIO EQU $103C
INIT EQU $103D
CONFIG EQU $103F

VELOC EQU $00
ACCAVG EQU $02
SNSSZE EQU $04

NEXTDMPR EQU $10
LASTDMPR EQU $B0

*RAM
    ORG $0100
RAM

CURSNS  rmb 1

SENSORS
VEL1 rmb 1
VEL2 rmb 1
VEL3 rmb 1
VEL4 rmb 1
VEL5 rmb 1
VEL6 rmb 1
VEL7 rmb 1
VEL8 rmb 1


*EEPROM
    ORG $B600

EEPROM
    LDS #$00C3  ;Initialize stack to RAM address

* Change TCNT prescaler  & enable timer overflow interrupt
```

```
    LDAA #$03
    STAA TMSK2

*Initialize D/A

    LDAA #$00
    LDAB #$00
INITDMPLOOP
    JSR WRITEDA
    ADDB NEXTDMPR
    CMPB LASTDMPR
    BLT INITDMPLOOP

*Initialize Variables

    LDAA #$08
    STAA CURSNS
    LDX #SENSORS
INITVLOOP
    CLR 0,X
    CLR 1,X
    INX
    INX
    CPX #VEL8
    BLE INITVLOOP

* Set up pseudovectors for interrupts
    LDAA #$7E   ; Jump opcode
    STAA PVIRQ  ; IRQ Interrupt
    STAA PVTOC
    LDX #SVCIRQ
    STX PVIRQ+1


    LDAA #$FF
    STAA DDRC  ;Set Port C for output

    LDAA #$80  ; Set bit 7 Port A for output
    STAA PACTL
```

```
* Put initial values in Ports A & C  (Starting first A2D
conversion)
    LDAA #$C8
    STAA PORTC
    LDAA #$C0
    STAA PORTA

    NOP

    LDAA #$00
    STAA PORTA ;End start pulse

    CLI ;Enable interrupts

LOOP ; Main Program Loop

  LDAA PORTA ; Checking for
  ANDA #$01
  BEQ SKYHOOK

  SEI
  LDAA DAMPMX
  LDAB #$30
  JSR WRITEDA
  LDAB #$80
  JSR WRITEDA
  LDAB #$20
  JSR WRITEDA
  LDAB #$90
  JSR WRITEDA
  LDAB #$00
  JSR WRITEDA
  LDAB #$60
  JSR WRITEDA
  LDAB #$10
  JSR WRITEDA
  LDAB #$70
  JSR WRITEDA
LOOP2
  LDAA PORTA
```

```
  ANDA #$01
  BNE LOOP2
  CLI

SKYHOOK
*Left front damper
  LDAA VEL1
  LDAB VEL2
  JSR CALCDMP
  LDAB #$30
  JSR WRITEDA
  LDAB #$80
  JSR WRITEDA

*Right Front
  LDAA VEL8
  LDAB VEL7
  JSR CALCDMP
  LDAB #$20
  JSR WRITEDA
  LDAB #$90
  JSR WRITEDA

*Left Rear
  LDAA VEL5
  LDAB VEL6
  JSR CALCDMP
  LDAB #$00
  JSR WRITEDA
  LDAB #$60
  JSR WRITEDA

*Right Rear
  LDAA VEL4
  LDAB VEL3
  JSR CALCDMP
  LDAB #$10
  JSR WRITEDA
  LDAB #$70
  JSR WRITEDA
```

```
  JMP LOOP

CALCDMP
* A - Body Velocity
* B - Axle Velocity

  CMPA #$10
  BGT POS
  CMPA #$EF
  BLT NEG
  BRA NODMP

NEG
  CBA
  BGE NODMP
  LDAA DAMPMX
  RTS

POS
  CBA
  BLE NODMP
  LDAA DAMPMX
  RTS

NODMP
  LDAA #$00
  RTS


* SVCIRQ
* Services IRQ interrupts. The IRQ interrupt is
* used here to signal an end of conversion for the A2D
SVCIRQ
   SEI

   LDAB CURSNS
   SUBB #$08
   LDX #SENSORS
   ABX
```

```
   LDAB PORTE
   SUBB #$80
   STAB 0,X

   LDAB CURSNS
   INCB
   BVC OKSNS
   LDAB #$08

OKSNS
   STAB CURSNS
   LDAA #$F0
   ANDA PORTC
   ABA
   STAA PORTC

   LDAA PORTA
   ORAA #$C0
   STAA PORTA

   NOP

   LDAA PORTA
   ANDA #$3F
   STAA PORTA

   CLI
   RTI

*Write data to D/A chip
*Registers:
* A - D/A value
* B - D/A address (In top 4 bits, zero in bottom 4)
WRITEDA
  PSHA
  CMPA DAMPMX
  BLS  OKDAMP
  LDAA DAMPMX
OKDAMP
  STAA PORTB
```

```
  LDAA PORTC
  ANDA #$0F
  ABA
  STAA PORTC
  ORAA #$C0
  STAA PORTC
  PULA
  RTS

       db 'v','a','r'
DAMPMX db $9A
GAIN DB $01
```

Vita

Neil McLellan began came to Tech in 1991, majoring in Computer Engineering. While an undergrad, he co-oped for a year at IBM Eduquest in Atlanta. He graduated with a B.S. in Computer in Engineering in December 1995. He then immediately began graduate school at Virginia Tech. For his Master's in Electrical Engineering his area of concentration was Controls. The first paper he published as a graduate student was "Simulation of Nonlinear Systems Using the Student Version of Matlab," in the Proceedings of IEEE Southeastcon, 1997. He completed his Master's in Electrical Engineering in July of 1998.